OUKA
The University of Osaka
Institutional Knowledge Archive

Title	Syntheses of U-Shaped Dibenzophenazine Cyclic Dimers and Their Photophysical Properties
Author(s)	難波, 直大
Citation	大阪大学, 2026, 博士論文
Version Type	VoR
URL	https://doi.org/10.18910/105424
rights	
Note	

The University of Osaka Institutional Knowledge Archive : OUKA

https://ir.library.osaka-u.ac.jp/

The University of Osaka

Doctoral Dissertation

Syntheses of U-Shaped Dibenzophenazine Cyclic Dimers and Their Photophysical Properties

Naohiro Namba

January 2026

Department of Applied Chemistry

Graduate School of Engineering

The University of Osaka

Preface

The studies presented in this Thesis were conducted under the supervision of Professor Dr. Satoshi Minakata, Department of Applied Chemistry, Graduate School of Engineering, The University of Osaka during the period of 2020–2026.

The objects of this Thesis cover the syntheses of U-shaped dibenzophenazine cyclic dimers and their photophysical properties. The author hopes sincerely that the fundamental work described in this Thesis contributes to further development of novel nitrogen-embedded extended π-conjugated macrocycles, functional material chemistry, and other related fields of chemistry.

Naohiro Namba

Department of Applied Chemistry

Graduate School of Engineering

The University of Osaka

Suita, Osaka

JAPAN

January 2026

Contents

General Introduction 1

Chapter 1 Development of Solubility-Enhanced 6,8-Diarylated Dibenzo[*a,j*]phenazine (DBPHZ) Building Blocks and Synthesis of DBPHZ Cyclic Homodimer 15

Chapter 2 Development of a Tetra-Functionalized Dibenzo[*a,j*]phenazine (DBPHZ) Building Block and Synthesis of Highly Soluble DBPHZ Cyclic Heterodimer 51

Chapter 3 Investigation of Photophysical Properties and Functional Exploration of Cyclic Dimers of DBPHZ 73

Conclusion 101

List of Publications 105

Copyrights 107

Acknowledgements 109

General Introduction

1. π-Conjugated Macrocycles Composed of Arylene Units and Their Progress

π-Conjugated macrocycles are defined as compounds in which aromatic units are connected either directly or via sp- or sp²-hybridized carbon atoms or are fused (Figure 1). Beyond the aesthetic appeal associated with their highly symmetric molecular architectures, these macrocycles exhibit unusual optical and electronic properties and functions that are not observed in acyclic π-conjugated molecules.[1] Such features arise from their conjugated frameworks without terminal ends and from electronic structures induced by molecular curvature and strain. Consequently, π-conjugated macrocycles have attracted considerable attention from both synthetic chemistry and materials science.

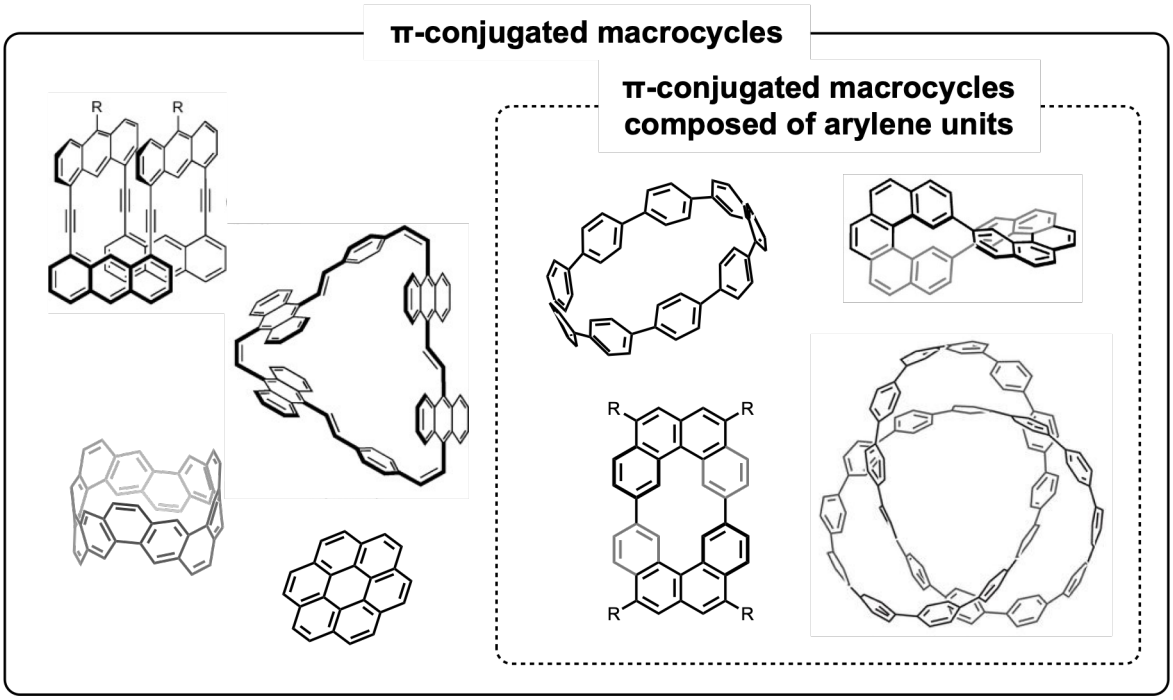


Figure 1. Chemical structures of π-conjugated macrocycles.

Among them, π-conjugated macrocycles composed of arylene units connected via single bonds (i.e., cycloarylenes) are particularly intriguing. They can construct a wide variety of nanocarbon frameworks ranging from two- to three-dimensional architectures, simply by altering the backbone structure of arylene units, the number of units, and their connection

patterns (Figure 2). Since these compounds can be regarded as substructures of nanographenes and carbon nanotubes, cycloarylenes are also important as model molecules toward the precise synthesis of nanocarbon materials.[2]

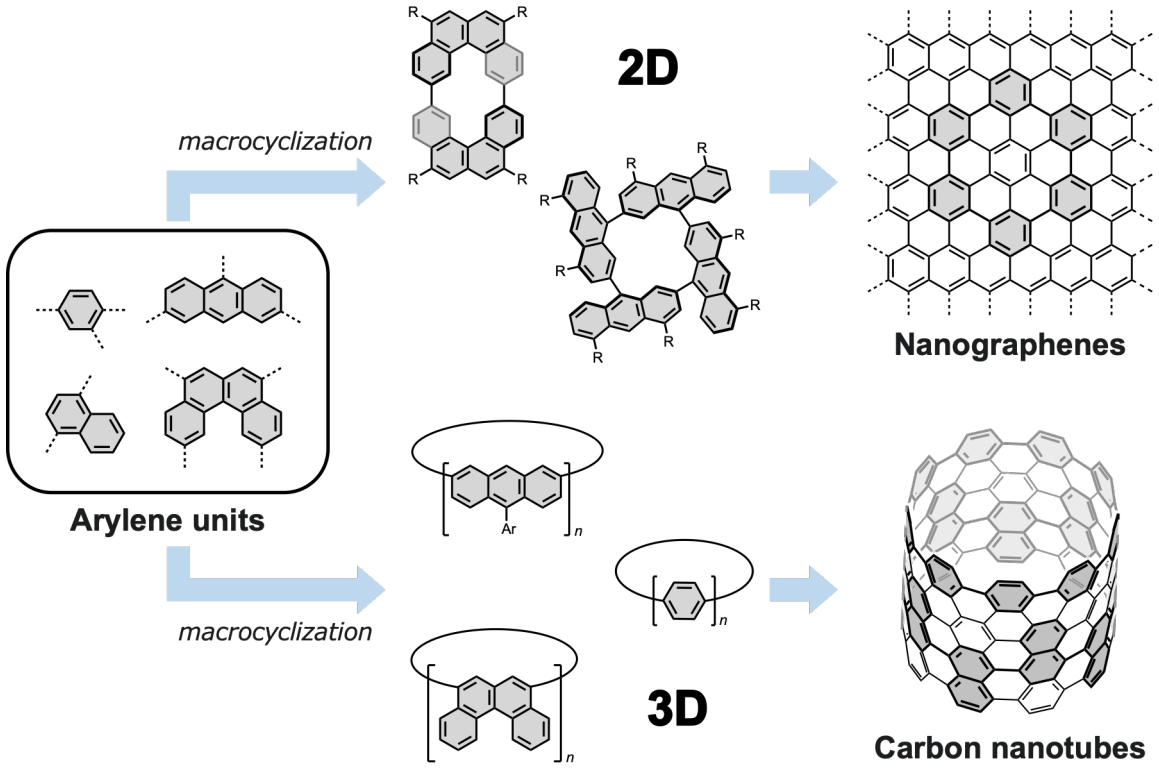


Figure 2. Structural diversity of cycloarylenes and their prospects.

A representative example of cycloarylenes is the family of cycloparaphenylenes (CPPs),[3] which constitute one of the shortest structural segments of single-walled carbon nanotubes (Figure 3a). Owing to their highly strained cyclic structures, CPPs had been regarded as a synthetically challenging target. However, in 2008, the first synthesis of CPPs was achieved by Jasti and Bertozzi,[3a] and around the same time, Itami[3b] and Yamago[3c] also opened this field. Inspired by these pioneering studies, structurally related cycloarylenes composed of π-extended arylene units have been actively developed over the past decade.[4] Prominent examples include cyclonaphthylenes ([*n*]CNAPs),[4a,4b] cycloanthrylenes ([*n*]CANTs),[4c–4f] and cyclopyrenylenes ([*n*]CPys).[4g,4h]

Notably, since reliable synthetic methods for CPPs were established, structurally innovative cycloarylenes such as nanocages,[5a,5b] catenanes,[5c,5d] and trefoil knots[5c] have been synthesized based on similar synthetic strategies, and the synthesis of cycloarylenes composed of chiral π-units[5e,5f] have also been realized (Figure 3b). Consequently, the systematic elucidation of structure–property relationships of hydrocarbon-based cycloarylenes has been steadily advanced.

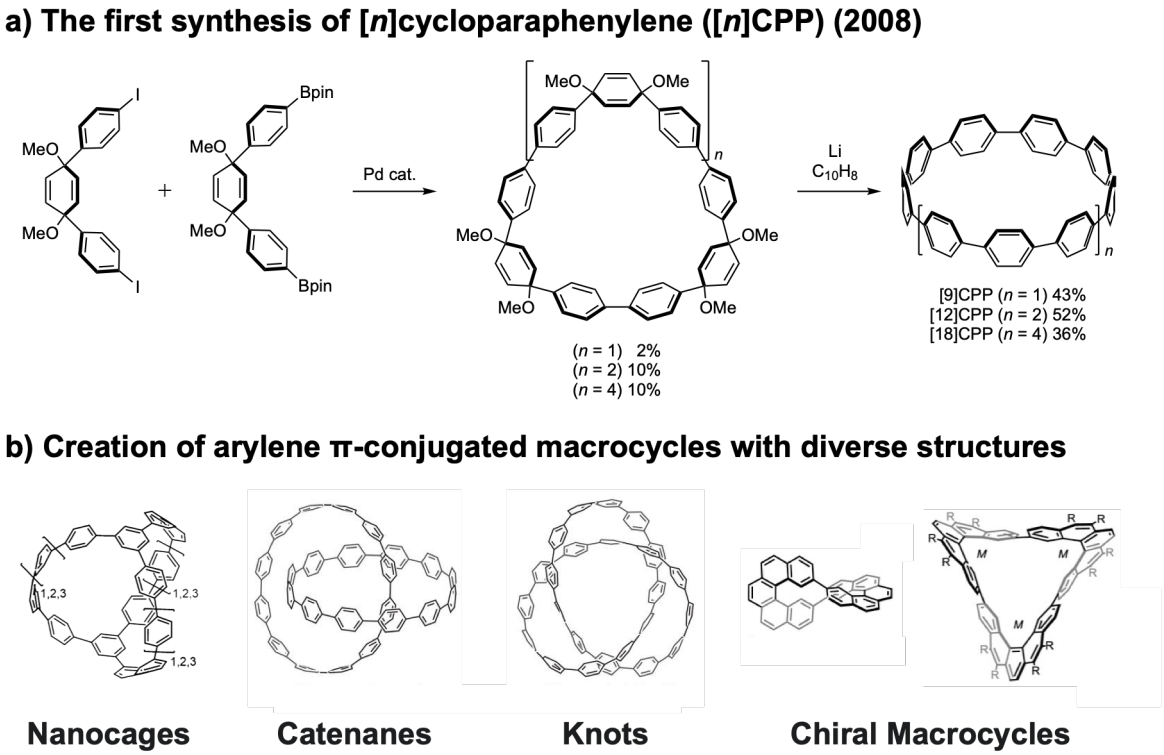


Figure 3. Progress in hydrocarbon-based cycloarylenes.

2. Challenges in Constructing π-Conjugated Macrocycles

Despite the impressive progress described above, π-conjugated macrocycles remain synthetically demanding targets, and the number of reported examples is still limited. To access such macrocycles efficiently, several fundamental issues must be overcome (Figure 4 and 5).

First, the formation of highly distorted macrocyclic structures from planar π-conjugated units is enthalpically disfavored (Figure 4). In addition, synthetic intermediates for ring closure

can adopt many conformations due to free rotation around each C–C single bond. Therefore, constraining such flexible linear precursors into a closed cyclic structure is entropically disfavored. As a result, macrocyclization reactions often compete with undesired oligomerization or polymerization, leading to low yield of the desired cyclic product and complicated separation from byproducts.

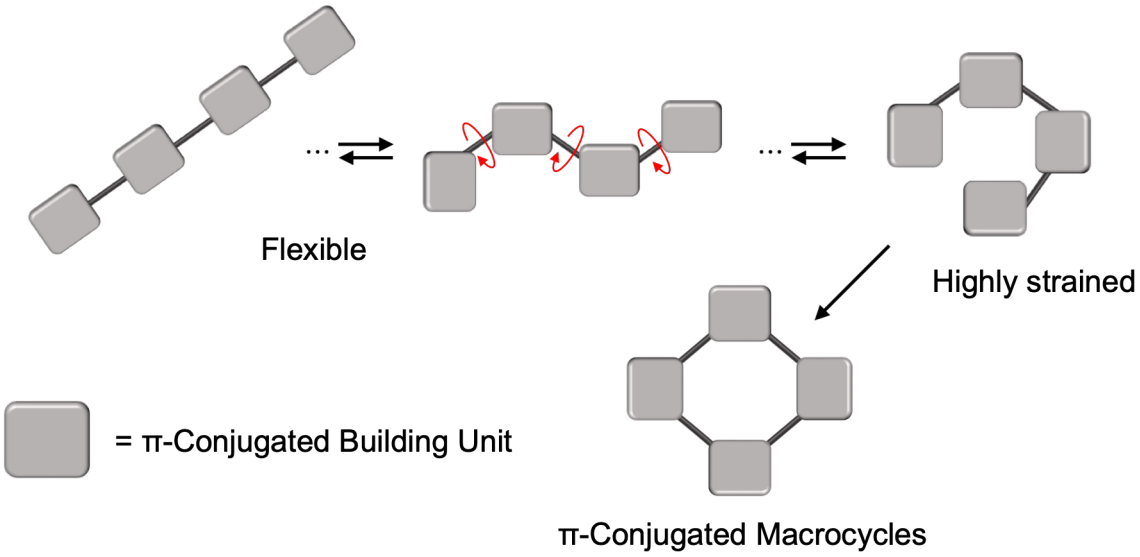


Figure 4. Ring-forming processes of π-conjugated macrocycles.

3. Solubility Issue in π-Extended Aromatic Compounds

Second, π-extended aromatic building blocks and macrocycles frequently suffer from poor solubility due to strong intermolecular interactions such as π–π stacking arising from their highly planar molecular structures (Figure 5). This not only decreases reaction efficiency but also severely restricts product isolation, purification, structural characterization, and property evaluation. To address such solubility issues, a common strategy is the introduction of bulky or flexible solubilizing substituents at the periphery of the π-framework, thereby sterically suppressing aggregation and ensuring sufficient solubility.[6]

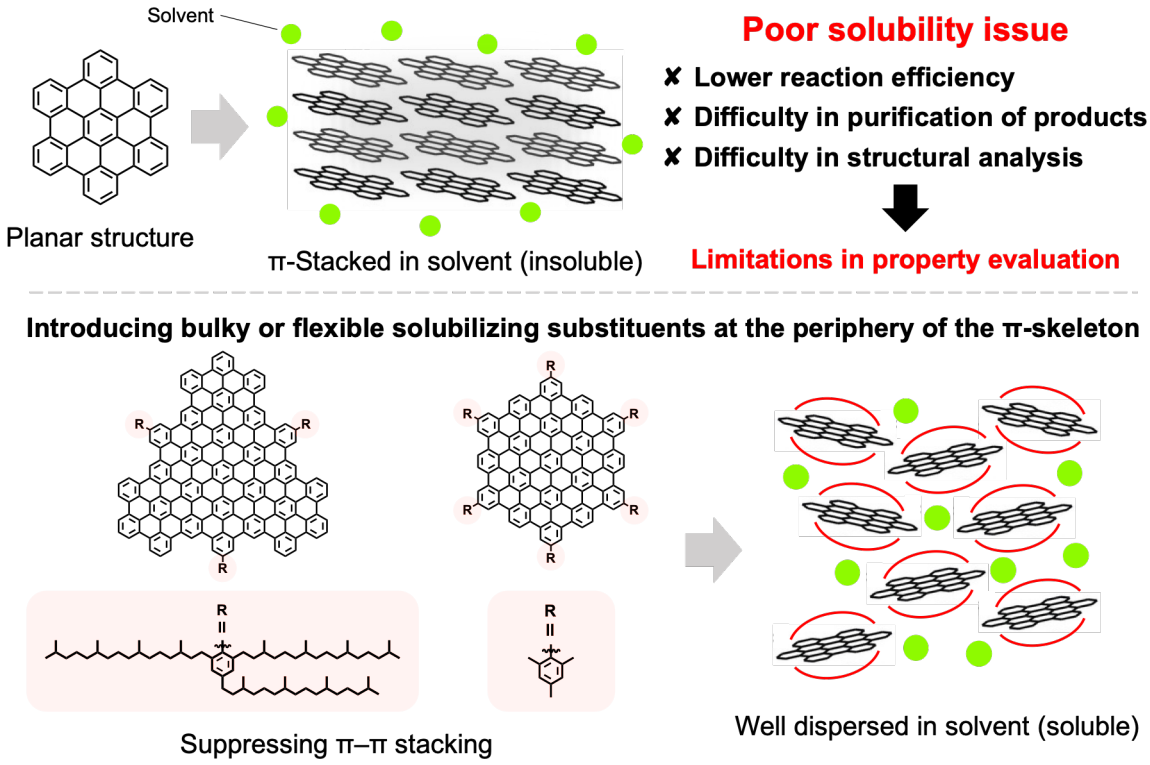


Figure 5. Solubility issue in π-extended aromatic compounds and their solutions.

4. Significance of Introducing Nitrogen Atoms into Cycloarylene π-Systems

As described in section 1, hydrocarbon-based cycloarylenes have provided powerful model systems for comprehending the properties of nanographenes and carbon nanotubes. However, purely hydrocarbon frameworks inherently limit the degree of tunability of electronic and supramolecular properties. In such systems, band gaps, frontier molecular orbital energies, and intermolecular interactions are primarily controlled by ring size and topology, and therefore it is difficult to introduce specific recognition sites or polar functionalities without perturbing the π-skeleton. To transform cycloarylenes from static structural models of nanocarbons into highly tunable functional materials, it is desirable to dope or functionalize the arylene backbone itself. To enhance the functions of π-conjugated macrocycles, one of the powerful approaches is the incorporation of heteroatoms into the molecular skeleton (Figure 6).[7] Although some pioneering examples of arylene macrocycles

incorporating heteroatoms of B, O, P, and S have been reported, their number remains limited.[7,8] In contrast, cycloarylenes in which aromatic units are replaced with heteroaromatic units containing nitrogen atoms offer several advantages (Figure 6). For example, pyrrole-type heterocycles endow the π-electronic system with electron-donating characters, whereas pyridine-type heterocycles confer electron-accepting properties. Thus, the electronic properties of nitrogen-embedded cycloarylenes (i.e., N-arylene macrocycles) can be widely tuned by varying the type of azaheterocycles to be incorporated. Moreover, the embedded nitrogen atoms can provide interacting sites for guest molecules via non-covalent interactions such as hydrogen bonding and metal coordination.

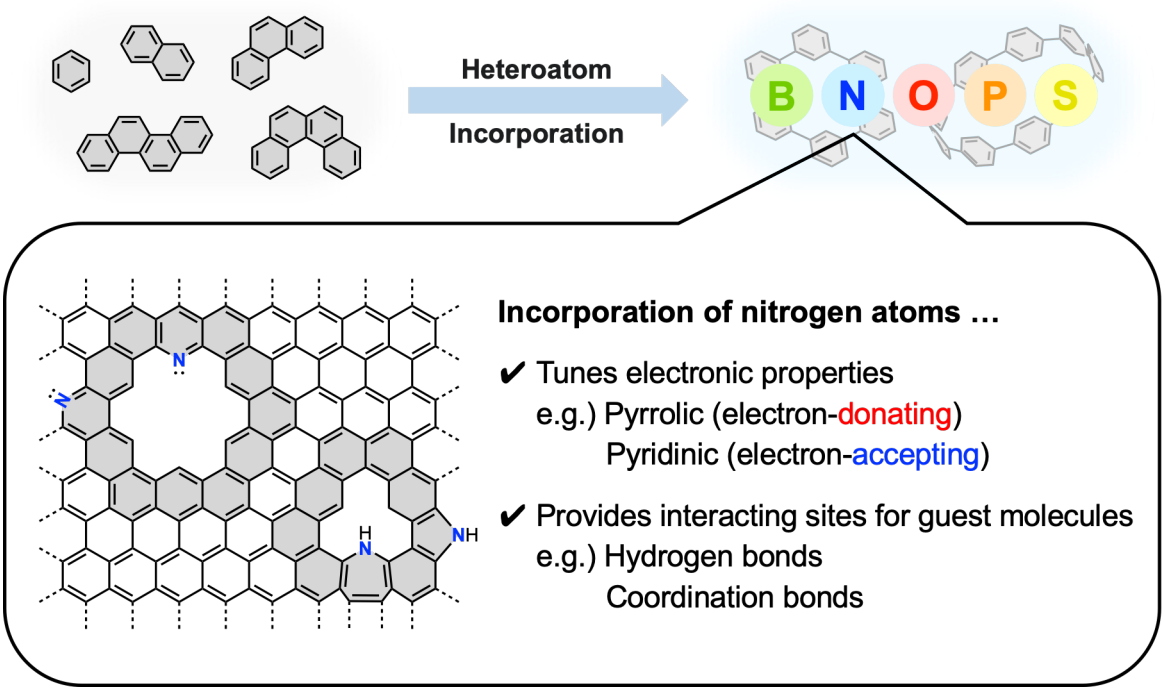


Figure 6. Design for fine-tuning molecular structures and physical properties of cycloarylenes.

In this context, Kumagai and co-workers have reported systematic studies on the synthesis of N-arylene macrocycles based on quinoline units (Figure 7a).[9] Among these, TriQuinoline (TQ),[9a] a cyclic trimer, exhibits high proton affinity at the central region where quinoline nitrogen atoms converge, resulting in pronounced hydrophilicity, whereas

TEtraQuinoline (TEQ),[9b] a cyclic tetramer, emits strong fluorescence upon protonation of nitrogen atoms or coordination to Zn^{2+} ions. Another notable example of N-arylene macrocycle is composed of carbazole and triazole units reported by Flood and co-workers (Figure 7b).[9c] This macrocycle displays high binding affinity toward anions whose sizes match the cavity of the inner ring, and it also undergoes well-defined self-assembly on a graphite surface.

As mentioned above, nitrogen-embedded cycloarylenes are expected to serve as functional compounds, fearturing exceptional optoelectronic behavior, host–guest recognition, and self-assembly properties. Therefore, the construction of new structures of N-arylene macrocycles and clarification of their properties is significantly important from the viewpoint of materials science.

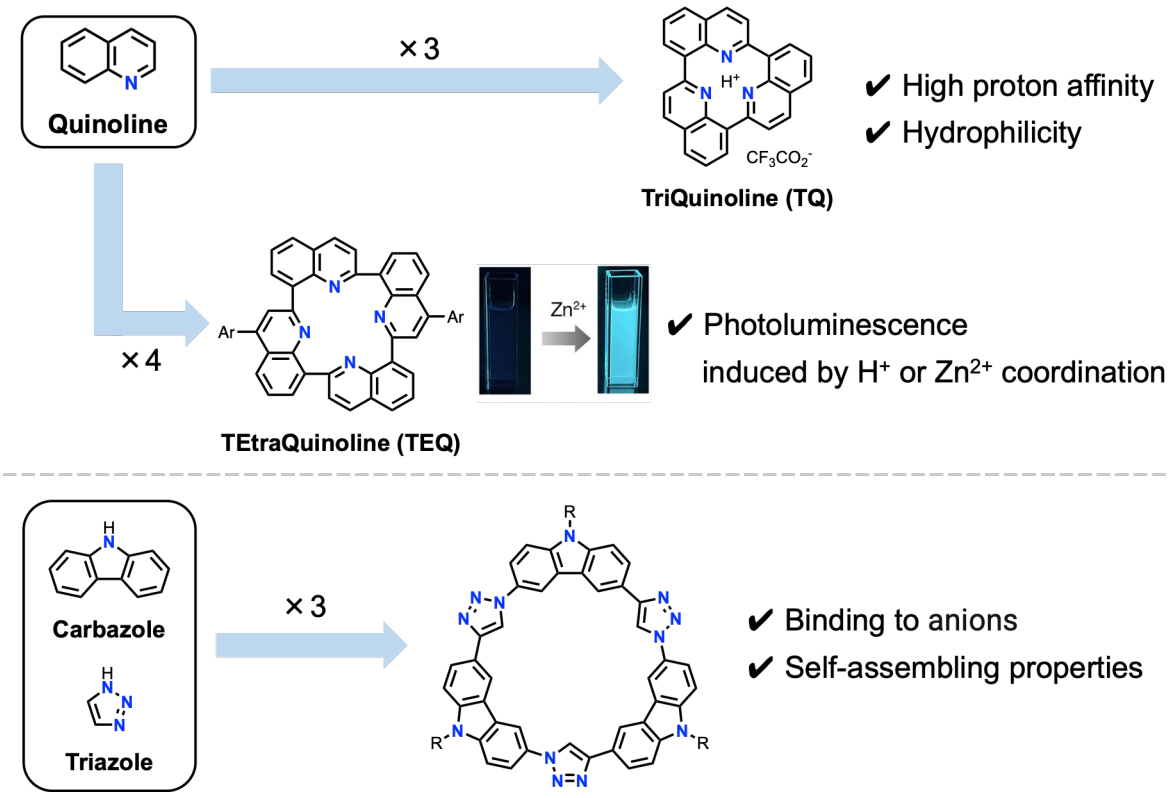


Figure 7. Examples of nitrogen-embedded cycloarylenes.

5. Shortage of Nitrogen-Embedded π-Extended Building Blocks

Focusing on previously reported cycloarylenes composed of nitrogen-embedded arylene units, most examples are constructed from tricyclic or smaller N-arylene skeletons (Figure 8).[7,9] In contrast, N-arylene macrocycles based on tetracyclic or more fused aromatic units are almost unexplored. To the best of my knowledge, a π-conjugated macrocycle constructed from azatriangulene units is the only reported example.[10] This situation reflects a more fundamental issue: there is a marked scarcity of nitrogen-embedded, π-extended building blocks suitable for macrocycle construction.

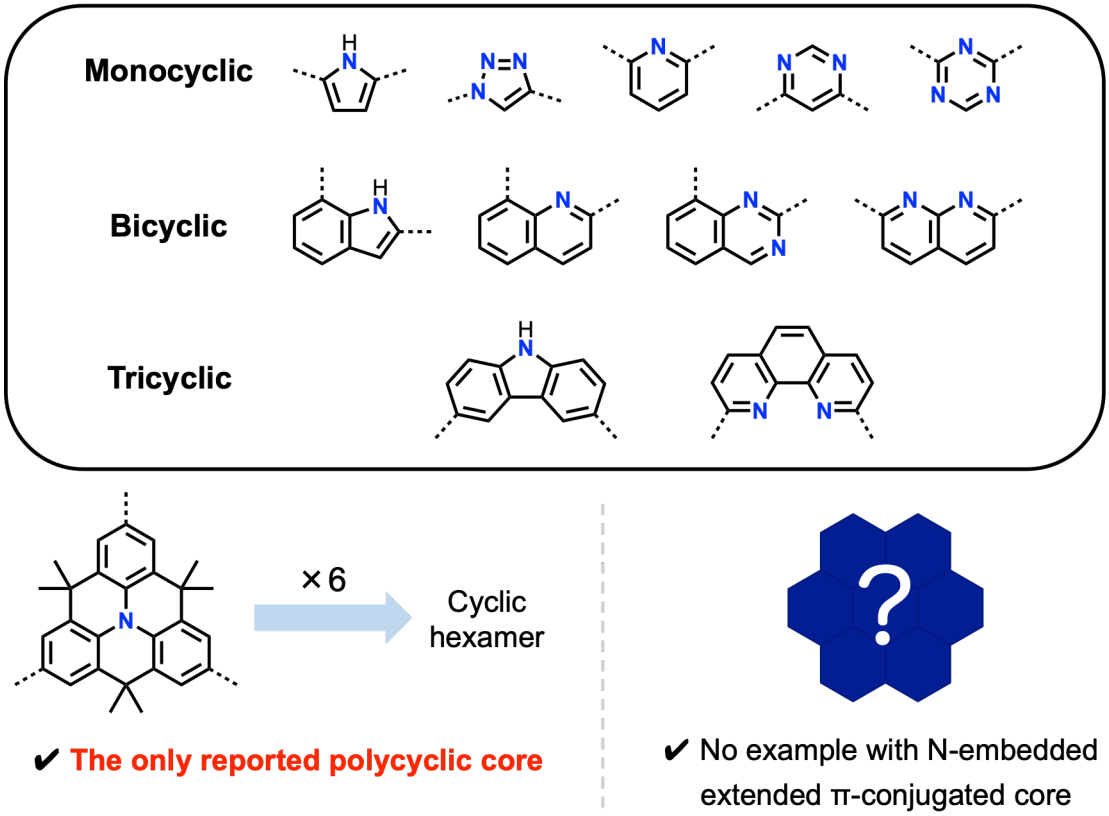


Figure 8. Classification of nitrogen-embedded π-extended building blocks.

6. Potential of Dibenzo[*a,j*]phenazines as Building Blocks and Functional Materials

Based on this background, the author focused on dibenzo[*a,j*]phenazine (DBPHZ) as a promising building block for the construction of N-arylene macrocycles (Figure 9).[11] DBPHZ

is a pentacyclic, nitrogen-containing π-conjugated compound, and is readily synthesized via an oxidative skeletal rearrangement of 1,1'-binaphthalene-2,2'-diamine derivatives.[11a] From a structural viewpoint, DBPHZ possesses a characteristic U-shaped geometry, and its 2,12-dihalogenated derivatives offer well-positioned reactive sites for macrocycle construction. Therefore, the author envisioned that DBPHZ could serve as a versatile building block for the facile construction of new cycloarylenes featuring nitrogen-embedded, π-extended skeletons. Moreover, DBPHZ derivatives exhibit excellent luminescent properties in both solution and the solid state, together with high electron-accepting abilities, making them attractive candidates for optoelectronic and photofunctional materials.[11b,11c] Macrocyclization of such U-shaped units is expected not only to generate topologically unique architectures but also to extend the effective π-conjugation length and enforce a defined spatial arrangement of the chromophore units. These features can lead to red-shifted absorption and emission as well as improved photoluminescence quantum yield (PLQY), which make DBPHZ-based cycloarylenes attractive emissive materials. Therefore, the resulting macrocycles provide a suitable platform for the systematic investigation of structures, photophysical properties, and emerging functions of this new class of nitrogen-embedded cycloarylenes.

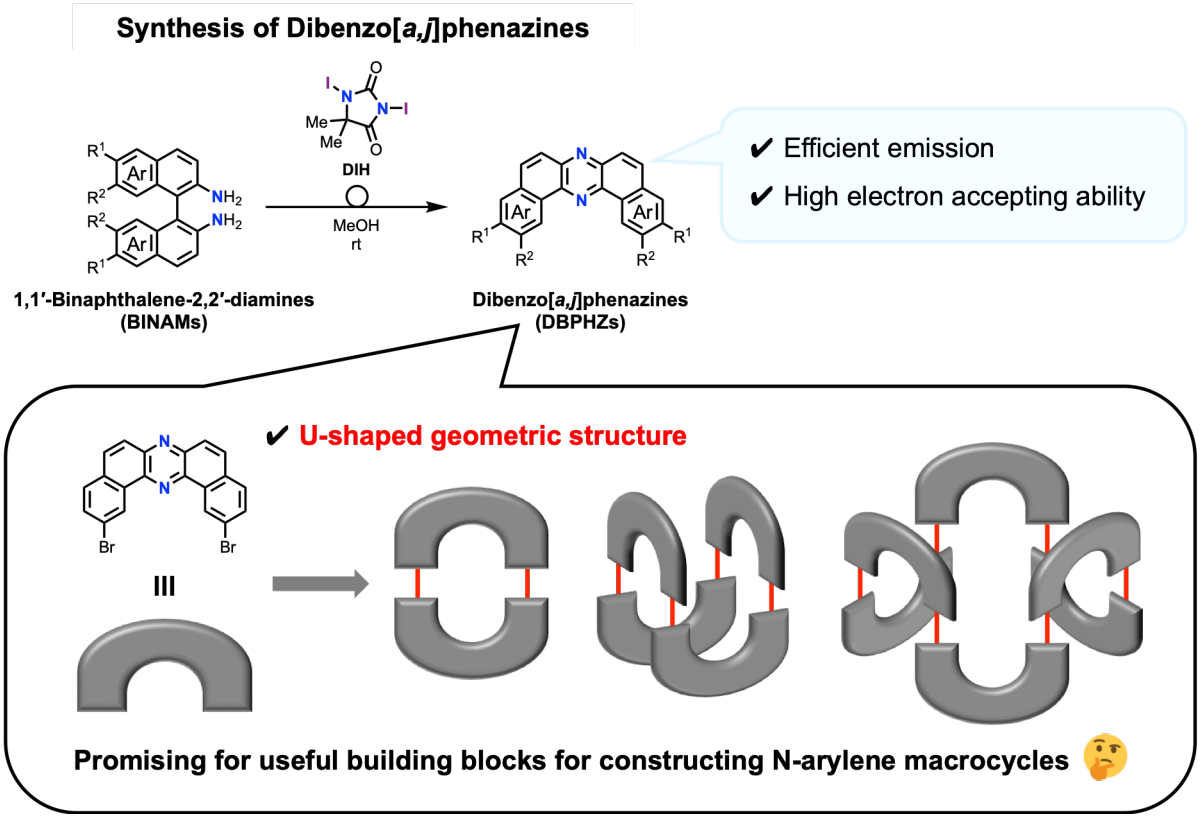


Figure 9. Working hypothesis: dibenzo[*a,j*]phenazines as building blocks for the construction of new N-arylene macrocycles.

7. Synopsis of This Thesis

On the basis of these backgrounds, the author has designed and developed new DBPHZ derivatives as building blocks for constructing macrocycles and synthesized novel nitrogen-embedded π-extended arylene macrocycles by utilizing these units. The structures and fundamental physicochemical properties of the resulting DBPHZ macrocycles have been investigated in detail. Furthermore, new functions of synthesized DBPHZ-based macrocycles have been explored by leveraging their structural and physical properties. This doctoral Thesis consists of General Introduction, three Chapters (Figure 10), and Conclusion.

In Chapter 1, the development of 6,8-diarylated dibenzo[*a,j*]phenazine building blocks with good solubility, the synthesis of DBPHZ cyclic homodimer by utilizing developed building blocks, and the structures and fundamental physicochemical properties of the

homodimer are described.

In Chapter 2, the development of a tetra-functionalized DBPHZ building block, the synthesis of solubility-enhanced DBPHZ cyclic heterodimer by utilizing the new building block, and the structures and fundamental physicochemical properties of the heterodimer are described.

In Chapter 3, the photophysical properties of the DBPHZ cyclic dimers synthesized in Chapters 1 and 2 are disclosed. The comparison with monomeric DBPHZ and functional studies based on the characteristic structures and properties of the cyclic dimers are described.

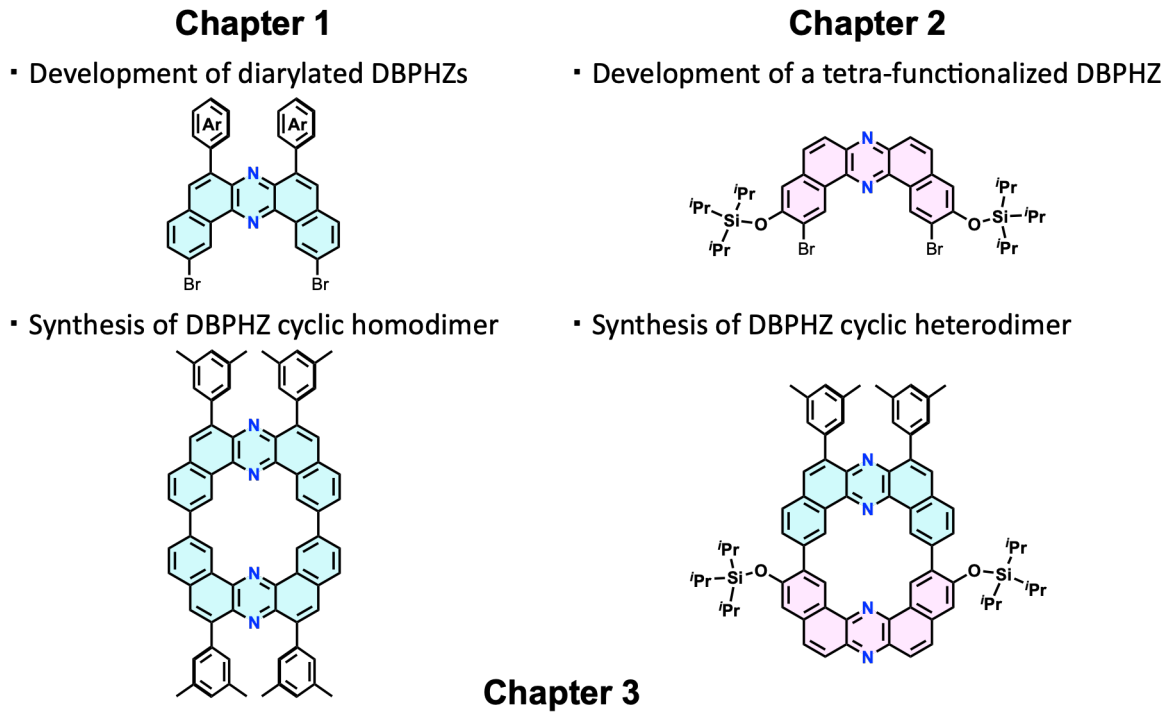


Figure 10. Summary of this Thesis.

8. References

1. Iyoda, M.; Yamakawa, J.; Rahman, M. J. *Angew. Chem. Int. Ed.* **2011**, *50*, 10522–10553.

2. (a) Omachi, H.; Segawa, Y.; Itami, K. *Acc. Chem. Res.* **2012**, *45*, 1378–1389. (b) Golder, M. R.; Jasti, R. *Acc. Chem. Res.* **2015**, *48*, 557–566.

3. (a) Jasti, R.; Bhattacharjee, J.; Neaton, J. B.; Bertozzi, C. R. *J. Am. Chem. Soc.* **2008**, *130*, 17646–17647. (b) Takaba, H.; Omachi, H.; Yamamoto, Y.; Bouffard, J.; Itami, K. *Angew. Chem. Int. Ed.* **2009**, *48*, 6112–6116. (c) Yamago, S.; Watanabe, Y.; Iwamoto, T. *Angew. Chem. Int. Ed.* **2010**, *49*, 757–759.

4. (a) Nakanishi, W.; Yoshioka, T.; Taka, H.; Xue, J. Y.; Kita, H.; Isobe, H. *Angew. Chem. Int. Ed.* **2011**, *50*, 5323–5326. (b) Yagi, A.; Segawa, Y.; Itami, K. *J. Am. Chem. Soc.* **2012**, *134*, 2962–2965. (c) Yamamoto, Y.; Wakamatsu, K.; Iwanaga, T.; Sato, H.; Toyota, S. *Chem. Asian J.* **2016**, *11*, 1370−1375. (d) Yamamoto, Y.; Tsurumaki, E.; Wakamatsu, K.; Toyota, S. *Angew. Chem. Int. Ed.* **2018**, *57*, 8199–8202. (e) Fujise, K.; Saibara, T.; Iwanaga, T.; Tsurumaki, E.; Toyota, S. *Chem. Lett.* **2019**, *48*, 166–169. (f) Shigihara, Y.; Tsurumaki, E.; Yamashina, M.; Toyota, S. *Org. Lett.* **2025**, *27*, 8668–8673. (g) Lorbach, D.; Keerthi, A.; Figueira-Duarte, T. M.; Baumgarten, M.; Wagner, M.; Müllen, K. *Angew. Chem. Int. Ed.* **2016**, *55*, 418–421. (h) Ikemoto, K.; Sato, S.; Isobe, H. *Chem. Lett.* **2016**, *45*, 217–219.

5. (a) Matsui, K.; Segawa, Y.; Namikawa, T.; Kamada, K.; Itami, K. *Chem. Sci.* **2013**, *4*, 84–88. (b) Matsui, K.; Segawa, Y.; Itami, K. *J. Am. Chem. Soc.* **2014**, *136*, 16452–16458. (c) Segawa, Y.; Kuwayama, M.; Hijikata, Y.; Fushimi, M.; Nishihara, T.; Pirillo, J.; Shirasaki, J.; Kubota, N.; Itami, K. *Science* **2019**, *365*, 272–276. (d) Segawa, Y.; Kuwayama, M.; Itami, K. *Org. Lett.* **2020**, *22*, 1067–1070. (e) Robert, A.; Dechambenoit, P.; Hillard, E. A.; Bock, H.; Durola, F. *Chem. Commun.* **2017**, *53*, 11540–11543. (f) Naulet, G.; Sturm, L.; Robert, A.; Dechambenoit, P.; Röhricht, F.; Herges, R.; Bock, H.; Durola, F. *Chem. Sci.* **2018**, *9*, 8930–8936.

6. (a) Yan, X.; Cui, X.; Li, B.; Li, L.-s. *Nano Lett.* **2010**, *10*, 1869–1873. (b) Zhao, X.-J.; Hou, H.; Fan, X.-T.; Wang, Y.; Liu, Y.-M.; Tang, C.; Liu, S.-H.; Ding, P.-P.; Cheng, J.; Lin, D.-H.; Wang, C.; Yang, Y.; Tan, Y.-Z. *Nat. Commun.* **2019**, *10*, 3057.

7. (a) Wang, X.-Y.; Yao, X.; Narita, A.; Müllen, K. *Acc. Chem. Res.* **2019**, *52*, 2491–2505. (b) Stępień, M.; Gońka, E.; Żyła, M.; Sprutta, N. *Chem. Rev.* **2017**, *117*, 3479–3716. (c)

Borissov, A.; Maurya, Y. K.; Moshniaha, L.; Wong, W.-S.; Żyła-Karwowska, M.; Stępień, M. *Chem. Rev.* **2022**, *122*, 565–788. (d) Sun, X.; Bai, J.; Wang, X.-Y.; Gong, H.-Y. *Coord. Chem. Rev.* **2024**, *518*, 216063. (e) An, D.; Gu, Y.; Wang, T.; Zhang, X.; Zhu, J.; Zhang, R.; Lu, X.; Liu, Y. *Adv. Mater.* **2025**, e06256.

8. (a) Shouda, T.; Nakanishi, K.; Sasamori, T.; Tokitoh, N.; Kuramochi, K.; Tsubaki, K. *J. Org. Chem.* **2017**, *82*, 7850–7855. (b) Kato, S.; Serizawa, Y.; Sakamaki, D.; Seki, S.; Miyake, Y.; Shinokubo, H. *Chem. Commun.* **2015**, *51*, 16944–16947. (c) Ito, H.; Mitamura, Y.; Segawa, Y.; Itami, K. *Angew. Chem. Int. Ed.* **2015**, *54*, 159–163. (d) Zhan, L.; Dai, C.; Zhang, G.; Zhu, J.; Zhang, S.; Wang, H.; Zeng, Y.; Tung, C.-H.; Wu, L.-Z.; Cong, H. *Angew. Chem. Int. Ed.* **2022**, *61*, e202113334.

9. (a) Adachi, S.; Shibasaki, M.; Kumagai, N. *Nat. Commun.* **2019**, *10*, 3820. (b) Xu, W.; Nagata, Y.; Kumagai, N. *J. Am. Chem. Soc.* **2023**, *145*, 2609–2618. (c) Lee, S.; Hirsch, B. E.; Liu, Y.; Dobscha, J. R.; Burke, D. W.; Tait, S. L.; Flood, A. H. *Chem. Eur. J.* **2016**, *22*, 560–569.

10. Schlütter, F.; Rossel, F.; Kivala, M.; Enkelmann, V.; Gisselbrecht, J.-P.; Ruffieux, P.; Fasel, R.; Müllen, K. *J. Am. Chem. Soc.* **2013**, *135*, 4550–4557.

11. (a) Takeda, Y.; Okazaki, M.; Minakata, S. *Chem. Commun.* **2014**, *50*, 10291–10294. (b) Takeda, Y.; Data, P.; Minakata, S. *Chem. Commun.* **2020**, *56*, 8884–8894. (c) Takeda, Y. *Acc. Chem. Res.* **2024**, *57*, 2219–2232.

Chapter 1

Development of Solubility-Enhanced 6,8-Diarylated Dibenzo[*a,j*]phenazine (DBPHZ) Building Blocks and Synthesis of DBPHZ Cyclic Homodimer

1-1. Design of π-Conjugated Macrocycles Composed of Dibenzo[*a,j*]phenazine

To design π-conjugated macrocycles composed of dibenzo[*a,j*]phenazine (DBPHZ), the author focused on a cyclic homodimer in which two DBPHZ units are connected at the 2,12-positions as the target molecule (Figure 1). Retrosynthetic analysis suggests that the homodimer can be assembled via a sequence of intermolecular and subsequent intramolecular Suzuki–Miyaura cross-coupling reactions between appropriately functionalized dibrominated and diborylated DBPHZ derivatives. The principal conformational freedom of the 1:1 coupled precursor for the macrocycle would be restricted to rotation about the C–C single bond connecting DBPHZ units. In addition, the remaining reactive sites are located at the positions where they can approach each other. Therefore, the intramolecular cross-coupling leading to the macrocycle is expected to be an entropically more favorable process compared to competing intermolecular cross-coupling reactions that produce higher-order cyclic or acyclic oligomers (Figure 1).

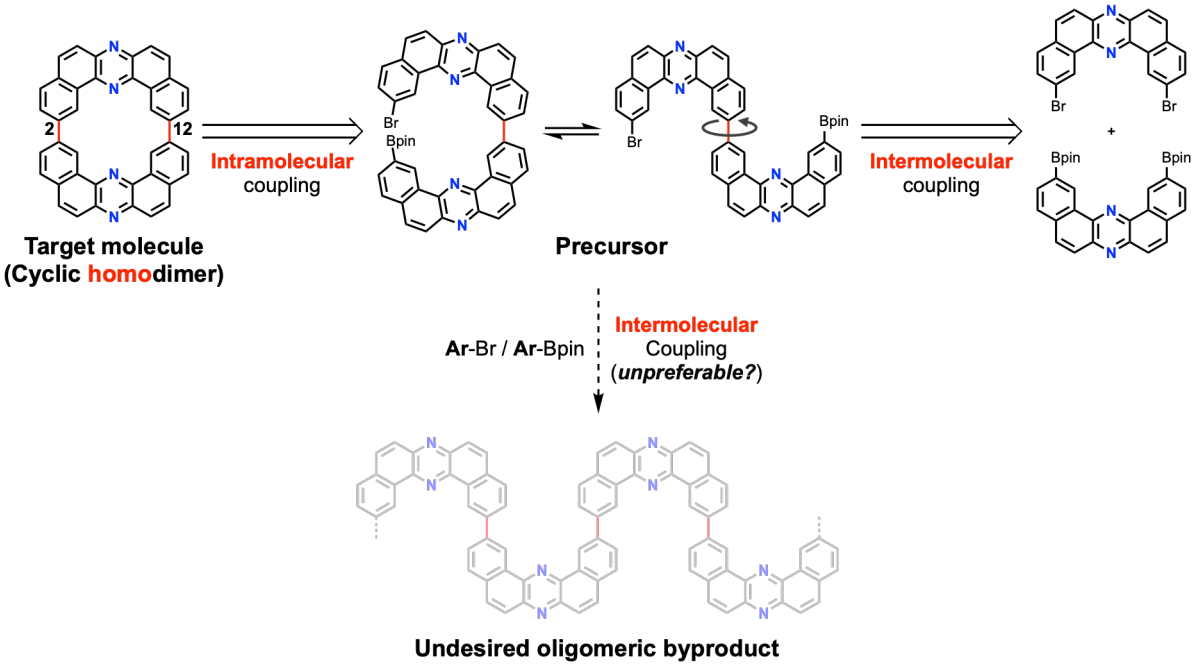


Figure 1. Design of π-conjugated macrocycles composed of DBPHZ and their retrosynthetic analysis.

1-2. Design of Solubility-Enhanced Dibenzo[*a,j*]phenazine Building Blocks

π-Extended DBPHZ macrocycles are expected to have planar structures, which would intensify intermolecular π–π stacking and lead to poor solubility (Figure 2a). Since processability is a crucial requirement in various physicochemical measurements, enhancing the solubility of DBPHZ building blocks is an important task. To develop DBPHZ building blocks with enhanced solubility, the author adopted a design strategy of introducing bulky aryl substituents at the 6,8-positions of DBPHZ (Figure 2b). These aryl substituents are expected to twist out of the DBPHZ plane due to their steric congestion, thereby suppressing intermolecular π–π stacking between DBPHZ units. Alkyl groups on the introduced aryl substituents should further enhance solubility through dispersion interactions with organic solvents. At the same time, dibromo functionalities at the 2,12-positions of DBPHZ, which serve as the reactive sites for the consecutive cross-couplings that construct the macrocyclic frameworks, must be retained during the introduction of the solubilizing groups. Previously, the Takeda and Minakata group reported the synthesis of a DBPHZ derivative bearing diphenyl substituents at the 6,8-positions.[1] This compound was synthesized via an oxidative skeletal rearrangement of a 1,1'-binaphthalene-2,2'-diamine (BINAM) precursor, in which the diphenyl units were introduced adjacent to the diamino groups through a Pd-catalyzed C–H arylation of *N,N'*-diacetylated biaryldiamines, as originally developed by Stahl and co-workers.[2] Although there is a report utilizing a similar C–H arylation strategy on BINAM frameworks to construct axially chiral bibenzo[*b*]carbazole derivatives,[3] the C–H arylation of BINAM substrates bearing halogen substituents has not been reported. Thus, it had remained uncertain whether such halogen functionalities were compatible with the Pd-catalyzed reaction conditions. Considering that the C–H arylation proceeds via a Pd(II)/Pd(IV) catalytic cycle, the author hypothesized that the C–Br bonds might remain intact throughout the transformation.

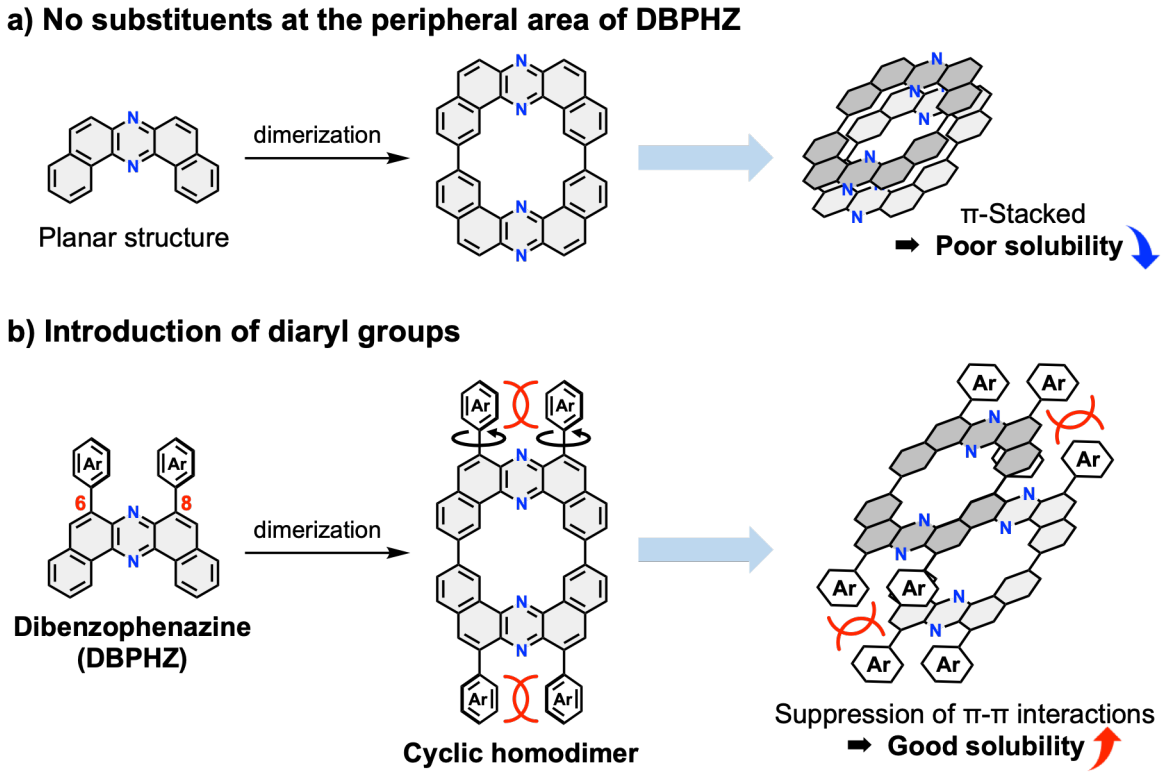
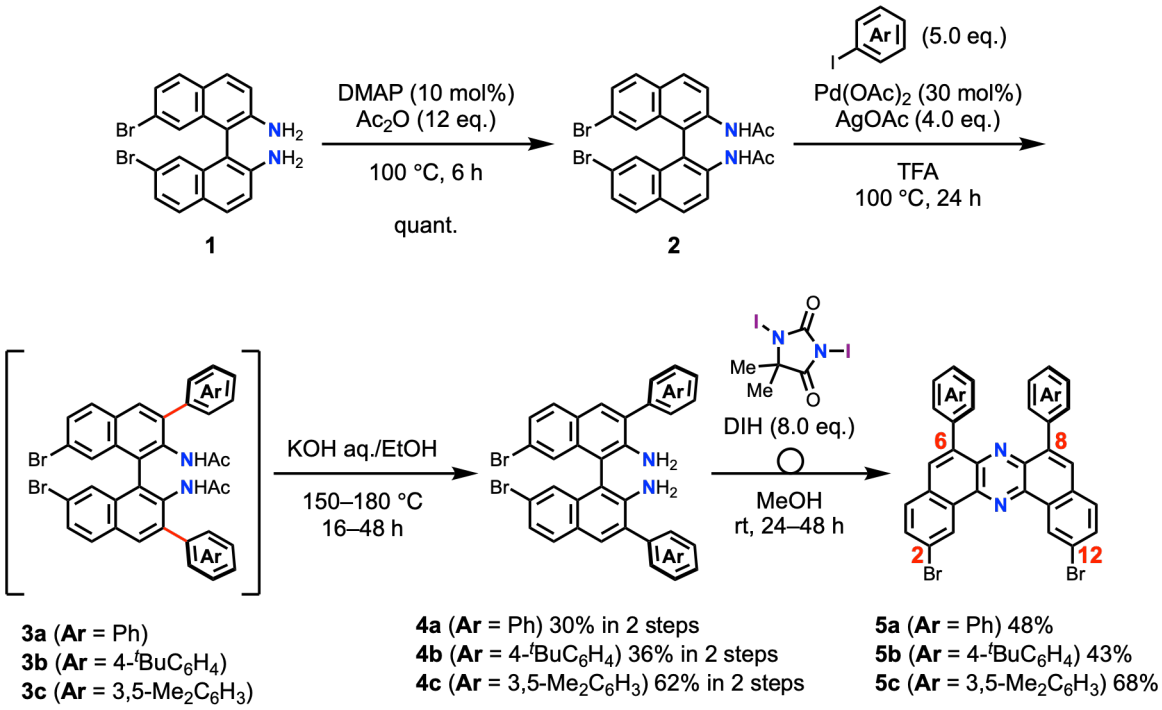


Figure 2. Design for improving the solubility of DBPHZ building blocks and the target dimer.

1-3. Synthesis of 6,8-Diarylated 2,12-Dibromodibenzo[*a*,*j*]phenazines

To examine the hypothesis described in the previous section and further explore the synthetic feasibility, the author commenced our study by preparing 6,6'-dibromo-BINAM (compound **1**) according to a reported procedure.[4] This compound was subjected to *N,N'*-diacetylation using acetic anhydride (Ac_2O) as both acylating reagent and solvent, in the presence of *N,N*-dimethyl-4-aminopyridine (DMAP) as a nucleophilic catalyst. The reaction proceeded cleanly to afford the desired diacetylated derivative **2** in quantitative yield (Scheme 1; for the detailed experimental procedures, see the section **1-11.**). With compound **2** in hand, the *N*-acetyl-directed C–H arylation was carried out using iodobenzene (5 equiv) as the arylating reagent, $Pd(OAc)_2$ (30 mol%) as the catalyst, and silver acetate (AgOAc) as the base (4 equiv) in trifluoroacetic acid (TFA) at 100 °C under reflux conditions (Scheme 1).[2] Gratifyingly, the arylation proceeded regioselectively to furnish the diphenylated dianilide **3a**.

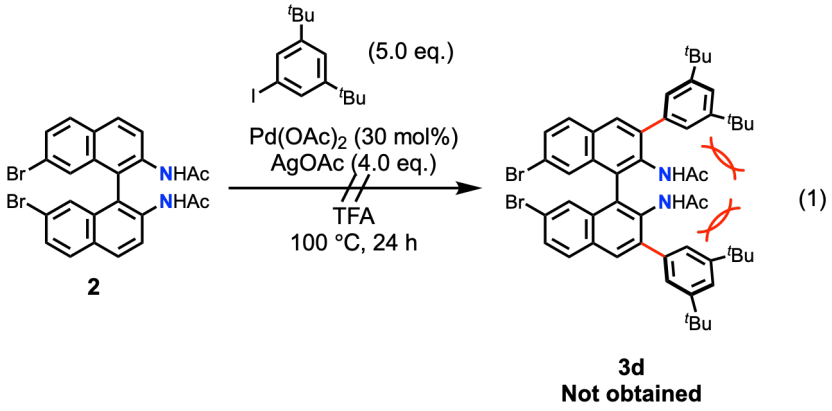
^{1}H NMR analysis of the crude product revealed the disappearance of the two sets of doublet signals at 8.34 and 7.96 ppm corresponding to the hydrogens at the 3/3' and 4/4' positions in **2** and the emergence of singlet signal at 8.04 ppm, indicating successful substitution. Moreover, MALDI-TOF mass spectrometry confirmed the presence of two bromine atoms in the product (M^+:$[M+2]^+$:$[M+4]^+$ = 1:2:1), providing strong evidence that the C–Br bonds remained intact during the transformation. These results suggest that the dibromo functionalities are indeed compatible with the Pd(II)/Pd(IV) catalytic cycle employed in this arylation. Despite the successful introduction of aryl groups, the crude product mixture contained inseparable byproducts, possibly due to multiple-arylative side reactions, making purification challenging. Therefore, the intermediate **3a**, roughly purified by column chromatography, was directly subjected to alkaline hydrolysis at an elevated temperature, which cleanly removed the *N*-acetyl groups to afford the corresponding diamine **4a**. Delightedly, compound **4a** was isolated in 30% yield over two steps. Subsequently, an oxidative skeletal rearrangement of **4a** was conducted using 1,3-diiodo-5,5-dimethylhydantoin (DIH) in methanol at room temperature.[1] This transformation proceeded smoothly to yield the desired 6,8-diphenylated 2,12-dibromo-DBPHZ **5a** in 48% yield.



Scheme 1. Synthetic route to 6,8-diarylated dibromodibenzo[*a,j*]phenazines.

Encouraged by these results, the author further explored the synthesis of structurally modified analogues to validate the synthetic protocol generality. Using 4-*tert*-butyl-iodobenzene as the arylating reagent under similar reaction conditions, the C–H arylation furnished the corresponding diarylated intermediate **3b**, as estimated by ^{1}H NMR spectroscopy. However, purification was again hampered by inseparable byproducts. Nevertheless, the roughly purified product was directly subjected to hydrolysis to afford diamine **4b**, which underwent oxidative skeletal rearrangement to provide the corresponding desired product **5b** in good yield. Similarly, 3,5-dimethylphenyl-substituted DBPHZ derivative **5c** was successfully synthesized from diamine **1** in four steps with good yield. These results demonstrate the robustness and modularity of our synthetic strategy for producing diverse 6,8-diarylated DBPHZ derivatives. The C–H arylation using 3,5-bis(*tert*-butyl)iodobenzene did not proceed successfully (eq 1). While the signals corresponding to residual starting material **2** and minor complex products were observed in the crude ^{1}H NMR spectrum, the formation of

the corresponding diaryl compound **3d** was not be conclusively determined. Although the reason why the reaction using this substrate does not proceed is not clear, steric repulsion between bulky *tert*-butyl groups and *N*-acetyl groups could not allow the Pd catalyst to form palladacycle intermediate for the arylation.



1-4. Structure of a 6,8-Diarylated DBPHZ Derivative in Single Crystal

To gain deeper insight into the molecular geometry and solid-state packing of the newly synthesized diarylated DBPHZ derivatives, the author attempted to grow single crystals of compounds **5a**–**5c**. As a result of these attempts, a single crystal suitable for X-ray diffraction analysis was obtained for only compound **5b**. Crystals of **5b** were successfully obtained by slow evaporation from a chloroform solution under ambient conditions.[5] The X-ray diffraction crystallographic analysis of **5b** revealed that the newly introduced two *tert*-butylphenyl substituents are considerably twisted relative to the central DBPHZ plane (Figure 3a). The dihedral angles between the DBPHZ core and the *tert*-butylphenyl substituents were found to be 43.8° and 37.0°. This significant torsion likely arises from steric repulsion between the closely positioned aryl rings and the planar π-conjugated DBPHZ core, resulting in a non-coplanar arrangement. In the single crystal, compound **5b** adopts an anti-parallel dimeric packing motif, wherein two DBPHZ molecules align face-to-face with an interplanar distance of 3.35 Å (Figure 3b). This arrangement appears to minimize steric congestion between the

adjacent aryl substituents while maintaining close π–π interactions.

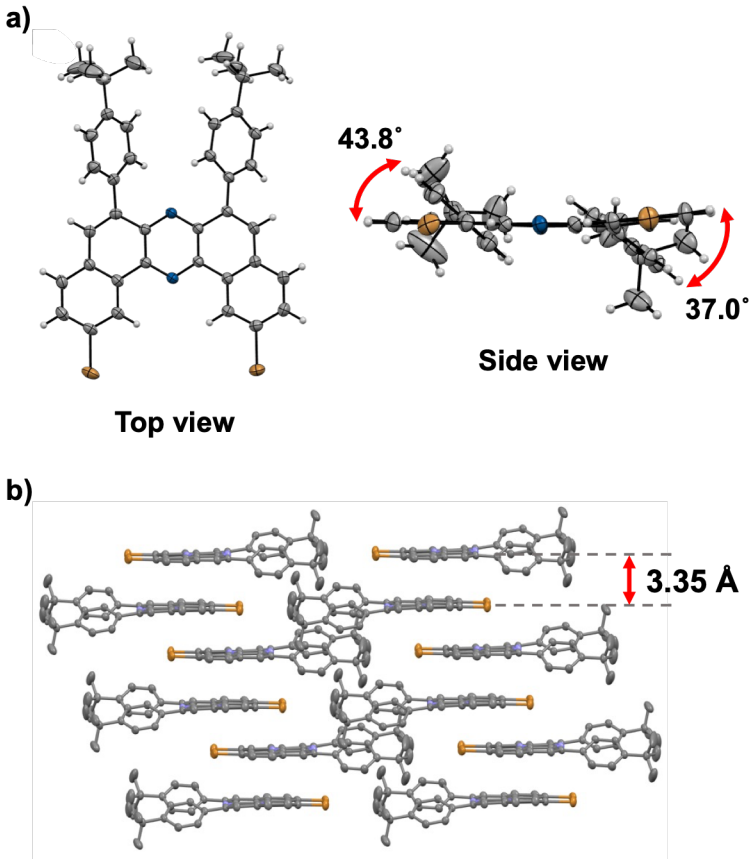


Figure 3. a) Structure in the crystal and b) packing structure of **5b**.

1-5. Comparison of Solubility in Organic Solvents

Having successfully synthesized new families of 6,8-diarylated DBPHZ derivatives, the author next evaluated their solubility in organic solvents (for the detailed procedures, see the section **1-11.**). The solubility data for dibromo compounds **5a**–**5c** and non-arylated DBPHZ **6** are illustrated in Figure 4. As a result, diethyl ether was found not to be a good solvent consistently for any compounds. In addition, the introduction of two phenyl groups (**5a**) did not markedly change the solubility compared to the reference compound **6**. However, DBPHZ derivatives bearing alkylated aryl substituents, such as 4-*tert*-butylphenyl (**5b**) and 3,5-dimethylphenyl (**5c**) groups, exhibited significantly higher solubility in toluene and chloroform than that of the unsubstituted analogue **6**. Given the antiparallel stacking motif of

DBPHZ units observed in the single crystals, just twisting the aryl substituents relative to the DBPHZ core is not sufficient to improve solubility. Rather, the enhanced solubility is attributed to increased London dispersion interactions associated with the alkyl substituents, which more effectively outcompete the inherently strong π–π interactions between the DBPHZ cores.

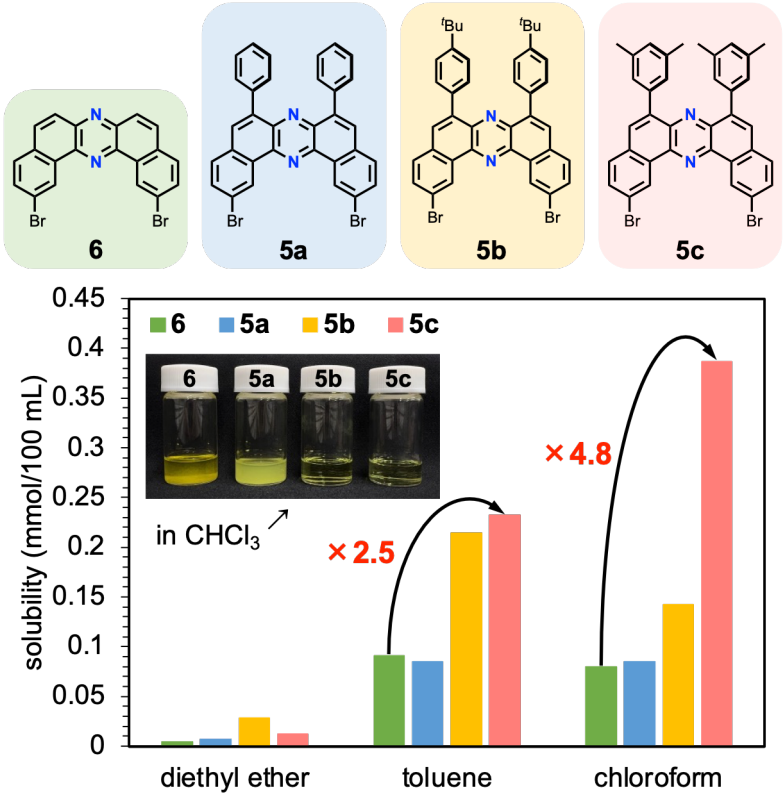
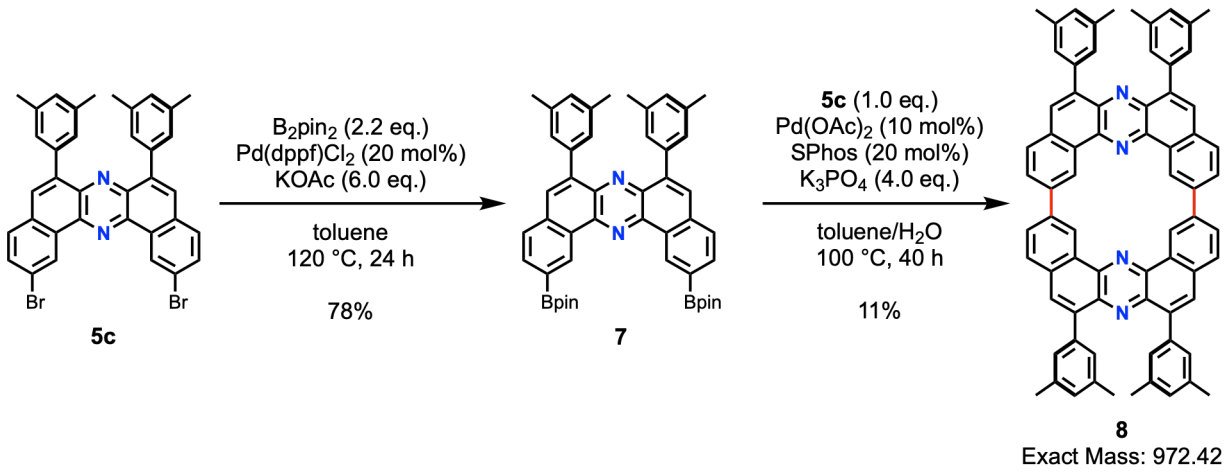


Figure 4. Comparison of solubility in organic solvents.

1-6. Synthesis of Cyclic Homodimer of U-Shaped DBPHZ

Based on the solubility of 6,8-diarylated DBPHZs, the 3,5-dimethylphenyl substituted DBPHZ **5c**, which exhibits the highest solubility, was utilized as a building block to synthesize the corresponding cyclic homodimer **8**. The synthetic route is shown in Scheme 2. Dibromo compound **5c** was converted to the corresponding aryl diboronic diester **7** in good yield via a Pd-catalyzed Miyaura borylation reaction.[6] Subsequently, a Pd-catalyzed Suzuki–Miyaura cross-coupling reaction[7] between dibromide **5c** and diboryl compound **7** yielded a yellow crude solid.



Scheme 2. Synthetic route to DBPHZ cyclic homodimer **8**.

Delightedly, MALDI-TOF mass spectrometry of the crude product confirmed the formation of cyclic dimer **8** (*m/z* = 973.4) along with the formation of cyclic/acyclic higher oligomers (*n* = 3–6), spaced by repeating DBPHZ units (*m/z* = 486.2) (Figure 5). However, the crude product was not dissolved completely in various organic solvents such as toluene, chloroform ($CHCl_3$), and ethyl acetate, even under heating conditions. Thus, the insoluble solid was first roughly separated by filtration and washed with $CHCl_3$ (Figure 6). The separated solid was slightly soluble in *o*-dichlorobenzene (*o*-DCB) (solubility: ~2.0 mg/4.0 mL at 25 °C). Therefore, repeated flash column chromatography using $CHCl_3$/*o*-DCB as the eluent and reprecipitation with *n*-hexane/*o*-DCB were performed on the separated solid, which successfully isolated the desired cyclic homodimer **8** in 11% yield. From the $CHCl_3$-soluble crude fraction, only cyclic homotrimer **9** was obtained in 7% yield after performing column chromatography and reprecipitation. These DBPHZ cyclic dimer **8** and trimer **9** were characterized with spectroscopic techniques (e.g., ^1H and ^{13}C NMR, IR, MS, and HRMS).

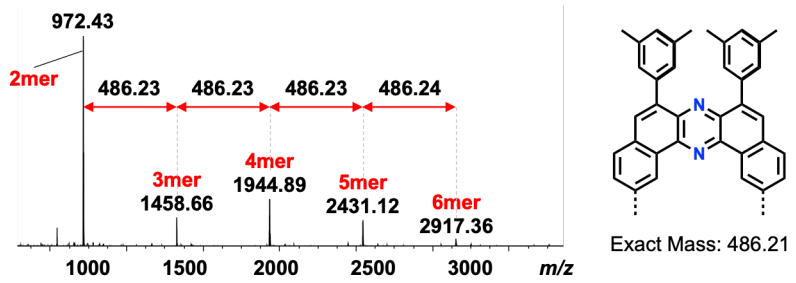


Figure 5. MALDI-TOF mass spectrum of the crude product.

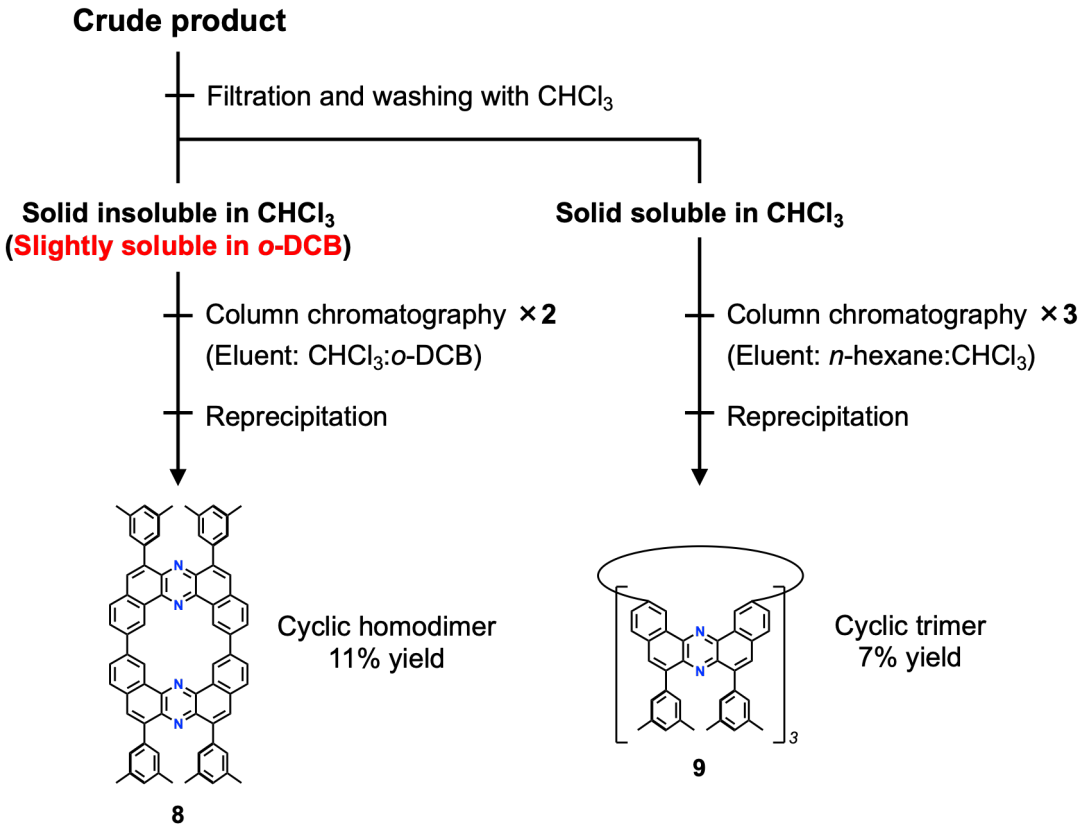


Figure 6. Purification processes for compounds **8** and **9**.

1-7. Structural Analysis of DBPHZ Cyclic Homodimer by ^{1}H NMR Spectroscopy

To elucidate the electronic structure of cyclic homodimer **8**, the ^{1}H NMR spectra of **8** and starting materials (**5c** and **7**) were measured in *o*-DCB-d_4 at room temperature (Figure 7). Each compound gave only one set of six signals originating from the DBPHZ and the introduced aryl groups, suggesting the highly symmetric structure of homodimer **8**.

Furthermore, the characteristic signal for the 1,13-positioned hydrogens of the DBPHZ core, typically observed in the lower field region below δ 9 ppm[1] (e.g., 9.67 ppm for **5c** and 10.38 ppm for **7**), was observed at the much lower field of δ 11.1 ppm for the homodimer **8**. This significant deshielding for homodimer **8** is attributable to the steric compression effect[8] from proximal hydrogen atoms and/or additional ring current effects from the connected DBPHZ unit. The NMR assignments were further supported by gauge-including atomic orbital (GIAO)-based density functional theory (DFT) calculations performed at the PBE0/6-31G(d,p) level, which reproduced the observed chemical shift trends (Figure 8).

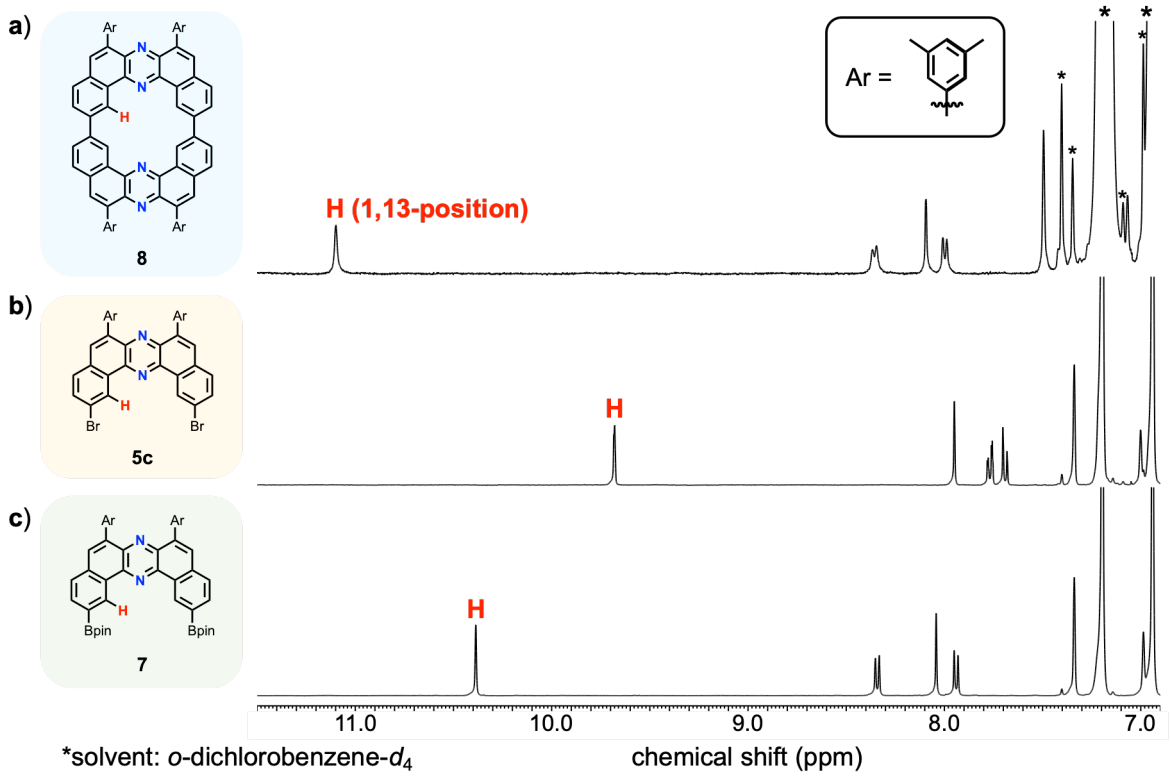


Figure 7. ^{1}H NMR spectra of the aromatic regime of compound **8**, **5c** and **7**.

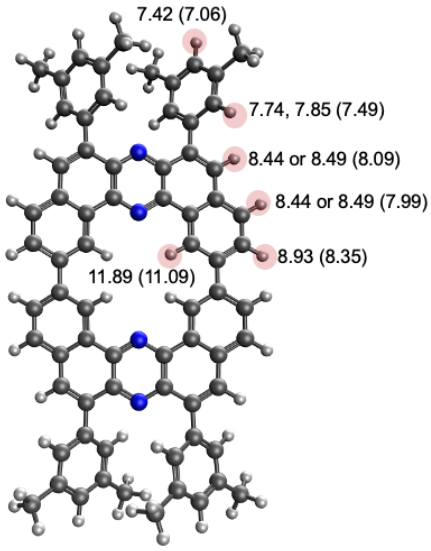


Figure 8. Comparison of chemical shifts between calculated (numbers shown) and experimental values (numbers shown in parentheses).

In addition, a very slight high-field shift of the DBPHZ signals was observed with increasing concentration ($\Delta\delta$ = 0.009–0.027 ppm) (Figure 9), suggesting weak association in solution, albeit markedly weaker than that seen for the related Penrose stairs hydrocarbon.[9]

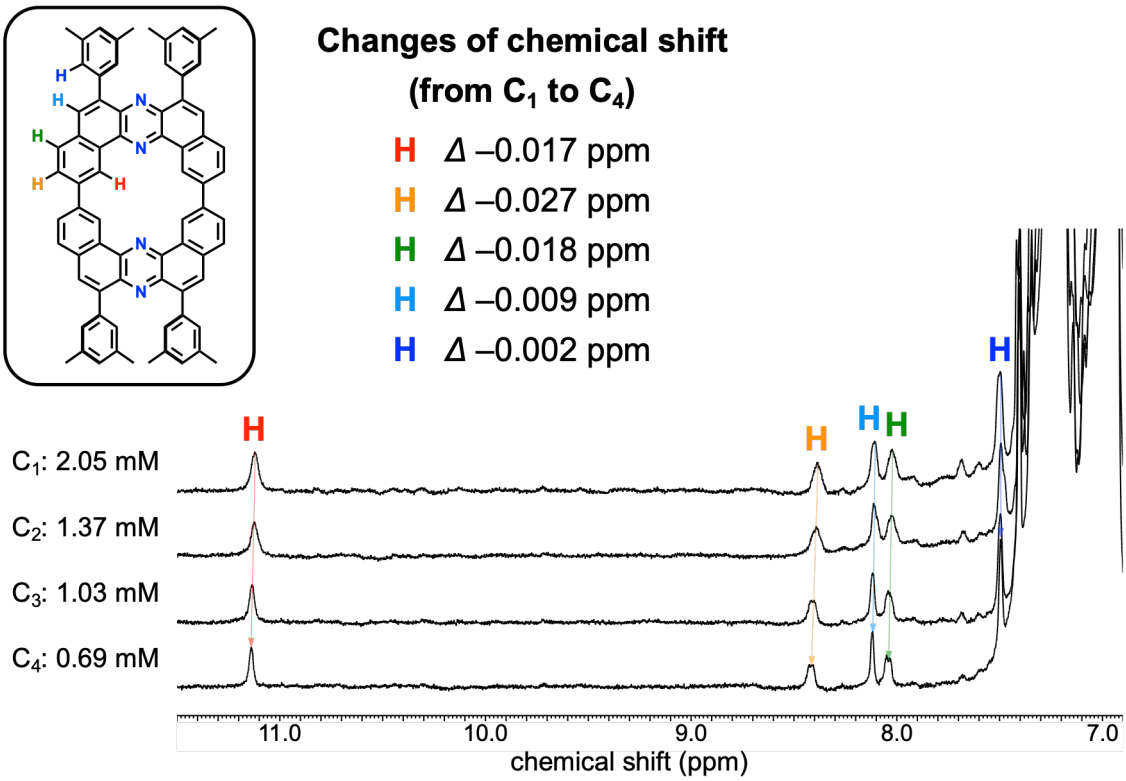


Figure 9. Concentration-dependent ^{1}H NMR spectra of **8** in *o*-DCB-d_4.

1-8. Structural Analysis of DBPHZ Cyclic Homodimer by DFT Calculations

The optimization study of the homodimer **8** conducted by quantum chemical calculations using the DFT method revealed that homodimer **8** adopts a "Penrose stairs-like" conformation, analogous to cyclobis[4]helicene (Figure 10a).[9a] The dihedral angle between the terminal benzene rings of each DBPHZ unit is 9.7° with a torsion angle of 13.8° across the biphenylene bridge (Figure 10b). The corresponding helix angle and torsional angle of its nitrogen-free hydrocarbon analogue, cyclobis[4]helicene, are significantly larger (22.7° and 29.8°, respectively; Figure 10a). This difference likely arises from reduced steric repulsion among the closely spaced aromatic C–H bonds upon introduction of nitrogen atoms.

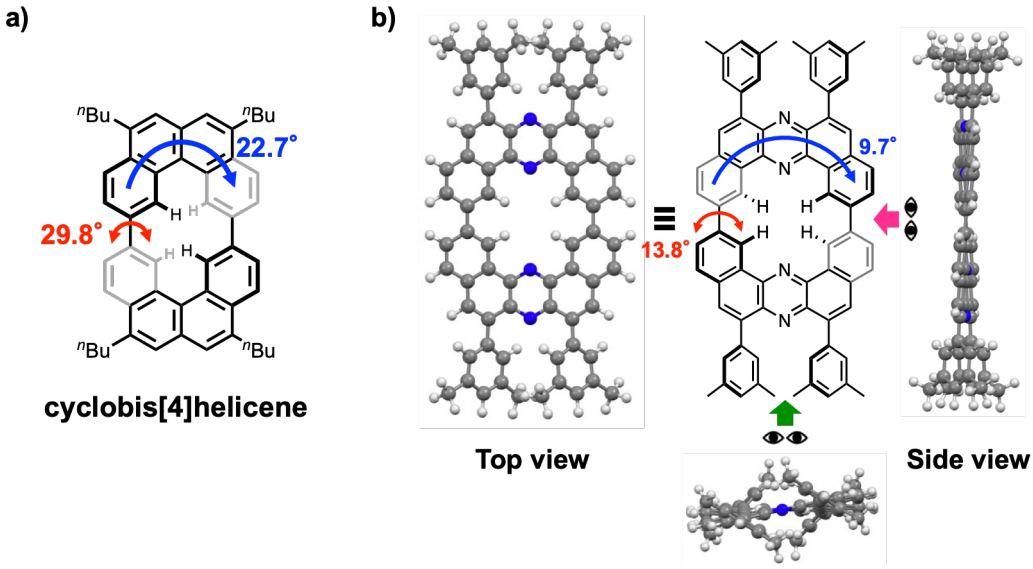


Figure 10. a) Structure in the crystal of cyclobis[4]helicene and b) optimized structure of **8** calculated at the PBE0/6-31G(d,p) level in $CHCl_3$.

Additionally, two DBPHZ units of **8** possess identical helicity, suggesting that the homodimer is chiral (Figure 11a). Time-dependent DFT (TD-DFT) calculations confirmed that its mirror-image counterpart exhibits the exactly mirrored electronic circular dichroism (ECD) spectrum (Figure 11b), thereby definitively establishing the molecule's chirality.

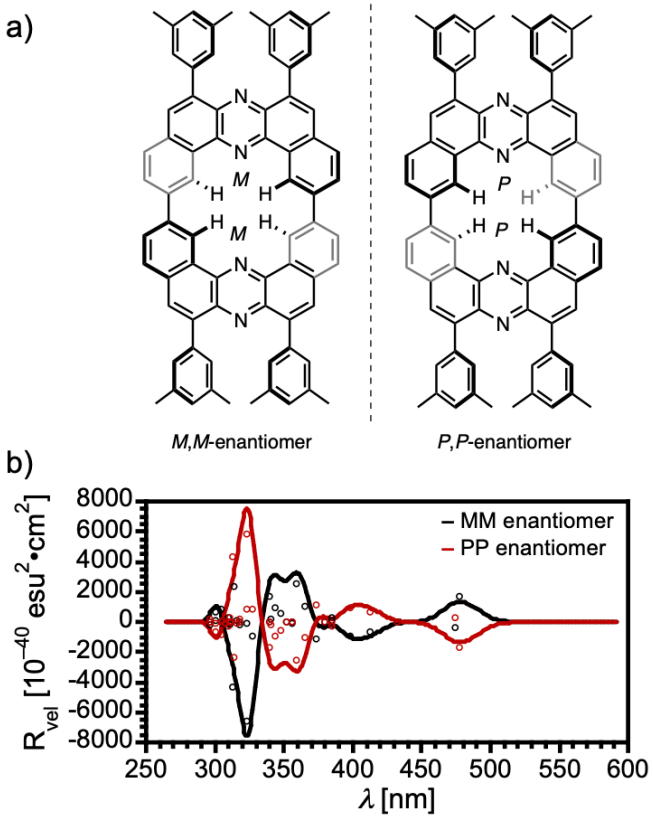


Figure 11. a) Chemical structures and b) calculated ECD spectra of the enantiomers of **8**.

1-9. Aromaticity of DBPHZ Cyclic Homodimer

To evaluate the aromatic character of the cyclic homodimer **8**, the harmonic oscillator model of aromaticity (HOMA) values and the nucleus-independent chemical shift (NICS) indices were calculated (Figure 12a and 12b, respectively). The HOMA values for rings A (pale green in Figure 12a) and C (pale blue in Figure 12a) in the DBPHZ scaffold are 0.911 and 0.849, respectively, which are close to that of a fully aromatic reference (0.976, representing an isolated diaryl unit). In contrast, ring B (pale red in Figure 12a) displays a significantly lower HOMA value of 0.466. Similarly, the NICS(1)$_{ave}$ values for rings A (–8.80 ppm) and C (–10.67 ppm) are comparable to that of the peripheral dimethylphenyl rings (–9.04 ppm), whereas ring B shows a markedly higher (less negative) value of −5.76 ppm (Figure 12b). Collectively, these results indicate that aromaticity in compound **8** is localized to rings A and C, rather than

delocalized over the entire macrocyclic framework, consistent with Clar's π-sextet representation (Figure 12c).

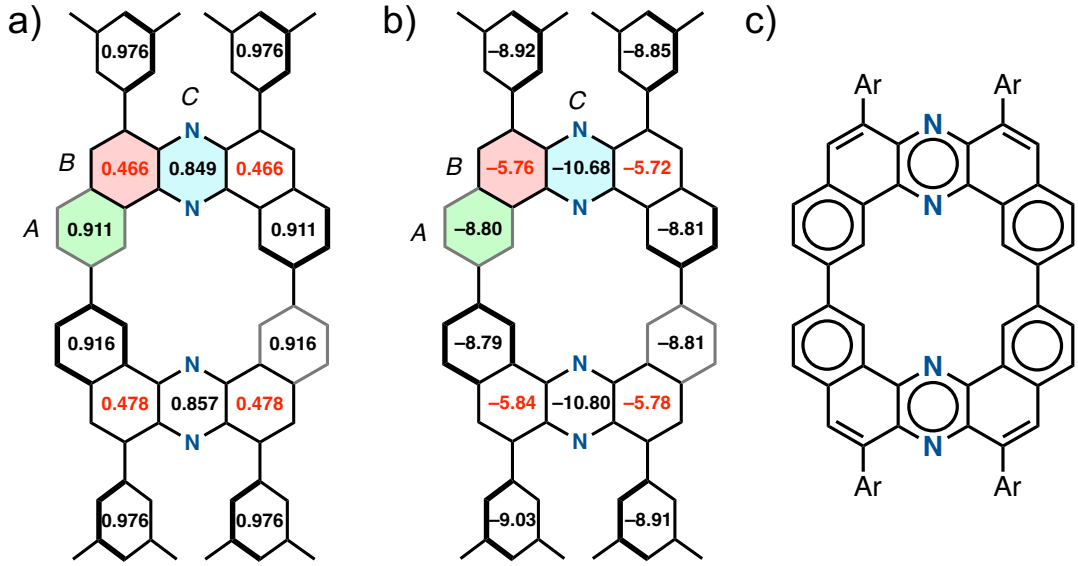


Figure 12. a) HOMAs of each ring, b) $NICS(1)_{ave}$ value for each ring calculated at the PBE0/6-311+G(d,p) level and c) Clar's sextet description of **8**.

1-10. Summary

In summary, Chapter 1 describes the development of a synthetic method for introducing diaryl units at the 6,8-positions of DBPHZ. The introduction of bulky diaryl substituents at the 6,8-positions of DBPHZ effectively improves solubility while preserving the 2,12-dibromo functionalities required for cross-coupling to construct the macrocyclic structure. Utilizing these solubility-enhanced building blocks, DBPHZ cyclic homodimer with a unique helical topology has been successfully synthesized. This compound represents the new class of nitrogen-embedded cycloarylenes.

1-11. Experimental Section

General Remarks.

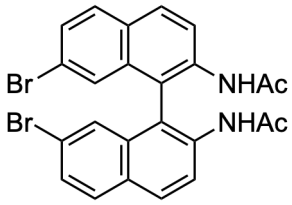
All reactions were carried out under an atmosphere of nitrogen unless otherwise noted. Products were purified by chromatography on silica gel Chromatorex BW-300 and NH-DM1020 (Fuji Silysia Chemical Ltd.). Analytical thin-layer chromatography (TLC) was performed on pre-coated silica gel glass plates (Merck silica gel 60 F_{254} TLC plate and Fuji Silysia Chromatorex NH, 0.25 mm thickness). Compounds were visualized with UV lamp. Melting points were determined using a Stanford Research Systems MPA100 OptiMelt Automated Melting Point System. All ^{1}H and ^{13}C NMR were recorded on a JEOL JNM-ECZL400S Spectrometer (^{1}H NMR: 400 MHz; ^{13}C NMR: 100 MHz). ^{1}H NMR chemical shifts were determined relative to tetramethylsilane (0.0 ppm) as an internal standard in $CDCl_3$, or the signals of residual non-deuterated acetone (2.04 ppm) in acetone-d_6, non-deuterated *o*-dichlorobenzene (6.94 ppm) in *o*-dichlorobenzene-d_4 and non-deuterated trifluoroacetic acid (11.50 ppm) in trifluoroacetic acid-d_1. ^{13}C NMR chemical shifts were determined relative to $CDCl_3$ (77.00 ppm) or trifluoroacetic acid-d_1 (116.60 ppm). Infrared spectra were acquired on a SHIMADZU IRAffinity-1 FT-IR Spectrometer. Mass spectra were obtained on a JEOL JMS-700 Mass Spectrometer. High-resolution mass spectra were obtained on a JEOL JMS-S3000 Mass Spectrometer.

Materials.

Acetic anhydride (Ac_2O) and trifluoroacetic acid (TFA) were purchased from FUJIFILM Wako Pure Chemical Corp. as Guaranteed Reagent or Wako Special Grade, respectively. Alcohol solvents (MeOH and EtOH) were purchased from FUJIFILM Wako Pure Chemical Corp. as Wako 1st Grade. 1,3-diiodo-5,5-dimethylhydantoin (DIH) was purchased from NIPPOH Chemicals Co., Ltd. Dehydrated toluene used for organic synthesis were purified by passing through a solvent purification system. 7,7'-dibromo-[1,1'-binaphthalene]-2,2'-diamine (**1**) [CAS No. 756822-96-5][4] and 2,12-dibromodibenzo[*a*,*j*]phenazine (**6**) [CAS No. 2757604-04-7][10] were synthesized according to the reported procedures. Other commercial reagents were purchased from TCI or Wako Pure Chemical Industries, Ltd. and used as received. PTFE inner vessel TVS-12T-100 (100 mL vessel) was purchased from Tainetsu Techno Corp.

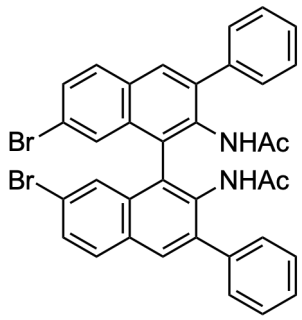
Synthetic Procedures and Spectroscopic Data of New Compounds.

***N,N'*-(7,7'-dibromo-[1,1'-binaphthalene]-2,2'-diyl)diacetamide (2) [CAS No. 3097787-28-2]**



The title compound **2** was prepared according to a similar method reported in the literature[2] with a slight modification. To a three-necked round-bottom flask (300 mL) equipped with a magnetic stirring bar, were added 7,7'-dibromo-[1,1'-binaphthalene]-2,2'-diamine (**1**) (8.87 g, 20.1 mmol) and 4-dimethylaminopyridine (DMAP) (122.3 mg, 1.00 mmol, 5 mol%). The flask was equipped with a three-way stopcock, sealed with two rubber septa, evacuated, and refilled with nitrogen gas for three times. To the flask, acetic anhydride (Ac_2O) (23 mL, 24.8 g, 243 mmol, 12 equiv.) was added, and the resulting mixture was stirred in an aluminum heating block set at 50 °C for 12 hours. The reaction mixture was allowed to cool down to room temperature, then hydrochloric acid (1 M, 120 mL) was slowly added to the reaction mixture and stirred vigorously at room temperature for 1 hour. The resulting precipitates were separated by suction filtration, washed off with deionized water (500 mL), and dried under vacuum in a desiccator to give the title compound **2** as a white to pale yellow solid in 99% yield (10.5 g, 19.9 mmol). mp 285.8 °C; R_f 0.05 (*n*-hexane/EtOAc 6:4); ^{1}H NMR (400 MHz, $CDCl_3$) δ 8.38 (d, J = 8.8 Hz, 2H), 8.03 (d, J = 8.8 Hz, 2H), 7.83 (d, J = 8.8 Hz, 2H), 7.56 (dd, J = 8.8, 2.0 Hz, 2H), 7.10 (d, J = 2.0 Hz, 2H), 6.85 (brs, 2H), 1.86 (s, 6H); ^{13}C NMR (100 MHz, $CDCl_3$) δ 169.3, 135.9, 133.5, 130.17, 130.15, 129.8, 129.4, 126.8, 122.8, 122.0, 120.0. 24.1; IR (ATR, cm^{-1}): 3304, 3236, 3186, 3103, 3074, 3051, 3010, 1658, 1614, 1583, 1492, 1421, 1400, 1365, 1348, 1327, 1305, 1276, 1149, 1083, 1068, 991, 977, 947, 923, 881, 869, 848, 839, 790, 771, 761; MS (EI^+, direct): *m/z* (relative intensity, %) 528 ($[M+4]^+$, 30), 526 ($[M+2]^+$, 47), 525 ($[M+1]^+$, 13), 524 (M^+, 29), 486 ($[M+4–Ac+1]^+$, 18), 484 ($[M+2–Ac+1]^+$, 32), 482 ($[M–Ac+1]^+$, 18), 444 (27), 442 (53), 440 (32), 427 ($[M+4–Ac–NHAc]^+$, 54), 425 ($[M+2–Ac–NHAc]^+$, 100), 423 ($[M–Ac–NHAc]^+$, 55), 346 (12), 344 (8), 265 (40); HRMS (MALDI-TOF, positive, CHCA matrix): *m/z* calcd for $C_{24}H_{18}Br_2N_2NaO_2$ ($[M+Na]^+$) 546.9627, found 546.9621.

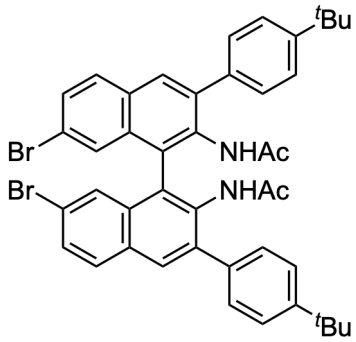
***N,N′*-(7,7'-dibromo-3,3'-diphenyl-[1,1'-binaphthalene]-2,2'-diyl)diacetamide (3a)**
[CAS No. 3097787-29-3]



The title compound **3a** was prepared according to a similar method reported in the literature[2] with a slight modification. To a two-necked reaction tube (50 mL) equipped with a magnetic stirring bar, were added diacetamide **2** (424.6 mg, 0.807 mmol), $Pd(OAc)_2$ (54.9 mg, 0.245 mmol, 30 mol%), and AgOAc (536.8 mg, 3.22 mmol, 4.0 equiv.). The reaction tube was sealed with two rubber septa, evacuated, and refilled with nitrogen gas through a syringe needle connected to a double manifold for three times. Trifluoroacetic acid (TFA) (4.0 mL) was added to the tube, and solids were dissolved. Iodobenzene (826.0 mg, 4.05 mmol, 5.0 equiv.) was added, and the resulting mixture was stirred at room temperature for 10 min. The reaction mixture was stirred in a Personal Organic Synthesizer (EYELA, *Chemi-Station*) equipped with a cooling system under a reflux condition (aluminum block temperature: 100 °C) for 24 hours. The reaction mixture was allowed to cool down to room temperature. $CHCl_3$ (50 mL) was added to the mixture, which was then filtered through a Celite pad, and the solvents were evaporated from the filtrate under reduced pressure. The mixture was neutralized with sat. $NaHCO_3$ aq. (50 mL) and extracted with $CHCl_3$ (30 mL×3). The combined organic extracts were dried over Na_2SO_4 and filtered, and the solvents in the filtrate were removed under reduced pressure to give viscous black-brown crude solid (823.5 mg). The solid residue was purified by flash column chromatography on silica gel (eluent: *n*-hexane/EtOAc 9:1–6:4) to give pale brown solid containing *N,N′*-(7,7'-dibromo-3,3'-diphenyl-[1,1'-binaphthalene]-2,2'-diyl)diacetamide (**3a**) (369.0 mg) and small quantities of impurities. The formation of **3a** was confirmed with ^{1}H NMR and MALDI-TOF MS. White solid; R_f 0.26 (*n*-hexane/EtOAc 6:4); ^{1}H NMR (400 MHz, acetone-d_6) δ 8.88 (brs, 2H), 8.08 (s, 2H), 8.03 (d, J = 8.4 Hz, 2H), 7.63 (dd, J = 8.4, 2.0 Hz, 2H), 7.59–7.56 (m, 4H), 7.44 (dd, J = 8.0, 7.2 Hz, 4H), 7.39–7.35 (m, 2H), 7.28 (br, 2H), 1.41 (brs, 6H); HRMS (MALDI-TOF, positive, CHCA matrix): *m/z* calcd for $C_{36}H_{26}Br_2N_2NaO_2$

([M+Na]$^+$) 699.0253, found 699.0234. Since the isolation of **3a** was difficult with chromatography and GPC, without further purification, the solid was employed in the following reaction.

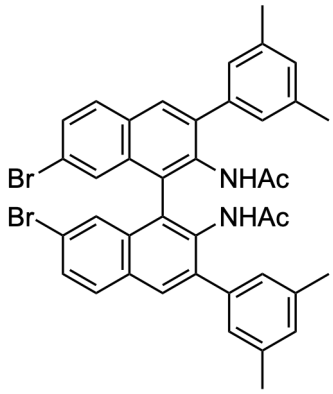
***N,N'*-(7,7'-dibromo-3,3'-bis(4-(*tert*-butyl)phenyl)-[1,1'-binaphthalene]-2,2'-diyl)diacetamide (3b) [CAS No. 3097787-30-6]**



The title compound **3b** was prepared following the procedure established for compound **3a**. To a two-necked reaction tube (50 mL) equipped with a magnetic stirring bar, were added diacetamide **2** (1.06 g, 2.01 mmol), $Pd(OAc)_2$ (135.1 mg, 0.602 mmol, 30 mol%), and AgOAc (1.35 g, 8.09 mmol, 4.0 equiv.). The reaction tube was sealed with two rubber septa, evacuated, and refilled with nitrogen gas through a syringe needle connected to a double manifold for three times. Trifluoroacetic acid (TFA) (10 mL) was added to the tube, and solids were dissolved. To the solution was added 1-(*tert*-butyl)-4-iodobenzene (2.64 g, 10.1 mmol, 5.0 equiv.), and the resulting mixture was stirred at room temperature for 10 min. The reaction mixture was stirred in a Personal Organic Synthesizer (EYELA, *Chemi-Station*) equipped with a cooling system under a reflux condition (aluminum block temperature: 100 °C) for 24 hours. The reaction mixture was allowed to cool down to room temperature. $CHCl_3$ (50 mL) was added to the mixture, which was then filtered through a Celite pad, and the solvents were evaporated from the filtrate under reduced pressure. The mixture was neutralized with sat. $NaHCO_3$ aq. (50 mL) and extracted with $CHCl_3$ (30 mL×3). The combined organic extracts were dried over Na_2SO_4 and filtered, and the solvents in the filtrate were removed under reduced pressure to give viscous black-brown crude solid (3.44 g). The solid residue was purified by flash column chromatography on silica gel (eluent: *n*-hexane/EtOAc 9:1–4:6) to give pale brown solid containing *N,N'*-(7,7'-dibromo-3,3'-bis(4-(*tert*-butyl)phenyl)-[1,1'-binaphthalene]-2,2'-diyl)diacetamide (**3b**) (1.09 g) and small quantities of impurities. The formation of **3b** was confirmed with ^{1}H

NMR and MALDI-TOF MS. White solid; R_f 0.60 (*n*-hexane/EtOAc 6:4); ^{1}H NMR (400 MHz, acetone-d_6) δ 8.87 (brs, 2H), 8.07 (s, 2H), 8.01 (d, J = 8.8 Hz, 2H), 7.62 (dd, J = 8.8, 2.0 Hz, 2H), 7.52 (d, J = 8.4 Hz, 4H), 7.49 (d, J = 8.4 Hz, 4H), 7.27 (br, 2H), 1.36 (s, 24H); HRMS (MALDI-TOF, positive, CHCA matrix): *m/z* calcd for $C_{44}H_{42}Br_2N_2NaO_2$ ($[M+Na]^+$) 811.1505, found 811.1507. Since the isolation of **3b** was difficult with chromatography and GPC, without further purification, the solid was employed in the following reaction.

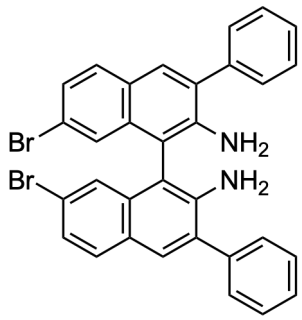
***N,N'*-(7,7'-dibromo-3,3'-bis(3,5-dimethylphenyl)-[1,1'-binaphthalene]-2,2'-diyl)diacetamide (3c) [CAS No. 3097787-31-7]**



The title compound **3c** was prepared following the procedure established for compound **3a**. To a two-necked reaction tube (50 mL) equipped with a magnetic stirring bar, were added diacetamide **2** (2.66 g, 5.05 mmol), $Pd(OAc)_2$ (339.2 mg, 1.51 mmol, 30 mol%), and AgOAc (3.37 g, 20.2 mmol, 4.0 equiv.). The reaction tube was sealed with two rubber septa, evacuated, and refilled with nitrogen gas through a syringe needle connected to a double manifold for three times. Trifluoroacetic acid (TFA) (20 mL) was added to the tube, and solids were dissolved. To the solution was added 1-iodo-3,5-dimethylbenzene (5.97 g, 25.7 mmol, 5.1 equiv.), and the resulting mixture was stirred at room temperature for 10 min. The reaction mixture was stirred in a Personal Organic Synthesizer (EYELA, *Chemi-Station*) equipped with a cooling system under a reflux condition (aluminum block temperature: 100 °C) for 24 hours. The reaction mixture was allowed to cool down to room temperature. $CHCl_3$ (100 mL) was added to the mixture, which was then filtered through a Celite pad, and the solvents were evaporated from the filtrate under reduced pressure. The mixture was neutralized with sat. $NaHCO_3$ aq. (100 mL) and extracted with $CHCl_3$ (50 mL×3). The combined organic extracts were dried over Na_2SO_4 and filtered, and the solvents in the filtrate were removed under reduced pressure to give viscous black-brown crude solid (6.83 g). The solid residue was

purified by flash column chromatography on silica gel (eluent: *n*-hexane/EtOAc 9:1–4:6) to give pale brown solid containing *N,N'*-(7,7'-dibromo-3,3'-bis(3,5-dimethylphenyl)-[1,1'-binaphthalene]-2,2'-diyl)diacetamide (**3c**) (2.69 g) and small quantities of impurities. The formation of **3c** was confirmed with ^{1}H NMR and MALDI-TOF MS. White solid; R_f 0.37 (*n*-hexane/EtOAc 6:4); ^{1}H NMR (400 MHz, acetone-d_6) δ 8.91 (brs, 2H), 8.04 (s, 2H), 8.02 (d, J = 8.8 Hz, 2H), 7.61 (dd, J = 8.8, 2.0 Hz, 2H), 7.27 (br, 2H), 7.17 (s, 4H), 6.99 (s, 2H), 2.32 (s, 12H), 1.39 (brs, 6H); HRMS (MALDI-TOF, positive, CHCA matrix): *m/z* calcd for $C_{40}H_{34}Br_2N_2NaO_2$ ($[M+Na]^+$) 755.0879, found 755.0882. Since the isolation of **3c** was difficult with chromatography and GPC, without further purification, the solid was employed in the following reaction.

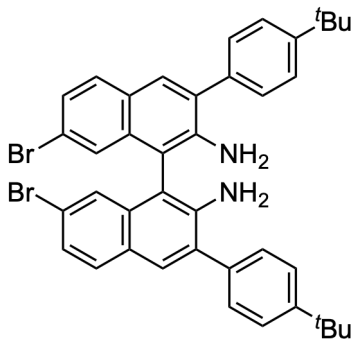
7,7'-dibromo-3,3'-diphenyl-[1,1'-binaphthalene]-2,2'-diamine (4a)
[CAS No. 3097787-32-8]



The title compound **4a** was prepared according to a similar method reported in the literature[2] with a slight modification. To a PTFE inner cylinder vessel (100 mL) equipped with a magnetic stirring bar, were added compound **3a** (369.0 mg) and EtOH (72 mL). After **3a** was dissolved under ultrasonication, KOH aq. (25 M, 6 mL) was added, and the mixture was stirred at room temperature until it became homogeneous. Then, the PTFE vessel was placed in an autoclave, sealed, and stirred in an aluminum heating block set at 180 °C for 16 hours. The reaction mixture was allowed to cool down to room temperature, transferred to a round-bottom flask (300 mL), and neutralized with sat. NH_4Cl aq. (50 mL). After EtOH was removed from the mixture under reduced pressure, the organic layer was extracted with $CHCl_3$ (30 mL×3). The combined organic extracts were dried over Na_2SO_4 and filtered, and the solvents in the filtrate were removed under reduced pressure to give brown crude solid (278.7 mg). The solid residue was purified by flash column chromatography on silica gel (eluent: *n*-hexane/EtOAc 98:2–8:2) to give the title compound **4a** as a pale yellow solid (146.4 mg, 0.246 mmol, 30% in

2 steps). mp 252.9 °C; R_f 0.22 (*n*-hexane/EtOAc 9:1); ^{1}H NMR (400 MHz, $CDCl_3$) δ 7.73 (s, 2H), 7.66 (d, J = 8.8 Hz, 2H), 7.62–7.59 (m, 4H), 7.52–7.48 (m, 4H), 7.44–7.40 (m, 2H), 7.33 (dd, J = 8.8, 2.0 Hz, 2H), 7.23 (d, J = 1.6 Hz, 2H) 3.92 (brs, 4H); ^{13}C NMR (100 MHz, $CDCl_3$) δ 141.7, 138.6, 134.2, 131.0, 130.0, 129.9, 129.2, 128.9, 127.9, 126.6, 126.0, 125.4, 121.5, 111.0; IR (ATR, cm^{-1}): 3456, 3361, 3327, 3180, 3047, 3028, 1734, 1618, 1581, 1571, 1481, 1444, 1423, 1411, 1377, 1355, 1307, 1265, 1222, 1176, 1155, 1130, 1101, 1064, 1002, 987, 939, 883, 869, 833, 798, 781, 759, 750, 729, 700; MS (EI^+, direct): *m/z* (relative intensity, %) 596 ($[M+4]^+$, 60), 594 ($[M+2]^+$, 100), 593 ($[M+1]^+$, 22), 592 (M^+, 52), 579 ($[M+4–NH_3]^+$, 7), 577 ($[M+2–NH_3]^+$, 14), 575 ($[M–NH_3]^+$, 8), 499 (13), 497 (12), 417 (30); HRMS (MALDI-TOF, positive, CHCA matrix): *m/z* calcd for $C_{32}H_{22}Br_2N_2$ (M^+) 592.0144, found 592.0144.

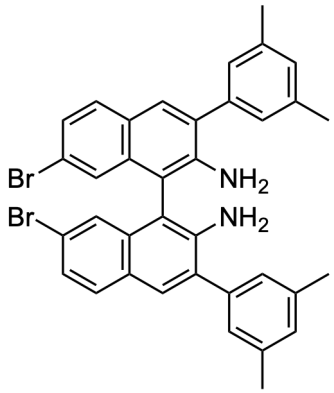
7,7'-dibromo-3,3'-bis(4-(tert-butyl)phenyl)-[1,1'-binaphthalene]-2,2'-diamine (4b)
[CAS No. 3097787-33-9]



The title compound **4b** was prepared following the procedure established for compound **4a**. To a PTFE inner cylinder vessel (100 mL) equipped with a magnetic stirring bar, were added compound **3b** (1.09 g) and EtOH (72 mL). After **3b** was dissolved under ultrasonication, KOH aq. (25 M, 6 mL) was added, and the mixture was stirred at room temperature until it became homogeneous. Then, the PTFE vessel was placed in an autoclave, sealed, and stirred in an aluminum heating block set at 180 °C for 24 hours. The reaction mixture was allowed to cool down to room temperature, transferred to a round-bottom flask (300 mL), and neutralized with sat. NH_4Cl aq. (50 mL). After EtOH was removed from the mixture under reduced pressure, the organic layer was extracted with $CHCl_3$ (30 mL×3). The combined organic extracts were dried over Na_2SO_4 and filtered, and the solvents in the filtrate were removed under reduced pressure to give brown crude solid (879.1 mg). The solid residue was purified by flash column chromatography on silica gel (eluent: *n*-hexane/EtOAc 98:2–8:2) to give the

title compound **4b** as a pale yellow solid (517.8 mg, 0.733 mmol, 36% in 2 steps). mp 295.3 °C; R_f 0.46 (*n*-hexane/EtOAc 9:1); ^{1}H NMR (400 MHz, $CDCl_3$) δ 7.72 (s, 2H), 7.65 (d, J = 8.4 Hz, 2H), 7.54 (d, J = 8.8 Hz, 4H), 7.51 (d, J = 8.4 Hz, 4H), 7.31 (dd, J = 8.4, 2.0 Hz, 2H), 7.22 (d, J = 2.0 Hz, 2H), 3.95 (brs, 4H), 1.38 (s, 18H); ^{13}C NMR (100 MHz, $CDCl_3$) δ 150.9, 141.9, 135.6, 134.1, 130.9, 129.9, 128.8, 126.6, 125.9, 125.8, 125.4, 121.4, 110.9, 34.6, 31.3 (one aryl carbon signal was not detected, probably due to the overlap of signals in this regime); IR (ATR, cm^{-1}): 3477, 3381, 3371, 2956, 2929, 2899, 2864, 1616, 1591, 1577, 1506, 1479, 1458, 1431, 1392, 1359, 1307, 1265, 1224, 1193, 1174, 1109, 1064, 1026, 1018, 993, 985, 937, 893, 867, 846, 835, 825, 790, 771, 748, 729; MS (EI^+, direct): *m/z* (relative intensity, %) 708 ($[M+4]^+$, 54), 706 ($[M+2]^+$, 100), 704 (M^+, 47), 628 (5), 626 (6), 570 (6), 568 (5), 339 (5), 338 (9), 337 (6); HRMS (MALDI-TOF, positive, CHCA matrix): *m/z* calcd for $C_{40}H_{38}Br_2N_2$ (M^+) 704.1396, found 704.1392.

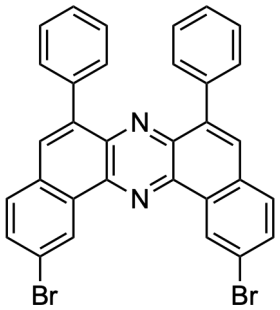
7,7'-dibromo-3,3'-bis(3,5-dimethylphenyl)-[1,1'-binaphthalene]-2,2'-diamine (4c)
[CAS No. 3097787-34-0]



The title compound **4c** was prepared following the procedure established for compound **4a**. The reaction was carried out in separate two batches. To a PTFE inner cylinder vessel (100 mL) equipped with a magnetic stirring bar, were added compound **3c** (1.35 g) and EtOH (72 mL). After **3c** was dissolved under ultrasonication, KOH aq. (25 M, 6 mL) was added, and the mixture was stirred at room temperature until it became homogeneous. Then, the PTFE vessel was placed in an autoclave, sealed, and stirred in an aluminum heating block set at 150 °C for 48 hours. The reaction mixture was allowed to cool down to room temperature, transferred to a round-bottom flask (300 mL), and neutralized with sat. NH_4Cl aq. (50 mL). After EtOH was removed from the mixture under reduced pressure, the organic layer was extracted with $CHCl_3$ (50 mL×3). The organic extracts from both batches were combined, dried over Na_2SO_4, filtered,

and the solvents in the filtrate were removed under reduced pressure to give brown crude solid (2.87 g). The solid residue was purified by flash column chromatography on acidic silica gel (eluent: *n*-hexane/EtOAc 98:2–7:3) to give the title compound **4c** as a pale yellow solid (2.02 g, 3.11 mmol, 62% in 2 steps). mp 304.5 °C; R_f 0.39 (*n*-hexane/EtOAc 9:1); ^{1}H NMR (400 MHz, $CDCl_3$) δ 7.70 (s, 2H), 7.64 (d, J = 8.4 Hz, 2H), 7.31 (dd, J = 8.4, 2.0 Hz, 2H), 7.23–7.19 (m, 6H), 7.05 (br, 2H), 3.93 (brs, 4H), 2.39 (s, 12H); ^{13}C NMR (100 MHz, $CDCl_3$) δ 141.8, 138.57, 138.51, 134.2, 131.2, 129.9, 129.7, 129.5, 126.9, 126.6, 125.9, 125.3, 121.4, 110.9, 21.3; IR (ATR, cm^{-1}): 3479, 3469, 3381, 3026, 3012, 2954, 2914, 2860, 2736, 1734, 1614, 1598, 1579, 1479, 1435, 1413, 1377, 1357, 1319, 1296, 1267, 1246, 1203, 1180, 1099, 1062, 1033, 995, 941, 900, 889, 867, 850, 798, 779, 773, 744, 719, 705; MS (EI^+, direct): *m/z* (relative intensity, %) 652 ($[M+4]^+$, 67), 650 ($[M+2]^+$, 100), 648 (M^+, 53), 635 ($[M+4–NH_3]^+$, 8), 633 ($[M+2–NH_3]^+$, 12), 631 ($[M–NH_3]^+$, 4); HRMS (MALDI-TOF, positive, CHCA matrix): *m/z* calcd for $C_{36}H_{30}Br_2N_2$ (M^+) 648.0770, found 648.0766.

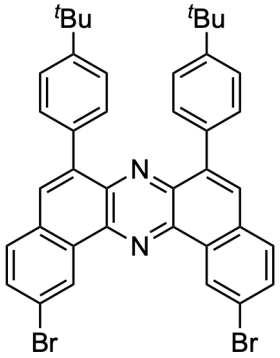
2,12-dibromo-6,8-diphenyldibenzo[*a*,*j*]phenazine (5a) [CAS No. 3097787-35-1]



The title compound **5a** was prepared according to a similar method reported in literature[1] with a slight modification. To a three-necked round-bottom flask (200 mL) equipped with a magnetic stirring bar, were added binaphthalenediamine **4a** (119.2 mg, 0.201 mmol) and MeOH (80 mL). The resulting suspension was stirred at room temperature under ultrasonication until **4a** was completely dissolved. The flask equipped with a ground-glass joint connected to a double manifold was sealed with a rubber septum and a glass stopper, evacuated, and refilled with nitrogen gas for three times. To the solution, 1,3-diiodo-5,5-dimethylhydantoin (DIH) (609.2 mg, 1.60 mmol, 8.0 equiv.) was added, and the resulting mixture was stirred at room temperature for 24 hours. $Na_2S_2O_3$ aq. (1 M, 40 mL) was added to the reaction mixture, and the organic layer was extracted with $CHCl_3$ (30 mL×3). The combined organic extracts were dried over Na_2SO_4 and filtered, and the solvents in the filtrate

were removed under reduced pressure to give yellowish brown crude solid (137.4 mg). The solid residue was purified by flash column chromatography on silica gel (eluent: *n*-hexane/$CHCl_3$ 9:1–6:4) to give the title compound **5a** as a yellow solid in 48% yield (56.9 mg, 0.096 mmol). Further purification to obtain samples for spectroscopic analysis was carried out by recrystallization from $CHCl_3$ solution at 0–10 °C. mp 350.3 °C (dec.); R_f 0.25 (*n*-hexane/$CHCl_3$ 8:2); ^{1}H NMR (400 MHz, $CDCl_3$) δ 9.72 (d, J = 2.0 Hz, 2H), 8.08 (s, 2H), 7.92 (dd, J = 8.4, 2.0 Hz, 2H), 7.85 (d, J = 8.4, 2H), 7.75–7.72 (m, 4H), 7.42–7.35 (m, 6H); ^{13}C NMR (100 MHz, $CDCl_3$) δ 141.3, 139.0, 138.7, 137.7, 132.8, 132.1, 131.8, 131.2, 130.8, 129.8, 127.9, 127.8, 127.5, 122.1; IR (ATR, cm^{-1}): 3055, 3026, 1587, 1573, 1564, 1537, 1494, 1471, 1444, 1427, 1377, 1336, 1323, 1280, 1253, 1215, 1182, 1166, 1149, 1076, 1066, 1028, 1010, 999, 910, 894, 848, 812, 806, 758, 729; MS (EI^+, direct): *m/z* (relative intensity, %) 592 ($[M+4]^+$, 55), 590 ($[M+2]^+$, 100), 589 ($[M+1]^+$, 95), 588 (M^+, 51), 511 ($[M+2–Br]^+$, 19), 509 ($[M–Br]^+$, 17), 430 ($[M–2Br]^+$, 5), 215 (26); HRMS (MALDI-TOF, positive, CHCA matrix): *m/z* calcd for $C_{32}H_{19}Br_2N_2$ ($[M+H]^+$) 588.9910, found 588.9911.

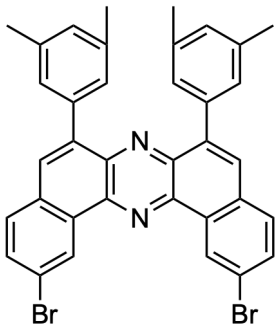
2,12-dibromo-6,8-bis(4-(*tert*-butyl)phenyl)dibenzo[*a,j*]phenazine (5b)
[CAS No. 3097787-36-2]



The title compound **5b** was prepared following the procedure established for compound **5a**. To a three-necked round-bottom flask (300 mL) equipped with a magnetic stirring bar, were added binaphthalenediamine **4b** (354.7 mg, 0.502 mmol) and MeOH (200 mL). The resulting suspension was stirred at room temperature under ultrasonication until **4b** was completely dissolved. The flask equipped with a ground-glass joint connected to a double manifold was sealed with a rubber septum and a glass stopper, evacuated, and refilled with nitrogen gas for three times. To the solution, 1,3-diiodo-5,5-dimethylhydantoin (DIH) (1.53 g, 4.03 mmol, 8.0 equiv.) was added, and the resulting mixture was stirred at room temperature

for 24 hours. $Na_2S_2O_3$ aq. (1 M, 100 mL) was added to the reaction mixture, and the organic layer was extracted with $CHCl_3$ (50 mL×3). The combined organic extracts were dried over Na_2SO_4 and filtered, and the solvents in the filtrate were removed under reduced pressure to give yellowish brown crude solid (381.2 mg). The solid residue was purified by flash column chromatography on silica gel (eluent: *n*-hexane/$CHCl_3$ 9:1–6:4) to give the title compound **5b** as a yellow solid in 43% yield (152.2 mg, 0.217 mmol). Further purification to obtain samples for spectroscopic analysis was carried out by recrystallization from $CHCl_3$ solution at 0–10 °C. mp 376.1 °C; R_f 0.46 (*n*-hexane/$CHCl_3$ 8:2); ^{1}H NMR (400 MHz, $CDCl_3$) δ 9.73 (d, J = 1.6 Hz, 2H), 8.10 (s, 2H), 7.91 (dd, J = 8.4, 1.6 Hz, 2H), 7.86–7.82 (m, 6H), 7.46 (d, J = 8.4 Hz, 2H), 1.42 (s, 18H); ^{13}C NMR (100 MHz, $CDCl_3$) δ 150.6, 141.4, 139.1, 138.4, 135.0, 132.8, 132.1, 131.9, 131.6, 130.6, 129.7, 127.9, 124.8, 122.0, 34.6, 31.5; IR (ATR, cm^{-1}): 2960, 2900, 2866, 1610, 1589, 1554, 1539, 1514, 1496, 1473, 1462, 1425, 1392, 1373, 1359, 1338, 1323, 1271, 1253, 1230, 1220, 1201, 1149, 1128, 1107, 1068, 1022, 1006, 962, 950, 935, 918, 896, 858, 837, 825, 806, 792, 738, 715; MS (EI$^+$, direct): *m/z* (relative intensity, %) 704 ([M+4]$^+$, 35), 702 ([M+2]$^+$, 81), 701 ([M+1]$^+$, 4), 700 (M$^+$, 40), 689 ([M+4–CH_3]$^+$, 21), 687 ([M+2–CH_3]$^+$, 44), 685 ([M–CH_3]$^+$, 20), 647 ([M+4–^{t}Bu]$^+$, 33), 645 ([M+2–^{t}Bu]$^+$, 49), 643 ([M–^{t}Bu]$^+$, 31), 633 ([M+4–CH_3–^{t}Bu]$^+$, 13), 631 ([M+2–CH_3–^{t}Bu]$^+$, 29), 629 ([M–CH_3–^{t}Bu]$^+$, 21), 551 (13), 549 (11), 337 (8), 336 (12), 335 (7); HRMS (MALDI-TOF, positive, CHCA matrix): *m/z* calcd for $C_{40}H_{35}Br_2N_2$ ([M+H]$^+$) 701.1162, found 701.1163.

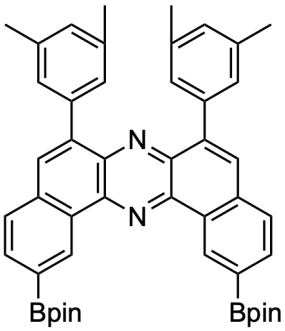
2,12-dibromo-6,8-bis(3,5-dimethylphenyl)dibenzo[*a*,*j*]phenazine (5c)
[CAS No. 3097787-37-3]



The title compound **5c** was prepared following the procedure established for compound **5a**. To a three-necked round-bottom flask (300 mL) equipped with a magnetic stirring bar, were added binaphthalenediamine **4c** (327.8 mg, 0.504 mmol) and MeOH (200 mL). The resulting mixture was stirred at room temperature under ultrasonication until **4c** was

completely dissolved. The flask equipped with a ground-glass joint connected to a double manifold was sealed with a rubber septum and a glass stopper, evacuated, and refilled with nitrogen gas for three times. To the solution, 1,3-diiodo-5,5-dimethylhydantoin (DIH) (1.53 g, 4.04 mmol, 8.0 equiv.) was added, and the resulting mixture was stirred at room temperature for 24 hours. $Na_2S_2O_3$ aq. (1 M, 100 mL) was added to the reaction mixture, and the organic layer was extracted with $CHCl_3$ (50 mL×3). The combined organic extracts were dried over Na_2SO_4 and filtered, and the solvents in the filtrate were removed under reduced pressure to give yellowish brown crude solid (464.4 mg). The solid residue was purified by flash column chromatography on silica gel (eluent: *n*-hexane/$CHCl_3$ 9:1–6:4) to give the title compound **5c** as a yellow solid in 68% yield (221.8 mg, 0.343 mmol). Further purification to obtain samples for spectroscopic analysis was carried out by recrystallization from $CHCl_3$ solution at 0–10 °C. mp 333.6 °C; R_f 0.46 (*n*-hexane/$CHCl_3$ 8:2); ^{1}H NMR (400 MHz, $CDCl_3$) δ 9.72 (d, J = 2.0 Hz, 2H), 8.07 (s, 2H), 7.91 (dd, J = 8.4, 2.0 Hz, 2H), 7.86 (d, J = 8.4 Hz, 2H), 7.31 (s, 4H), 7.03 (s, 2H), 2.21 (s, 12H); ^{13}C NMR (100 MHz, $CDCl_3$) δ 141.4, 139.0, 138.9, 137.5, 136.9, 132.7, 132.0, 131.9, 130.8, 129.7, 129.2, 128.7, 127.8, 121.9, 21.2; IR (ATR, cm^{-1}): 3008, 2968, 2953, 2914, 2860, 2729, 1899, 1598, 1585, 1562, 1539, 1496, 1469, 1442, 1421, 1371, 1336, 1290, 1273, 1257, 1213, 1186, 1157, 1145, 1130, 1066, 1029, 997, 952, 933, 902, 887, 869, 848, 829, 808, 775, 736, 727; MS (EI^+, direct): *m/z* (relative intensity, %) 648 ($[M+4]^+$, 55), 646 ($[M+2]^+$, 100), 645 ($[M+1]^+$, 37), 644 (M^+, 52), 633 ($[M+4–CH_3]^+$, 59), 631 ($[M+2–CH_3]^+$, 97), 629 ($[M–CH_3]^+$, 61), 552 ($[M+2–CH_3–Br]^+$, 11), 550 ($[M–CH_3–Br]^+$, 15); HRMS (MALDI-TOF, positive, CHCA matrix): *m/z* calcd for $C_{36}H_{27}Br_2N_2$ ($[M+H]^+$) 645.0536, found 645.0535.

6,8-bis(3,5-dimethylphenyl)-2,12-bis(4,4,5,5-tetramethyl-1,3,2-dioxaborolan-2-yl)dibenzo[*a*,*j*]phenazine (7) [CAS No. 3097787-37-3]



The title compound **7** was prepared according to a similar method reported in the literature[6] with a slight modification. A two-necked reaction tube (50 mL) equipped with a magnetic stirring bar and two rubber septa were dried in a vacuum oven at 80 °C for 2 hours before use. To the tube, were added 2,12-dibromo-6,8-bis(3,5-dimethylphenyl)dibenzo[*a*,*j*]phenazine (**5c**) (1.30 g, 2.01 mmol), bis(pinacolato)diboron (B_2pin_2) (1.13 g, 4.45 mmol, 2.2 eq.), Pd(dppf)Cl_2 (293.4 mg, 0.401 mmol, 20 mol%), and KOAc (1.19 g, 12.1 mmol, 6.0 eq.). The reaction tube was sealed with two rubber septa, evacuated, and refilled with nitrogen gas through a syringe needle connected to a double manifold for three times. Dehydrated toluene (20 mL) was added to the tube, and the resulting mixture was stirred at room temperature for 10 min. The reaction mixture was stirred in a Personal Organic Synthesizer (EYELA, *Chemi-Station*) equipped with a cooling system under a reflux condition (aluminum block temperature: 120 °C) for 24 hours. The reaction mixture was allowed to cool down to room temperature. Water (10 mL) was added to the mixture, and the organic layer was extracted with $CHCl_3$ (50 mL×3). The combined organic extracts were dried over Na_2SO_4 and filtered, and the solvents in the filtrate were removed under reduced pressure to give yellowish brown crude solid (2.87 g). The solid residue was purified by flash column chromatography on silica gel (eluent: *n*-hexane/EtOAc 95:5–6:4) to give yellow solid of diboryldibenzophenazine **7** containing small quantities of B_2pin_2. The solid was triturated with *n*-hexane (20 mL) under ultrasonication, which was then filtered to give the title compound **7** as a yellow solid in 78% yield (1.16 g, 1.57 mmol). Mp 309.5 °C (dec.); R_f 0.48 (*n*-hexane/EtOAc 8:2); ^{1}H NMR (400 MHz, $CDCl_3$) δ 10.18 (br, 2H), 8.19 (dd, J = 8.0, 1.2 Hz, 2H), 8.10 (s, 2H), 7.97 (d, J = 8.0 Hz, 2H), 7.36 (s, 4H), 7.02 (s, 2H), 2.21 (s, 12H), 1.49 (s, 24H); ^{13}C NMR (100 MHz, $CDCl_3$) δ 140.9, 140.3, 139.6, 138.0, 136.8, 135.3, 134.6, 132.8, 131.2, 130.0, 129.0, 128.8, 127.3, 84.0, 25.1, 21.2 (the signal corresponding to

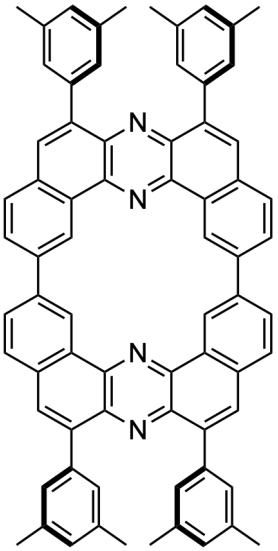
the aryl carbon directly connected to the boron atom was not detected, probably due to the quadrupolar relaxation); IR (ATR, cm^{-1}): 3055, 2974, 2916, 2862, 2729, 1610, 1508, 1460, 1444, 1371, 1352, 1319, 1261, 1213, 1145, 1130, 1111, 1087, 1060, 1039, 997, 960, 941, 908, 893, 885, 875, 856, 844, 835, 819, 777, 756, 738, 719, 700; MS (EI^+, direct): *m/z* (relative intensity, %) 740 (M^+, 100), 725 ($[M–CH_3]^+$, 39), 614 ($[M–Bpin+1]^+$, 18), 541 (22), 370 ($[M/2]^+$, 15); HRMS (MALDI-TOF, positive, CHCA matrix): *m/z* calcd for $C_{48}H_{51}B_2N_2O_4$ ($[M+H]^+$) 741.4045, found 741.4063.

*Synthesis of DBPHZ cyclic homodimer **8** and homotrimer **9***

The title compound **8** was prepared according to a similar method reported in the literature[7] with a slight modification. A two-necked reaction tube (50 mL) equipped with a magnetic stirring bar and two rubber septa were dried in a vacuum oven at 80 °C for 2 hours before use. Dehydrated toluene and deionized water were degassed through freeze-pump-thaw cycling for three times before use. To the tube, were added 2,12-dibromo-6,8-bis(3,5-dimethylphenyl)dibenzo[*a*,*j*]phenazine (**5c**) (130.2 mg, 0.201 mmol), 6,8-bis(3,5-dimethylphenyl)-2,12-bis(4,4,5,5-tetramethyl-1,3,2-dioxaborolan-2-yl)dibenzo[*a*,*j*] phenazine (**7**) (149.7 mg, 0.202 mmol), $Pd(OAc)_2$ (4.5 mg, 0.020 mmol, 10 mol%), 2-dicyclohexylphosphino-2',6'-dimethoxybiphenyl (SPhos) (17.0 mg, 0.041 mmol, 20 mol%), and K_3PO_4 (170.2 mg, 0.802 mmol, 4.0 eq.). The reaction tube was sealed with two rubber septa, evacuated, and refilled with nitrogen gas through a syringe needle connected to a double manifold for three times. Dehydrated toluene (20 mL) and deionized water (2.0 mL) were added to the tube, and the resulting mixture was stirred at room temperature for 10 min. The reaction mixture was stirred in a Personal Organic Synthesizer (EYELA, Chemi-Station) equipped with a cooling system (aluminum block temperature: 100 °C) for 40 hours. The reaction mixture was allowed to cool down to room temperature. Water (50 mL) was added to the mixture, and the organic layer was extracted with $CHCl_3$ (100 mL×3). The combined organic extracts were dried over Na_2SO_4 and filtered, and the solvents in the filtrate were removed under reduced pressure to give yellowish crude solid. The insoluble solids (crude A) and the components soluble in $CHCl_3$ (crude B) were separated by suction filtration from the crude product. The crude A was purified by flash column chromatography on NH silica gel (eluent: $CHCl_3$/*o*-dichlorobenzene 1:1–0:10) twice to give yellow solid containing cyclic homodimer **8** and small quantities of impurities, which was then reprecipitated from *o*-dichlorobenzene/*n*-hexane (1:20) to provide the dimer **8** in 11% yield (21.0 mg, 21.6 μmol)

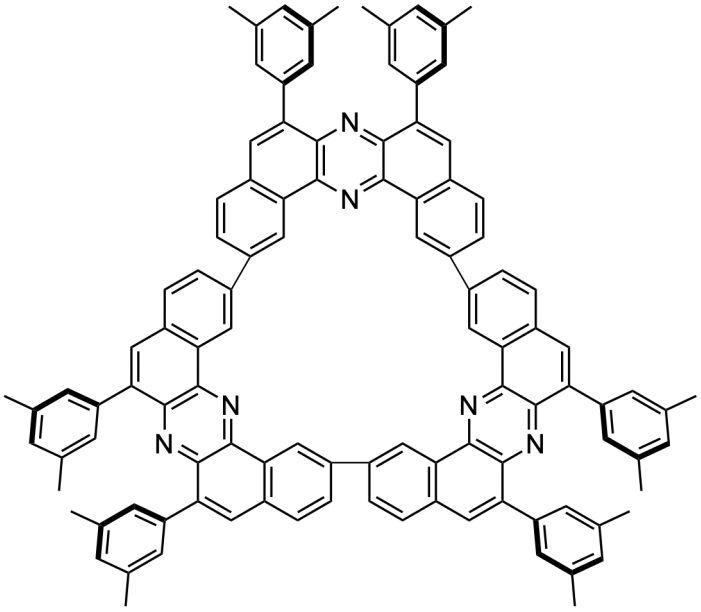
as a mustard yellow solid. The crude B was purified by flash column chromatography on NH silica gel (eluent: *n*-hexane/$CHCl_3$ 95:5–8:2) for three times to give yellow solid containing cyclic homotrimer **9** and small quantities of impurities, which was then reprecipitated from $CHCl_3$/*n*-hexane (1:10) to provide the trimer **9** in 7% yield (10.0 mg, 6.85 μmol) as a yellow solid.

3,7,16,20-tetrakis(3,5-dimethylphenyl)-4,6:17,19-di(azeno)-1,25:9,11:12,14:22,24-tetraethenotetrabenzo[*b*,*h*,*k*,*q*][1,10]diazacyclooctadecine (Cyclic homodimer) (8)
[CAS No. 3097787-37-3]



Cyclic homodimer **8**: mp 281.1 °C (dec.); R_f 0.85 ($CHCl_3$/*o*-dichlorobenzene 100:1); ^{1}H NMR (400 MHz, *o*-DCB-d_4) δ 11.09 (s, 4H), 8.35 (d, J = 8.0 Hz, 4H), 8.09 (d, J = 0.8 Hz, 4H), 7.99 (d, J = 8.0 Hz, 4H), 7.49 (s, 8H), 7.06 (s, 4H), 2.30 (s, 24H); ^{1}H NMR (400 MHz, TFA-d_1) δ 11.65 (s, 4H), 8.94 (dd, J = 8.8, 1.6 Hz, 4H), 8.65 (s, 4H), 8.47 (d, J = 8.8 Hz, 2H), 7.39 (s, 4H), 7.17 (s, 8H), 2.38 (s, 24H); ^{13}C NMR (100 MHz, TFA-d_1) δ 146.0, 143.8, 141.7, 140.6, 135.5, 134.5, 133.4, 133.2, 132.7, 131.6, 131.5, 130.7, 128.0, 124.3, 21.9; Since the solubility of **8** in *o*-dichlorobenzene is low to gain sufficient ^{13}C NMR signals, ^{13}C NMR spectrum was obtained in TFA-d_1; IR (ATR, cm^{-1}): 3012, 3001, 2914, 2860, 2727, 2679, 1732, 1597, 1525, 1506, 1473, 1456, 1373, 1328, 1303, 1280, 1226, 1207, 1136, 1066, 1058, 1035, 997, 948, 885, 846, 829, 802, 763, 744, 738, 707, 700; HRMS (MALDI-TOF, positive, dithranol matrix): *m/z* calcd for $C_{72}H_{53}N_4$ ($[M+H]^+$) 973.4265, found 973.4261.

$1^6,1^8,2^6,2^8,3^6,3^8$-hexakis(3,5-dimethylphenyl)-1,2,3(2,12)-tridibenzo[*a*,*j*]phenazinacyclopropaphane (Cyclic homotrimer) (9)



Cyclic homotrimer **9**: mp 316.6 °C (dec.); R_f 0.14 (*n*-hexane/$CHCl_3$ 8:2); ^1H NMR (400 MHz, $CDCl_3$) δ 9.49 (d, J = 2.0 Hz, 8H), 8.03 (s, 8H), 7.99 (d, J = 8.0 Hz, 8H), 7.77 (dd, J = 8.0, 2.0 Hz, 8H), 7.36 (s, 16H), 7.00 (s, 8H), 2.25 (48H); ^{13}C NMR (100 MHz, $CDCl_3$) δ 140.8, 139.9, 139.0, 137.87, 137.84, 137.0, 132.6, 130.76, 130.74, 130.6, 129.1, 128.5, 128.2, 124.8, 21.2; IR (ATR, cm^{-1}): 3012, 3001, 2914, 2860, 2727, 2679, 1732, 1597, 1525, 1506, 1473, 1456, 1373, 1328, 1303, 1280, 1226, 1207, 1136, 1066, 1058, 1035, 997, 948, 885, 846, 802, 763, 738, 707, 700; HRMS (MALDI-TOF, positive, CHCA matrix): *m/z* calcd for $C_{108}H_{79}N_6$ ($[M+H]^+$) 1459.6361, found 1459.6370.

Single Crystal X-Ray Crystallographic Analysis.

Crystallographic analysis of compound **5b**: The single crystal suitable for the X-ray crystallographic analysis was grown from a solution of chloroform by slow evaporation. A clear light yellow needle crystal with dimensions of 0.300 × 0.100 × 0.100 mm^3 was mounted on a suitable support. Data were collected using an Rigaku XtaLAB P200 diffractometer with graphite monochromated CuKα radiation (λ = 1.54184 Å) to a $2\theta_{max}$ value of 149.1° at 213 K. The cell refinements were performed with a software CrysAlisPro 1.171.39.20a.[11] The crystal structure was solved by direct methods (SHELXT Version 2018/3).[12] All calculations were performed with the observed reflections [I > 2σ(I)] with the program Olex2 1.5 crystallographic software packages,[13] except for refinement which was performed by SHELXL.[14] The non-hydrogen atoms were refined anisotropically, and hydrogen atoms were refined using the riding model. The crystal data are summarized in Table 1. CCDC-2466943 contains the supplementary crystallographic data for **5b**, which are available free of charge from the Cambridge Crystallographic Data Center (CCDC) via www.ccdc.cam.ac.uk/data_request/cif.

Table 1. Summary of the crystallographic data of compound **5b**.

Empirical Formula	$C_{41}H_{35}Br_2Cl_3N_2$	
Formula Weight	821.88	
Crystal System	*Triclinic*	
Space Group	*P-1* (#2)	
Unit cell dimensions	a = 9.2037(4) Å	α = 89.702(4)°
	b = 10.4287(5) Å	β = 88.626(4)°
	c = 18.7556(49 Å	γ = 86.462(4)°
V	1796.25(14) Å^3	
Z	2	
Density (calculated)	1.520 g/cm^3	
Absorption coefficient	5.164 mm^{-1}	
R_1 [I>2σ(I)]	0.0369	
wR_2 (all data)	0.1013	
Crystal size	0.300 × 0.100 × 0.100 mm^3	
Goodness-of-fit on F^2	1.058	
Reflections collected/unique	7057/18584 [R(int) = 0.0353]	

Investigation of the Solubility of DBPHZs in Organic Solvents

A 15 mL vial was charged with DBPHZ **5a**–**5c** and **6** (1.0–5.0 mg) and 0.5 mL of Et_2O, $CHCl_3$ or toluene. The mixture was subjected to ultrasonication at room temperature for 5 min. If DBPHZ did not dissolve completely, an additional 0.25 mL portion of the same solvent was added, and ultrasonication was resumed for another 5 min. This process was repeated, adding 0.25–0.50 mL aliquots of solvent and ultrasonication, until dissolution was achieved.

Measuring Procedure for Concentration-Dependence of ^{1}H NMR of homodimer 8.

A 15 mL vial was charged with compound **8** (2.0 mg, 2.05 mmol) and 1.00 mL of *o*-DCB-d_4 to prepare *Solution A* (2.05 mM). Into a standard NMR tube, 0.60 mL of *Solution A* was transferred, and the ^{1}H NMR spectrum was recorded. Subsequently, an additional 0.30 mL of *o*-DCB-d_4 was added to the tube, and a second ^{1}H NMR spectrum was acquired. Further experiments were performed by adding additional portions of *o*-DCB-d_4 (0.30 mL and 0.60 mL, respectively), with ^{1}H NMR spectra recorded after each addition.

Quantum Chemical Calculations

All quantum chemical calculations were performed using Gaussian 16. Geometry optimizations were carried out at the PBE0/6-31G(d,p) level with the IEFPCM solvation model ($CHCl_3$). NMR shielding tensors were computed using the GIAO method and referenced to TMS at the same level of theory. Geometry coordinates are available as xyz files online. Electronic circular dichroism (ECD) spectra were simulated using time-dependent DFT (TD-DFT) theory, computing 40 excited states based on the ground-state geometry optimized at the PBE0/6-311+G(d,p) level in conjunction with the IEFPCM solvation model (toluene). Nucleus-independent chemical shift (NICS (1)) and were computed using the GIAO method at the PBE0/6-311+G(d,p) level. HOMAs and NICS values were analyzed by py.Aroma *ver.* 4.[15]

1-12. References

1. Takeda, Y.; Okazaki, M.; Minakata, S. *Chem. Commun.* **2014**, *50*, 10291–10294.
2. Scarborough, C. C.; McDonald, R. I.; Hartmann, C.; Sazama, G. T.; Bergant, A.; Stahl, S. S. *J. Org. Chem.* **2009**, *74*, 2613–2615.
3. Takishima, R.; Nishii, Y.; Miura, M. *Org. Lett.* **2021**, *23*, 1349–1354.
4. Lim, Y.-K.; Jung, J.-W.; Lee, H.; Cho, C.-G. *J. Org. Chem.* **2004**, *69*, 5778–5781.
5. Deposition number 2466943 (for **5b**) contains the supplementary crystallographic data for this paper. These data are provided free of charge by the joint Cambridge Crystallographic Data Centre and Fachinformationszentrum Karlsruhe Access Structures service.
6. Ishiyama, T.; Murata, M.; Miyaura, N. *J. Org. Chem.* **1995**, *60*, 7508–7510.
7. Barder, T. E.; Walker, S. D.; Martinelli, J. R.; Buchwald, S. L. *J. Am. Chem. Soc.* **2005**, *127*, 4685–4696.
8. (a) Cheney, B. V. *J. Am. Chem. Soc.* **1968**, *90*, 5386–5390. (b) Zeng, Z.; Qasem, A. M. A.; Blagbrough, I. S.; Woodman, T. J. *Org. Biomol. Chem.* **2024**, *22*, 7915–7935.
9. (a) Nakanishi, W.; Matsuno, T.; Ichikawa, J.; Isobe, H. *Angew. Chem. Int. Ed.* **2011**, *50*, 6048–6051. (b) Matsuno, T.; Kogashi, K.; Sato, S.; Isobe, H. *Org. Lett.* **2017**, *19*, 6456–6459.
10. Hosono, T.; Decarli, N. O.; Crocomo, P. Z.; Goya, T.; de Sousa, L. E.; Tohnai, N.; Minakata, S.; de Silva, P.; Data, P.; Takeda, Y. *J. Mater. Chem. C* **2022**, *10*, 4905–4913.
11. Rigaku Oxford Diffraction (2015), Software CrysAlisPro 1.171.39.20a Rigaku Corporation, Tokyo, Japan.
12. G. M. Sheldrick, G *Acta Cryst.* **2015**, *A71*, 3-8.
13. O. V. Dolomanov, L. J. Bourhis, R. J. Gildea, J. A. K. Howard, H. Puschmann, *J. Appl. Cryst.* **2009**, *42*, 339–341.
14. G. M. Sheldrick, *Acta Cryst.* **2015**, *C71*, 3–8.
15. Wang, Z. *Chemistry* **2024**, *6*, 1692–1703.

Chapter 2

Development of a Tetra-Functionalized Dibenzo[*a,j*]phenazine (DBPHZ) Building Block and Synthesis of Highly Soluble DBPHZ Cyclic Heterodimer

2-1. Design of Tetra-Functionalized Dibenzo[*a,j*]phenazine for Solubility Enhancement

As described in Chapter 1, the introduction of alkylated aryl substituents at the 6,8-positions of DBPHZ effectively improved the solubility of these DBPHZ derivatives and enabled the synthesis of DBPHZ cyclic homodimer **8** via double Suzuki–Miyaura cross-coupling (Figure 1a). Nevertheless, the solubility of **8** itself remains insufficient: it dissolves only in limited aromatic solvents such as *o*-dichlorobenzene and toluene, and even then, its solubility is below the μM level. This poor solubility complicates purification and severely restricts detailed measurements of the macrocycle. Therefore, further improvement in the solubility of DBPHZ-based macrocycles is required.

To address this issue, the author designed a novel tetra-functionalized DBPHZ building block **10** to ensure the solubility of both the target macrocycle and synthetic intermediates for the macrocycle (Figure 1b). Specifically, the designed DBPHZ **10** possesses two bromo functionalities at the 2,12-positions as reactive sites, and two sterically demanding siloxy groups (TIPSO–) at the 3,11-positions as solubilizing substituents. The dibromo functionalities at the 2,12-positions are geometrically well aligned for macrocycle formation. Moreover, the bulky siloxy substituents adjacent to the ring-connecting sites are expected to twist the entire π-conjugated framework, owing to steric repulsion between the siloxy groups and the bay-positioned C–H bonds. This overall twisting of the dimeric structure, together with the presence of peripheral diaryl groups, is anticipated to suppress intermolecular interactions and thereby enhance solubility in organic solvents.

As described in Chapter 1, London dispersion interactions between alkyl groups and solvent molecules are effective for enhancing the solubility of DBPHZ derivatives. Given this finding, the author planned to introduce alkylated silyl groups into the DBPHZ core. Since the Si–C bond is longer than the C–C bond, intermolecular steric repulsion of silyl groups is expected to be greater than that of simple alkyl groups. Also, from the synthetic viewpoint,

siloxy groups are easily installed to the DBPHZ core by silylation of hydroxy groups (HO–). Furthermore, the siloxy groups are expected to be convertible into good leaving groups such as triflate (TfO–) and tosylate (TsO–) for extending π-conjugation via Pd-catalyzed coupling reactions.

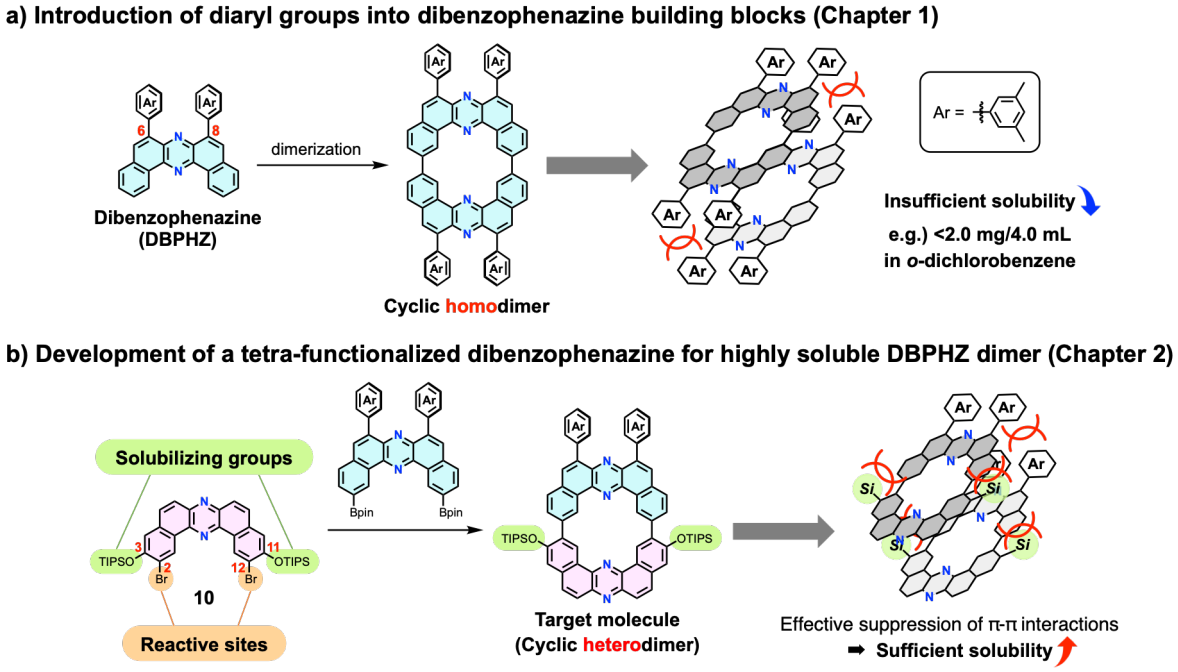
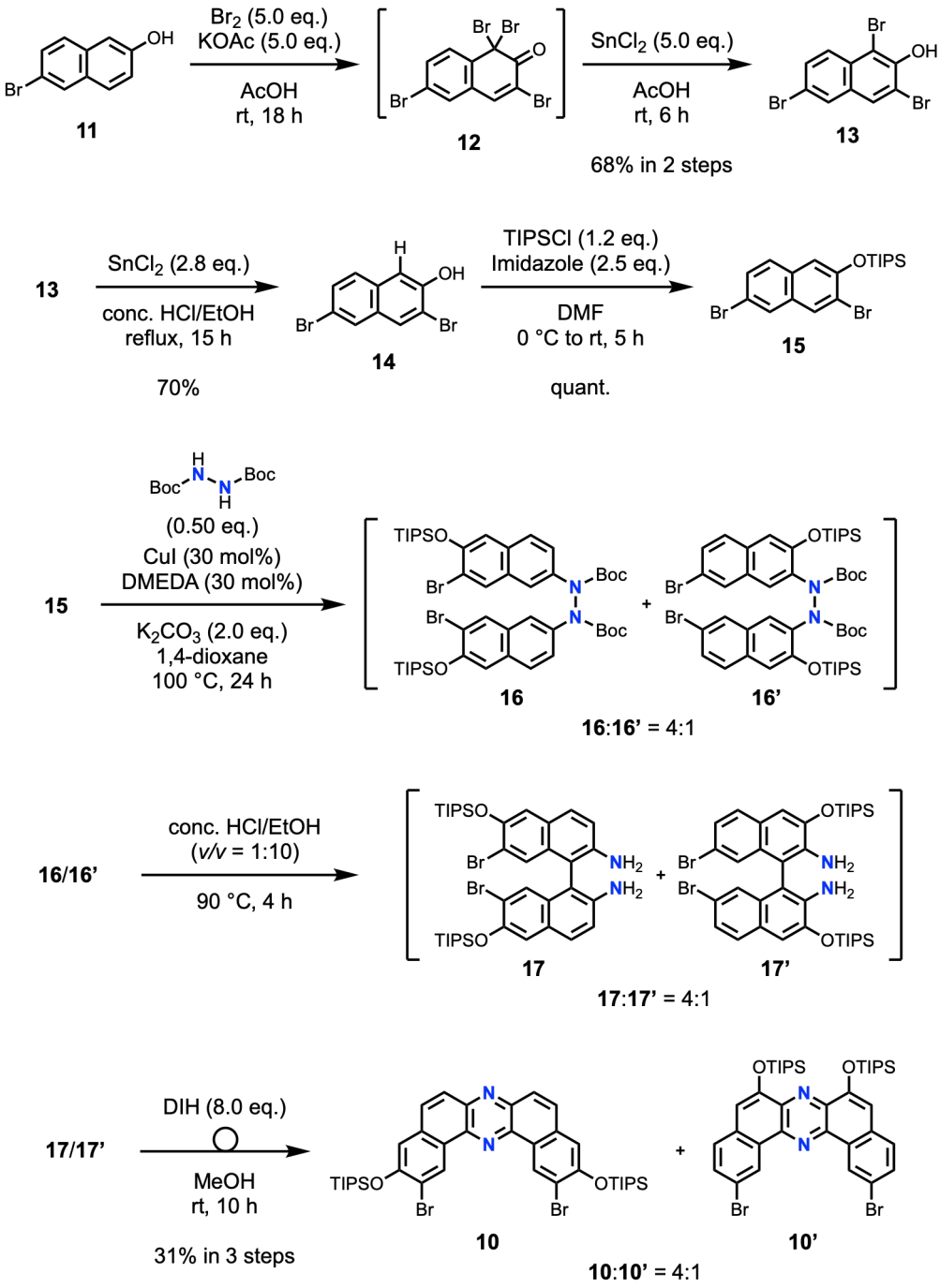


Figure 1. a) Previous and b) new design for improving solubility of DBPHZ cyclic dimers.

2-2. Synthesis of Tetra-Functionalized Dibenzo[*a*,*j*]phenazine and Solubility Enhancement

The synthetic route of the tetra-functionalized DBPHZ is outlined in Scheme 1 (for the detailed experimental procedures, see the section **2-8.**). Initially, monobromo-2-naphthol **11** was tribrominated with bromine to produce tetrabromonaphthalen-2-one **12** by following reported procedures[1] with slight modifications. Since compound **12** is readily decomposed under air or in silica gel to form complex mixtures, the crude product was employed in the following reaction without further purification. Subsequently, reduction of the bromo groups in **12** was performed using $SnCl_2$ as a reductant. However, due to the large amount of inorganic

solid byproducts generated from $SnCl_2$ after the reaction, the work-up and purification of the crude mixture was found to be complicated. Thus, a two-step reduction protocol was adopted. First, reduction of **12** using $SnCl_2$ at room temperature yielded tribromo-2-naphthol **13** in 60% over two steps. Subsequently, reduction of **13** with $SnCl_2$ under reflux conditions gave 3,6-dibromo-2-naphthol **14** in 70% yield in a regioselective manner. The phenoxy group of **14** was then silylated[2] with triisopropylsilylchloride (TIPSCl) in the presence of imidazole as a base to give 2,7-dibromo-siloxynaphthalene **15** in quantitative yield. Importantly, a Cu-catalyzed Ullmann-type N-amination[3] of **15** with *N,N′*-bis(Boc)-protected hydrazine (**15**:hydrazine = 2:1) afforded the desired biaryl hydrazine **16** and its regioisomer **16'** with moderate regioselectivity (4:1). The regioselectivity likely arises at the oxidative addition step, wherein the sterically less-demanding bromide undergoes oxidative addition preferentially. Since these isomers were obtained as an inseparable mixture, the mixture was carried forward to the next transformation. Deprotection of the *N*-Boc groups of **16**/**16'** under acidic condition[4], followed by a [3,3]-sigmatropic rearrangement and subsequent tautomerization, successfully afforded the corresponding 1,1'-binaphthalene-2,2'-diamine (BINAM) derivatives **17**/**17'** as a mixture containing a small quantity of impurities. Although the original isomeric ratio was preserved, further purification was difficult. Therefore, subjecting the BINAM mixture (**17**/**17'**) directly to the oxidative skeletal rearrangement conditions[5] successfully produced tetra-functionalized DBPHZs **10**/**10'** (**10**/**10'** = 4:1) in 31% yield over three steps, starting from **15**. Even though the separation of the regioisomers again proved very challenging, they were obtained without deteriorating any functionalities. Notably, dibromo DBPHZs **10**/**10'** with siloxy groups dissolved well even in nonpolar solvents such as diethyl ether (solubility: 4.0 mg/1.0 mL at 20 °C).



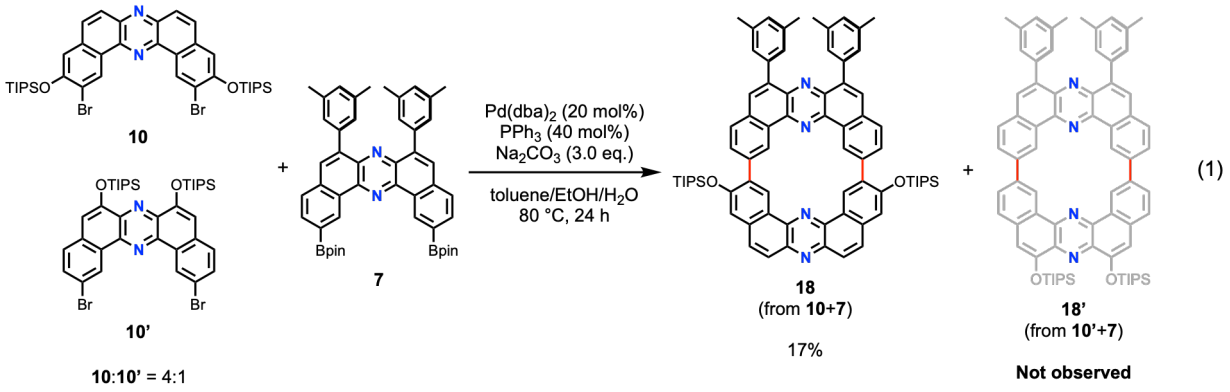
Scheme 1. Synthetic route to tetra-functionalized DBPHZ **10**.

2-3. Synthesis of Cyclic Heterodimer of U-Shaped DBPHZ

With the highly soluble tetra-functionalized DBPHZ building block **10** in hand, the synthesis of DBPHZ cyclic heterodimer was carried out (eq 1). Most importantly, a Pd-catalyzed Suzuki–Miyaura cross-coupling reaction[6] between the mixture of dibromide

10/**10'** and 6,8-diarylated diboryl compound **7** in a diluted condition (~8 mM)[7] successfully afforded a yellow crude solid. MALDI-TOF mass spectrometry of the crude product confirmed the formation of heterodimer **18** (*m/z* = 1109.56 for $[M+H]^+$) (Figure 2). In contrast to the case of the homodimer, the entire crude product was soluble in chloroform. Thus, purification was performed by simple silica gel column chromatography and reprecipitation without any difficulties to give the desired cyclic heterodimer **18** in 17% yield. Product **18** was fully characterized by spectroscopic and mass analysis (e.g., ^{1}H and ^{13}C NMR, IR, MS, and HRMS).

On the other hand, another cyclic heterodimer **18'**, arising from the minor dibromide **10'**, was not isolated, and its formation was not definitively confirmed. For compound **10'**, the reduced steric hindrance at the reaction site compared to the major compound **10** may have led to side reactions of oligomerization, resulting in a lower yield of heterodimer **18'**. Although 92% of the mass was recovered, only 17% corresponded to product **18**. The crude ^{1}H NMR spectrum was broad, and the major byproducts were not identified.



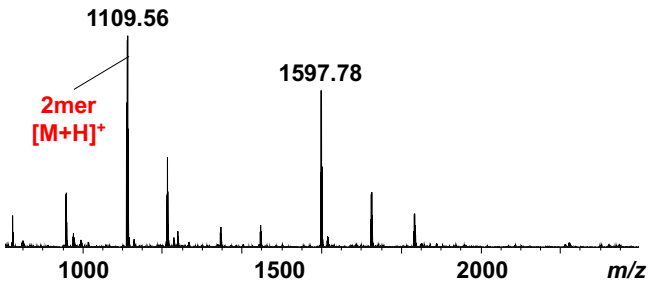


Figure 2. MALDI-TOF mass spectrum of crude product.

2-4. Solubility Enhancement of Heterodimer

The solubility of heterodimer **18** in organic solvents was investigated and compared with that of homodimer **8** (Figure 3 and Table S1). Notably, heterodimer **18** dissolves readily in common organic solvents at room temperature or under heated conditions. This stands in contrast to homodimer **8**, which exhibits only slight solubility (the upper limit concentration is in the μM range) in some aromatic solvents such as *o*-dichlorobenzene (*o*-DCB) (~2 mg/4 mL). This indicates that, as expected from the molecular design, the introduction of the siloxy groups significantly improved solubility by suppressing intermolecular interactions.

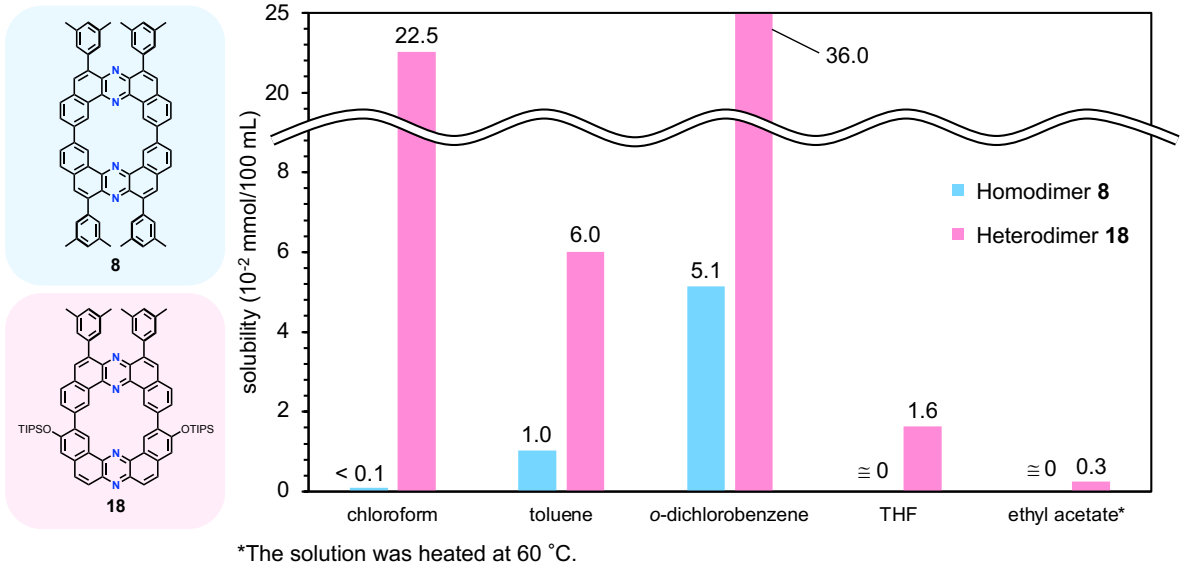


Figure 3. Solubility of DBPHZ cyclic dimers in organic solvents.

2-5. Structural Analysis of DBPHZ Cyclic Heterodimer by ^{1}H NMR Spectroscopy

To elucidate the electronic structure of cyclic heterodimer **18**, the ^{1}H NMR spectra of **18** and starting materials (**10** and **7**) were measured in $CDCl_3$ at room temperature (Figure 4). Heterodimer **18** showed well-resolved aromatic signals (Figure 4a). Compared with homodimer **8** (Figure 4d), the spectrum of **18** exhibited a clear decrease in molecular symmetry from D_2 to C_2, consistent with the coexistence of two distinct C_2 symmetric DBPHZ units. The most distinctive signal corresponds to the hydrogens at the 1,13-positions of the DBPHZ core,

which are commonly observed in the downfield region (δ > 9 ppm).[5] Compared with the corresponding ^{1}H NMR signals in precursors **10** (δ = 9.71 ppm; Figure 4b) and **7** (δ = 10.18 ppm; Figure 4c), the signals of heterodimer **18** were detected in the further downfield region (δ = 10.58 and 10.52 ppm; Figure 4a). This downfield shift indicates the steric compression effect[8] from proximal hydrogen atoms and/or an additional deshielding effect caused by the diatropic ring current from the adjacent DBPHZ unit. In contrast, the signals of **18** were observed with a slight upfield shift compared to that of the homodimer **8** measured in *o*-DCB-d_4 (δ = 11.1 ppm; Fig. 4d).

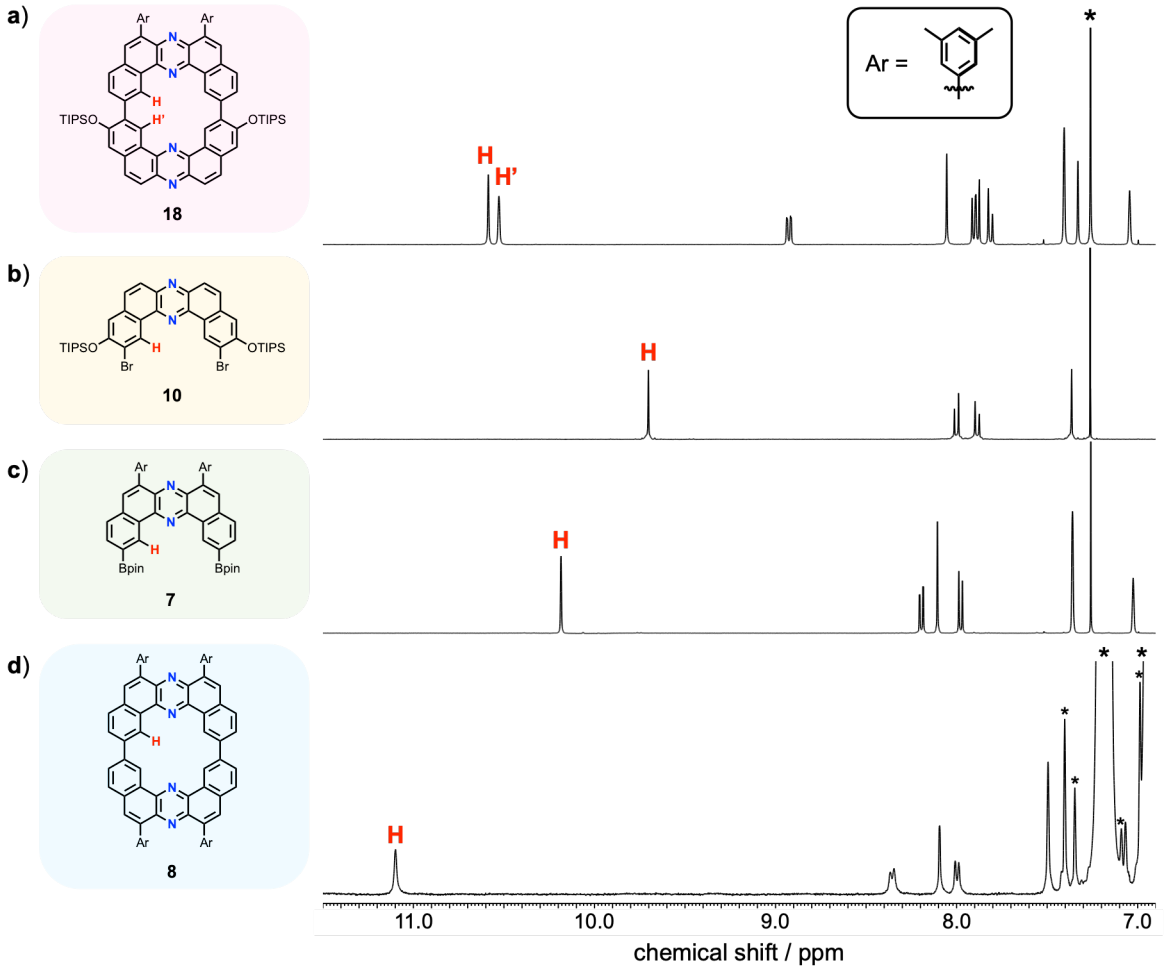


Figure 4. The aromatic region of ^{1}H NMR spectra of a) **18**, b) **10**, c) **7** and d) **8**.

2-6. Structural Analysis of DBPHZ Cyclic Heterodimer by DFT Calculations

Despite repeated attempts to obtain single crystals of heterodimer **18**, no crystals suitable for X-ray crystallographic analysis were obtained. This is likely due to its enhanced solubility in organic solvents. To explore its geometry, quantum chemical calculations using the DFT method were conducted (Figure 5). The optimized structure of compound **18** revealed a dihedral angle between the terminal benzene rings of the DBPHZ unit is 18.8° and a twist angle of the biphenylene bridge is 24.1°. In contrast, the corresponding helix angle and torsional angle for homodimer **8** are significantly smaller (9.7° and 13.8°, respectively). This difference is attributed to increased steric congestion at the connecting point of the two DBPHZ units. The introduction of sterically demanding siloxy groups adjacent to the biphenylene bridge causes the DBPHZ core to bend more and the biaryl unit to twist further.

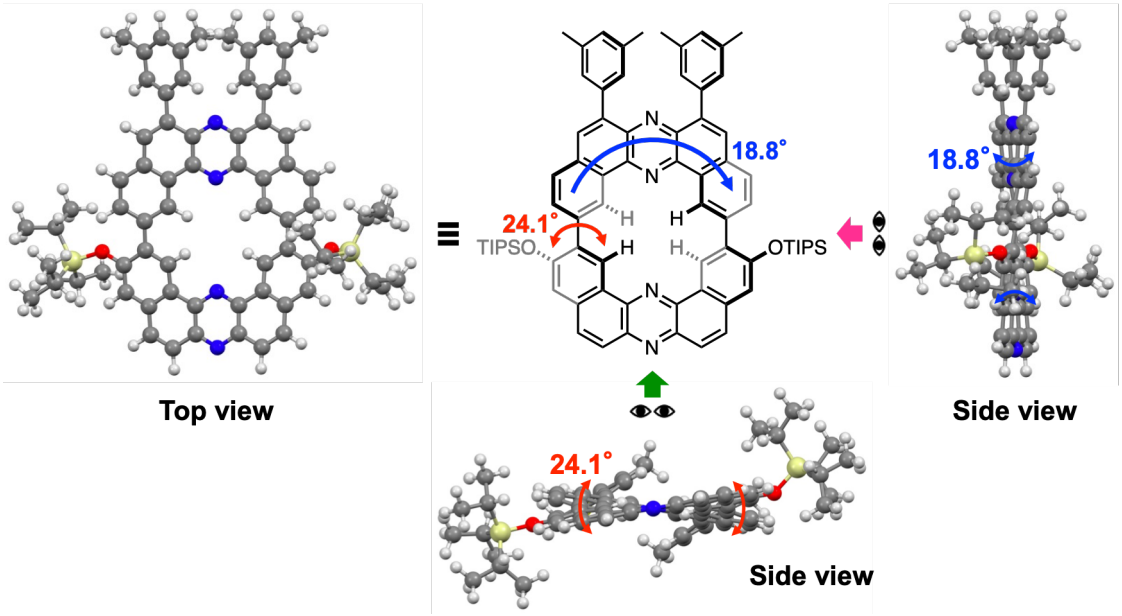


Figure 5. Optimized structure of **18** calculated at the PBE0/6-31G(d,p) level in $CHCl_3$.

2-7. Summary

In Chapter 2, the author described the design and synthesis of a new tetra-functionalized DBPHZ building block **10** to improve the solubility of DBPHZ cyclic dimers. The concise

synthetic route has been established while retaining all key functional groups, and the resulting compound **10** exhibits significantly improved solubility in nonpolar solvents. Moreover, DBPHZ cyclic heterodimer **18** has been successfully synthesized by utilizing **10** as a key building block. In clear contrast to the poorly soluble homodimer **8**, heterodimer **18** dissolves readily in common organic solvents, confirming the effectiveness of the introduction of siloxy groups. ^{1}H NMR spectroscopy and DFT calculations showed that **18** adopts a C_2 symmetric, more highly helical and twisted geometry than **8** due to increased steric congestion near the biphenylene bridge. This steric congestion, introduced by the siloxy groups, is attributed to the solubility enhancement of heterodimer **18**. Thus, the study described in Chapter 2 has established a practical strategy for enhancing the solubility of DBPHZ cyclic dimers, providing a robust platform for the photophysical studies disclosed in Chapter 3.

2-8. Experimental Section

General Remarks.

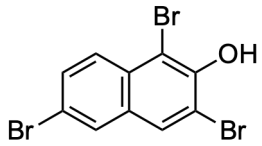
All reactions were carried out under an atmosphere of nitrogen unless otherwise noted. Products were purified by chromatography on silica gel Chromatorex BW-300 and NH-DM1020 (Fuji Silysia Chemical Ltd.). Analytical thin-layer chromatography (TLC) was performed on pre-coated silica gel glass plates (Merck silica gel 60 F_{254} TLC plate and Fuji Silysia Chromatorex NH, 0.25 mm thickness). Compounds were visualized with UV lamp. Melting points were determined using a Stanford Research Systems MPA100 OptiMelt Automated Melting Point System. All ^{1}H and ^{13}C NMR were recorded on a JEOL JNM-ECZL400S Spectrometer (^{1}H NMR: 400 MHz; ^{13}C NMR: 100 MHz). ^{1}H NMR chemical shifts were determined relative to tetramethylsilane (0.0 ppm) as an internal standard in $CDCl_3$. ^{13}C NMR chemical shifts were determined relative to $CDCl_3$ (77.00 ppm). Infrared spectra were acquired on a SHIMADZU IRAffinity-1 FT-IR Spectrometer. Mass spectra and high-resolution mass spectra were obtained on JEOL JMS-700 Mass Spectrometer or JEOL JMS-S3000 Mass Spectrometer.

Materials.

Dehydrated toluene used for organic synthesis was purified by passing through a solvent purification system. Other commercial reagents were purchased from TCI or Wako Pure Chemical Industries, Ltd., and were used as received.

Synthetic Procedures and Spectroscopic Data of New Compounds.

1,3,6-tribromonaphthalen-2-ol (13) [CAS No. 2623-40-7]

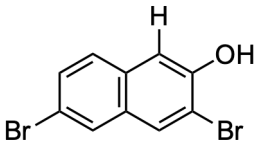


The title compound **13** was prepared according to a similar method reported in the literature[1] with a slight modification. To a three-necked round-bottom flask (300 mL) equipped with a magnetic stirring bar, were added 6-bromo-2-naphthol (**11**) (6.98 g, 31.3 mmol) and KOAc (15.3 g, 156 mmol, 5.0 eq.). To the flask, acetic acid (AcOH) (50 mL) was added, and the resulting suspension was stirred at room temperature under ultrasonication until solids were completely dissolved. To the resulting solution, Br_2 (25.0 g, 156 mmol, 5.0 eq.) was added dropwise over 10 minutes using a Pasteur pipette. The flask was sealed with two rubber septa and a glass stopper, and the resulting mixture was stirred at room temperature for 18 hours. The reaction mixture was poured into ice water (400 mL). The resulting precipitates were separated by suction filtration, washed off with deionized water (200 mL), and dried under vacuum in a desiccator to give a pale yellow solid (27.7 g) containing **12** and small quantities of impurities. Compound **12** is readily decomposed under air or in silica gel to form complex mixtures. Therefore, the crude product was employed in the following reaction without further purification.

To a three-necked round-bottom flask (300 mL) equipped with a magnetic stirring bar, were added the crude solid (27.7 g), $SnCl_2$ (29.6 g, 156 mmol, 5.0 eq.), and acetic acid (AcOH) (80 mL). The flask was sealed with three rubber septa, and the resulting suspension was stirred at room temperature for 16 hours. The reaction mixture was poured into 20% hydrochloric acid (90 mL). The resulting precipitates were separated by suction filtration and dried under vacuum in a desiccator to give white solid (30.7 g). The solid was dissolved in $CHCl_3$, and the solution was washed with water. The aqueous layer was extracted with $CHCl_3$ (50 mL×3). The combined organic extracts were dried over Na_2SO_4 and filtered, and the solvents in the filtrate were removed under reduced pressure to give brown crude solid (13.2 g). The obtained solid was recrystallized from acetone (100 mL) to give the title compound **13** as a white solid (7.15 g, 18.8 mmol, 60% in 2 steps). mp 129 °C; R_f 0.45 (*n*-hexane/EtOAc 8:2); ^{1}H NMR (400 MHz, $CDCl_3$) δ 7.95 (s, 1H), 7.91 (d, J = 8.8 Hz, 1H), 7.86 (d, J = 2.0 Hz, 1H), 7.63 (dd, J = 8.8, 2.0 Hz, 1H), 6.21 (s, 1H); ^{13}C NMR (100 MHz, $CDCl_3$) δ 147.5, 131.4, 130.5, 130.45, 130.42,

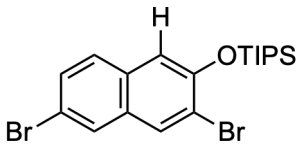
129.0, 127.6, 119.0, 112.0, 106.3; IR (ATR, cm^{-1}): 3402 (br), 3385, 3342, 1575, 1550, 1483, 1375, 1352, 1300, 1240, 1176, 1139, 1070, 1020, 931, 891, 808, 767; MS (EI^+, direct): *m/z* (relative intensity, %): 384 ($[M+6]^+$, 31), 382 ($[M+4]^+$, 95), 380 ($[M+2]^+$, 100), 378 (M^+, 33), 272 (13), 193 (13), 191 (16); HRMS (EI^+, direct): *m/z* calcd for $C_{10}H_5Br_3O$ (M^+) 377.7890, found 377.7888.

3,6-dibromonaphthalen-2-ol (14) [CAS No. 102153-55-9]



The title compound **14** was prepared according to a similar method reported in the literature[1] with a slight modification. To a three-necked round-bottom flask (200 mL) equipped with a magnetic stirring bar, were added 1,3,6-tribromonaphthalen-2-ol (**13**) (7.15 g, 18.8 mmol) and $SnCl_2$ (9.96 g, 52.5 mmol, 2.8 eq.). To the flask, EtOH (75 mL) and conc. HCl (7.5 mL) were added. The flask was equipped with an air-cooled condenser tube (Asynt, CondenSyn™) and sealed with two rubber septa. The resulting mixture was stirred in an aluminum heating block under a reflux condition (aluminum block temperature: 90 °C) for 15 hours. The reaction mixture was allowed to cool down to room temperature and neutralized with sat. $NaHCO_3$ aq. (100 mL). $CHCl_3$ (100 mL) was added to the mixture and the solution was washed with water. The aqueous layer was extracted with $CHCl_3$ (50 mL×3). The combined organic extracts were dried over Na_2SO_4 and filtered. The solvents in the filtrate were removed under reduced pressure to give white crude solid (5.91 g). The obtained solid was recrystallized from $CHCl_3$ to give the title compound **14** as a white solid in 69% yield (3.93 g, 13.0 mmol). mp 124 °C; R_f 0.25 (*n*-hexane/EtOAc 8:2); ^1H NMR (400 MHz, $CDCl_3$) δ 7.93 (s, 1H), 7.84 (d, J = 2.0 Hz, 1H), 7.56 (d, J = 8.8 Hz, 1H), 7.50 (dd, J = 8.8, 2.0 Hz, 1H), 7.35 (s, 1H), 5.64 (s, 1H); ^{13}C NMR (100 MHz, $CDCl_3$) δ 149.7, 132.3, 130.27, 130.22, 128.6, 128.2, 118.0, 113.6, 110.78 (one aryl carbon signal was not detected, probably due to the overlap of signals in this regime); IR (ATR, cm^{-1}): 3498 (br), 3062, 3047, 3028, 2981, 1581, 1485, 1454, 1409, 1265, 1192, 1149, 1138, 1062, 997, 916, 902, 875, 854, 804, 734; MS (EI^+, direct): *m/z* (relative intensity, %): 304 ($[M+4]^+$, 48), 302 ($[M+2]^+$, 100), 300 (M^+, 51), 223 ($[M–Br+2]^+$, 3), 221 ($[M–Br]^+$, 4), 142 ($[M–2Br]^+$, 6), 113 (14); HRMS (EI^+, direct): *m/z* calcd for $C_{10}H_6Br_2O$ (M^+) 299.8785, found 299.8789.

Synthesis of ((3,6-dibromonaphthalen-2-yl)oxy)triisopropylsilane (15)



The title compound **15** was prepared according to a similar method reported in the literature[2] with a slight modification. To a two-necked round-bottom flask (100 mL) equipped with a magnetic stirring bar, were added 3,6-dibromonaphthalen-2-ol (**14**) (1.70 g, 5.63 mmol), imidazole (985.3 mg, 14.1 mmol, 2.5 eq.), and dehydrated DMF (12 mL). The flask was sealed with two rubber septa, evacuated, and refilled with nitrogen gas through a syringe needle connected to a double vacuum manifold for three times. The flask was cooled to 0 °C in an ice bath, and triisopropylsilylchloride (TIPSCl) (1.43 mL, 1.30 g, 6.74 mmol, 1.2 eq.) was added dropwise to the flask through the septum with a syringe. After the completion of addition of TIPSCl, the resulting mixture was allowed to warm up to room temperature and stirred for 5 hours. Water (12 mL) was added to the flask, and the organic layer was extracted with EtOAc (15 mL×3), and washed twice with brine (15 mL×2). The combined organic extracts were dried over Na_2SO_4 and filtered, and the solvents in the filtrate were removed under reduced pressure to give yellow crude oil (2.69 g). The crude residue was purified by flash column chromatography on silica gel (eluent: *n*-hexane) to give the title compound **15** as a white solid in 99% yield (2.56 g, 5.59 mmol). mp 41 °C; R_f 0.80 (*n*-hexane/EtOAc 8:2); ^{1}H NMR (400 MHz, $CDCl_3$) δ 7.96 (s, 1H), 7.82 (s, 1H), 7.51 (d, J = 8.8 Hz, 1H), 7.47 (dd, J = 8.8, 1.2 Hz, 1H), 7.16 (s, 1H), 1.39 (septet, J = 7.6 Hz, 3H), 1.16 (d, J = 7.6 Hz, 18H); ^{13}C NMR (100 MHz, $CDCl_3$) δ 150.8, 131.9, 131.2, 130.4, 129.6, 128.4, 127.9, 118.3, 117.9, 114.0, 18.0, 12.9; IR (ATR, cm^{-1}): 2943, 2926, 2889, 2864, 1579, 1481, 1456, 1382, 1355, 1303, 1253, 1211, 1165, 1139, 1062, 1012, 987, 927, 879, 862, 792; MS (EI^+, direct): *m/z* (relative intensity, %): 460 ($[M+4]^+$, 5), 458 ($[M+2]^+$, 10), 456 (M^+, 5), 417 ($[M+4–^iPr]^+$, 51), 415 ($[M+2–^iPr]^+$, 100), 413 ($[M–^iPr]^+$, 48), 380 (9), 378 (8), 337 (11), 335 (11); HRMS (EI^+, direct): *m/z* calcd for $C_{19}H_{26}Br_2OSi$ (M) 456.0120, found 456.0111.

2,12-dibromo-3,11-bis(triisopropylsiloxy)dibenzo[*a,j*]phenazine
(Tetra-functionalized DBPHZ) (10)

*Synthesis of di-tert-butyl 1,2-bis(7-bromo-6-(triisopropylsiloxy)naphthalen-2-yl)hydrazine -1,2-dicarboxylate (**16**) (Step 1)*

Compound **16** was prepared according to a similar method reported in the literature[3] with a slight modification. To a two-necked reaction tube (50 mL) equipped with a magnetic stirring bar, were added compound **15** (3.21 g, 7.00 mmol), 1,2-bis(*tert*-butoxycarbonyl)hydrazine (813.0 mg, 3.50 mmol, 0.50 eq.), CuI (404 mg, 2.1 mmol, 30 mol%), K_2CO_3 (1.93 g, 14.0 mmol, 2.0 eq.), and *N,N'*-dimethylethylenediamine (DMEDA) (185 mg, 2.10 mmol, 30 mol%). The reaction tube was sealed with two rubber septa, evacuated, and refilled with nitrogen gas through a syringe needle connected to a double vacuum manifold for three times. Dehydrated 1,4-dioxane (20 mL) was added to the tube, and the resulting mixture was stirred at room temperature for 10 min. The reaction mixture was stirred in a Personal Organic Synthesizer (EYELA, *Chemi-Station*) equipped with a cooling system under a reflux condition (aluminum block temperature: 105 °C) for 36 hours. The reaction mixture was allowed to cool down to room temperature. $CHCl_3$ (50 mL) was added to the mixture, which was then filtered through a Celite pad, and the solvents were evaporated from the filtrate under reduced pressure. The concentrated mixture was extracted with $CHCl_3$ (30 mL×3). The combined organic extracts were dried over Na_2SO_4 and filtered, and the solvents in the filtrate were removed under reduced pressure to give viscous brown crude solid (3.67 g). The solid residue was purified by flash column chromatography on NH silica gel (eluent: *n*-hexane/EtOAc 10:0–9:1) to give the mixture of the title compound **16** and its regioisomer **16'** with small quantities of impurities as a white solid (1.88 g, **16**:**16'** = 4:1 determined by the integration of diagnostic signals). These regioisomers were not separated by silica gel column chromatography, HPLC, and GPC. Therefore, the product mixture was used for the next reaction as is. R_f 0.55 (*n*-hexane/EtOAc 2:8, NH silica); ^{1}H NMR (400 MHz, $CDCl_3$) mixture of **16**:**16'** ~ 4:1 δ 8.22 (s, 0.44H, minor isomer), 7.95 (s, 2H, major isomer), 7.90–7.40 (br, 7H, both isomers), 7.15 (s, 2H, major isomer), 7.09 (s, 0.62H, minor isomer), 1.55 (s, 25H, both isomers), 1.38 (septet, J = 7.6 Hz, 8H, both isomers), 1.15 (d, J = 7.2 Hz, 42H, both isomers); ^{13}C NMR (100 MHz, $CDCl_3$) mixture of **16**:**16'** ~ 4:1 δ 153.2 (br), 152.3, 150.4, 139.0, 137.5 (br), 132.0, 131.5 (br), 130.0, 129.37, 129.30, 126.8 (br), 122.3 (br), 117.6, 114.1, 113.8, 112.0, 82.6, 28.2, 18.1, 18.0, 13.0, 12.9 (Four carbon signals in the aromatic region and two in the aliphatic region were not

observed, likely due to overlap or broadening of signals); IR (ATR, cm^{-1}): 2941, 2866, 2164, 1718, 1589, 1458, 1365, 1336, 1296, 1251, 1149, 1060, 1010, 997, 939, 881, 852, 792, 736; MS (ESI^+, direct): *m/z* (relative intensity, %): 1011 ($[M+Na+4]^+$, 71), 1009 ($[M+2+Na]^+$, 100), 1007 ($[M+Na]^+$, 48), 931 (36), 929 (27); HRMS (ESI, positive, MeCN): *m/z* calcd for $C_{48}H_{70}N_2O_6NaSi_2Br_2$ ($[M+Na]^+$) 1007.3031, found 1007.3038.

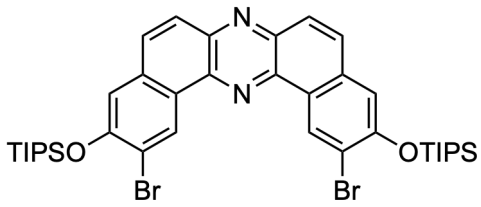
*Synthesis of 7,7'-dibromo-6,6'-bis(triisopropylsiloxy)-[1,1'-binaphthalene]-2,2'-diamine (**17**) (Step 2)*

Compound **17** was prepared according to a similar method reported in the literature[4] with a slight modification. To a three-necked flask (100 mL) equipped with a magnetic stirring bar, were added a mixture of **17** and **17'** (0.60 g), EtOH (5.0 mL), and conc. HCl (0.5 mL). The flask was equipped with an air-cooled condenser tube (Asynt, CondenSyn™) and sealed with three rubber septa. The resulting mixture was stirred in an aluminum heating block under a reflux condition (aluminum block temperature: 90 °C) for 12 hours. The reaction mixture was allowed to cool down to room temperature and neutralized with sat. $NaHCO_3$ aq. (50 mL). The organic layer was extracted with $CHCl_3$ (50 mL×3). The combined organic extracts were dried over Na_2SO_4 and filtered, and the solvents in the filtrate were removed under reduced pressure to give viscous brown crude solid (0.430 g). The solid residue was purified by flash column chromatography on silica gel (eluent: *n*-hexane/$CHCl_3$ 95:5–8:2) to give the mixture of the title compound **17** and its regioisomer **17'** with small quantities of impurities as brown solids (65.2 mg, **17**:**17'** = 4:1 determined by the integration of diagnostic signals). These regioisomers were not separated by silica gel column chromatography, HPLC, and GPC. Therefore, the product mixture was used for the next reaction as is. R_f 0.15 (*n*-hexane/EtOAc 2:8); ^1H NMR (400 MHz, $CDCl_3$) mixture of **17**:**17'** ~ 4:1 δ 7.60–7.57 (m, 3.2H, both isomers), 7.50 (s, 0.54H, minor isomer), 7.25–7.22 (m, 3.3H, both isomers), 7.18 (s, 2H, major isomer), 7.13 (s, 0.56H, minor isomer), 7.09 (d, J = 8.4 Hz, 3.2H, both isomers), 3.58 (br, 7H, both isomers), 1.39 (septet, J = 7.6 Hz, 10.8H, both isomers), 1.16 (d, J = 6.4 Hz, 58H, both isomers); ^{13}C NMR (100 MHz, $CDCl_3$) δ 149.8, 147.9, 141.5, 141.3, 134.7, 130.0, 129.5, 129.1, 128.3, 127.9, 119.3, 119.0, 118.1, 114.8, 113.0, 111.2, 110.0, 94.5, 18.1, 18.0, 13.0, 12.9 (Two carbon signals in the aromatic region and one in the aliphatic region were not observed, likely due to overlap or broadening of signals); IR (ATR, cm^{-1}): 3471, 3373, 2943, 2864, 1618, 1587, 1483, 1458, 1381, 1352, 1257, 1170, 1145, 1108, 920, 877, 842, 812; MS (FAB^+, direct, NBA matrix): *m/z*

(relative intensity, %) 788 ($[M+4]^+$, 6), 7.86 ($[M+2]^+$, 9), 785 ($[M+1]^+$,4), 784 (M^+, 4), 754 (5), 708 (8), 706 (7), 664 (6), 662 (6), 350 (16), 348 (14), 270 (39), 115 (25), 87 (39), 73 (62), 59 (100), 45 (23); HRMS (FAB^+, direct): *m/z* calcd for $C_{38}H_{54}Br_2N_2O_2Si_2$ (M^+) 784.2091, found 784.2064.

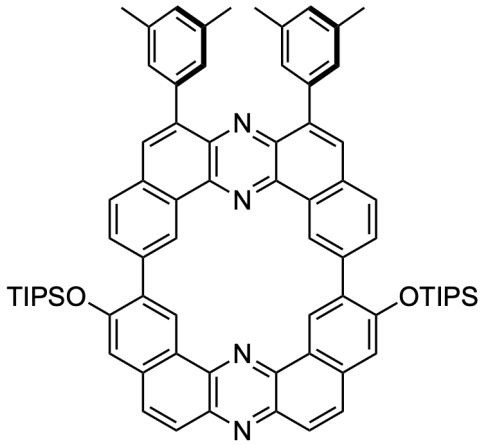
*Synthesis of 2,12-dibromo-3,11-bis(triisopropylsiloxy)dibenzo[a,j]phenazine (**10**) (Step 3)*

The title compound **10** was prepared according to a similar method reported in the literature[5] with a slight modification. To a two-necked round-bottom flask (100 mL) equipped with a magnetic stirring bar, were added a mixture of **17** and **17'** (399.0 mg, 0.507 mmol) and MeOH (20 mL). The resulting suspension was stirred at room temperature under ultrasonication until the solid was completely dissolved. The flask equipped with a ground-glass joint connected to a double vacuum manifold was sealed with a rubber septum and a glass stopper, evacuated, and refilled with nitrogen gas for three times. To the solution, 1,3-diiodo-5,5-dimethylhydantoin (DIH) (1.55 g, 4.08 mmol, 8.0 equiv.) was added, and the resulting mixture was stirred at room temperature for 10 hours. $Na_2S_2O_3$ aq. (1 M, 100 mL) was added to the reaction mixture, and the organic layer was extracted with $CHCl_3$ (30 mL×3). The combined organic extracts were dried over Na_2SO_4 and filtered, and the solvents in the filtrate were removed under reduced pressure to give yellowish brown crude solid (404 mg). The solid residue was purified by flash column chromatography on silica gel (eluent: *n*-hexane/EtOAc 97:3–8:2) to give yellow solid containing compound **10** and its regioisomer **10'** with small quantities of impurities, which was then reprecipitated from $CHCl_3$/*n*-hexane (> 1:20) to provide compound **10** and its regioisomer **10'** in 31% yield in 3 steps (240 mg, 0.306 mmol) as a yellow solid. R_f 0.40 (*n*-hexane/EtOAc 8:2, silica gel); ^1H NMR (400 MHz, $CDCl_3$) **10**:**10'** ~ 4:1 δ 9.92 (s, 0.48H, minor isomer), 9.68 (s, 2H, major isomer), 7.98 (d, J = 9.2 Hz, 2.51H, both isomers), 7.88–7.85 (m, 2.55H, both isomers), 7.35 (s, 2H, major isomer), 7.29 (s, 0.44H, minor isomer), 1.46 (septet, J = 7.6 Hz, 8.6H, both isomers), 1.21 (d, J = 7.2 Hz, 44H, both isomers); The major regioisomer **10** was isolated by silica-gel chromatography during the recovery of unreacted starting materials in the subsequent step aimed at synthesizing compound **18**. (14 mg).



Tetra-functionalized DBPHZ **10**: mp 218 °C (dec.); ^{1}H NMR (400 MHz, $CDCl_3$) δ 9.70 (s, 2H), 8.00 (d, J = 9.2 Hz, 2H), 7.88 (d, J = 9.6 Hz, 2H), 7.36 (s, 2H), 1.47 (septet, J = 7.2 Hz, 6H), 1.21 (d, J = 8.0 Hz, 36H); ^{13}C NMR (100 MHz, $CDCl_3$) δ 153.9, 141.6, 139.8, 133.7, 131.1, 130.2, 127.6, 126.0, 117.7, 116.1, 18.0, 13.0; IR (ATR, cm^{-1}): 2864, 1587, 1462, 1442, 1344, 1278, 1249, 1149, 1001, 904, 877, 862, 815, 788; MS (FAB^+, direct, NBA matrix): *m/z* (relative intensity, %): 785 ($[M+4+H]^+$, 30), 783 ($[M+2+H]^+$, 45), 781 ($[M+H]^+$, 21), 705 ($[M+4–Br]^+$, 9), 703 ($[M+2–Br]^+$, 11), 657 (10), 655 (13), 653 (11), 138 (10), 115 (17), 87 (27), 73 (44), 59 (100), 45 (20); HRMS (FAB^+, direct): *m/z* calcd for $C_{38}H_{51}Br_2N_2O_2Si_2$ ($[M+H]^+$) 781.1850, found 781.1861.

3,7-bis(3,5-dimethylphenyl)-29,33-bis((triisopropylsilyl)oxy)-4,6:17,19-di(azeno)-1,25:9,11:12,14:22,24-tetraethenotetrabenzo[*b*,*h*,*k*,*q*][1,10]diazacyclooctadecine (Cyclic heterodimer) (18)



The title compound **17** was prepared according to a similar method reported in the literature[6] with a slight modification. A two-necked reaction tube (50 mL) equipped with a magnetic stirring bar and two rubber septa were dried in a vacuum oven at 80 °C for 2 hours before use. Dehydrated toluene and deionized water were degassed through freeze-pump-thaw cycling three times before use. To the tube, were added a mixture of **10** and **10'** (234 mg, 0.299 mmol, **10**:**10'**=4:1), 2,12-diboryl-6,8-diaryl dibenzo[*a*,*j*]phenazine **7** (222 mg, 0.300 mmol, 1.0 eq. against the total amount of **9**/**9'**), $Pd(dba)_2$ (34 mg, 59 mmol, 20 mol%), PPh_3 (31 mg, 0.12

mmol, 40 mol%), and Na_2CO_3 (95 mg, 0.90 mmol, 3.0 eq.). The reaction tube was sealed with two rubber septa, evacuated, and refilled with nitrogen gas through a syringe needle connected to a double vacuum manifold for three times. Dehydrated toluene (18 mL), dehydrated EtOH (4.5 mL), and deionized water (4.5 mL) were added to the tube, and the resulting mixture was stirred at room temperature for 10 min. The reaction mixture was stirred in a Personal Organic Synthesizer (EYELA, *Chemi-Station*) equipped with a cooling system (aluminum block temperature: 80 °C) for 24 hours. The reaction mixture was allowed to cool down to room temperature, and toluene and EtOH were removed under reduced pressure. Water (50 mL) was added to the mixture, and the organic layer was extracted with $CHCl_3$ (100 mL×3). The combined organic extracts were dried over Na_2SO_4 and filtered, and the solvents in the filtrate were removed under reduced pressure to give yellowish crude solid (473 mg). The solid residue was purified by flash short column chromatography on NH silica gel (eluent: *n*-hexane/$CHCl_3$ = 9:1–5:5) to give yellow solid containing cyclic heterodimer **18** and small quantities of impurities, which was then reprecipitated from $CHCl_3$/*n*-hexane (> 1:20) to provide the dimer **18** in 17% yield (55.4 mg, 49.9 mmol) as a yellow solid. mp 321 °C; R_f 0.80 (*n*-hexane/$CHCl_3$ 1:1, NH silica); ^{1}H NMR (400 MHz, $CDCl_3$) δ 10.58 (s, 2H), 10.52 (s, 2H), 8.92 (dd, J = 8.0, 1.2 Hz, 2H), 8.05 (s, 2H), 7.90 (d, J = 8.0 Hz, 2H), 7.88 (d, J = 9.2 Hz, 2H), 7.81 (d, J = 9.2 Hz, 2H), 7.40 (s, 4H), 7.33 (s, 2H), 7.04 (s, 2H), 2.25 (s, 12H), 1.36 (septet, J = 7.6 Hz, 6H), 1.10 (d, J = 7.2 Hz, 36H); ^{13}C NMR (100 MHz, $CDCl_3$) δ 155.4, 141.6, 141.0, 140.9, 139.9, 138.2, 138.1, 136.8, 135.8, 133.6, 132.2, 130.8, 130.7, 130.6, 130.4, 130.1, 128.9, 128.7, 127.4, 127.1, 126.7, 125.7, 123.8, 117.4, 21.3, 17.9, 13.2; IR (ATR, cm^{-1}): 2945, 2866, 1602, 1539, 1496, 1473, 1456, 1373, 1344, 1290, 1197, 1153, 1141, 1076, 1008, 995, 916, 875, 864, 846, 819, 790; MS (FAB$^+$, direct, NBA matrix): *m/z* (relative intensity, %) 1109 ([M+H]$^+$, 5), 1065 ([M–*i*Pr]$^+$, 4), 307 (44), 289 (31), 154 (100), 138 (83), 137 (99), 136 (98), 107 (64), 91 (25), 90 (42), 89 (62), 77 (51); HRMS (MALDI-TOF, positive, DCTB matrix): *m/z* calcd for $C_{74}H_{76}N_4O_2Si_2$ (M$^+$) 1108.5501, found 1108.5497.

Investigation of the Solubility of Heterodimer in Organic Solvents

A 15 mL vial was charged with heterodimer **18** (2.0 mg) and 0.5 mL of each solvents ($CHCl_3$, toluene, and THF). The mixture was subjected to ultrasonication at room temperature for 5 min. If **18** did not dissolve completely, an additional 0.5 mL portion of the same solvent was added, and ultrasonication was resumed for another 5 min. This process was repeated, adding 0.25–0.50 mL aliquots of solvent and ultrasonication, until dissolution was achieved. Since compound **18** was slightly soluble in EtOAc, it was placed in a 200 mL round-bottom flask, and EtOAc (10 mL portions) was added repeatedly while heating at 60 °C in a water bath until the dissolution of **18** was completely achieved. Compound **18** showed very poor solubility in acetone, MeCN, and EtOH (Table 1).

Table 1. Summary of the solubility of heterodimer **18** in various organic solvents.

Solvent	Solubility
$CHCl_3$	2 mg / 0.8 mL
toluene	2 mg / 3 mL
THF	2 mg / 11 mL
EtOAc*	2 mg / 70 mL
Acetone	< 0.1 mg / 4.5 mL
MeCN	< 0.1 mg / 4.5 mL
EtOH	< 0.1 mg / 4.5 mL

*The solution was heated at 60 °C in water bath.

Quantum Chemical Calculations

All quantum chemical calculations were performed using Gaussian 16. Geometry optimizations were carried out at the PBE0/6-31G(d,p) level with the IEFPCM solvation model ($CHCl_3$). Geometry coordinates are available as xyz files online.

2-9. References

1. Pangeni, D.; Nesterov, E. E. *Macromolecules* **2013**, *46*, 7266–7273.
2. Goyard, D.; Kónya, B.; Chajistamatiou, A. S.; Chrysina, E. D.; Leroy, J.; Balzarin, S.; Tournier, M.; Tousch, D.; Petit, P.; Duret, C.; Maurel, P.; Somsák, L.; Docsa, T.; Gergely, P.; Praly, J.-P.; Azay-Milhau, J.; Vidal, S. *Eur. J. Med. Chem.* **2016**, *108*, 444–454.
3. Klapars, A.; Huang, X.; Buchwald, S. L. *J. Am. Chem. Soc.* **2002**, *124*, 7421–7428.
4. Lim. Y.-K.; Jung, J.-W.; Lee, H.; Cho, C.-G. *J. Org. Chem.* **2004**, *69*, 5778–5781.
5. Takeda, Y.; Okazaki, M.; Minakata, S. *Chem. Commun.* **2014**, *50*, 10291–10294.
6. Zhou, P.; Fu, Y.; Wang, M.; Qiu, R.; Wang, Y.; Stoddart, J. F.; Wang, Y.; Chen, H. *J. Am. Chem. Soc.* **2023**, *145*, 18800–18811.
7. (a) Martí-Centelles, V.; Pandey, M. D.; Burguete, M. I.; Luis, S. V. *Chem. Rev.* **2015**, *115*, 8736–8834. (b) Caso, C.; Altmann, K.-H. *Chem. Eur. J.* **2025**, *31*, e202402664.
8. (a) Cheney, B. V. *J. Am. Chem. Soc.* **1968**, *90*, 5386–5390. (b) Zeng, Z.; Qasem, A. M. A.; Blagbrough, I. S.; Woodman, T. J. *Org. Biomol. Chem.* **2024**, *22*, 7915–7935.

Chapter 3

Investigation of Photophysical Properties and Functional Exploration of Cyclic Dimers of Dibenzo[*a,j*]phenazine

3-1. Introduction

Dibenzo[*a,j*]phenazine (DBPHZ) derivatives are promising emissive materials exhibiting fluorescence both in solution and in the solid state.[1] In addition to their high electron-accepting character, the rigid, U-shaped π-conjugated framework and embedded nitrogen atoms make DBPHZ attractive as a building block for functional macrocyclic architectures. When two DBPHZ units are covalently linked to form a cyclic dimer, new photophysical features that cannot be realized by monomeric DBPHZ are expected to emerge. Macrocyclization extends the effective π-conjugation length, leading to red-shifted absorption and emission. The enforced proximity of two chromophore units and the defined geometric structure form a highly planar architecture, potentially inducing further environment- or aggregation-dependent color changes such as excimer emission. Moreover, the presence of multiple pyrazine nitrogen atoms in a confined macrocyclic framework would offer an opportunity for multi-step acid responsiveness and other stimuli-induced optical changes through a host-guest interaction.

In this Chapter, the photophysical properties of the DBPHZ cyclic dimers synthesized in Chapter 1 (homodimer **8**) and Chapter 2 (heterodimer **18**) are investigated and compared with those of monomeric DBPHZ. Furthermore, functions that arise from their characteristic structures and properties were explored. As a result, acid-responsive behavior and aggregation-dependent emission in thin films were found.

3-2. Photophysical Properties of the Cyclic Homodimer of DBPHZ

First, the author focused on the cyclic homodimer of DBPHZ prepared in Chapter 1 and investigated its fundamental photophysical properties. The homodimer **8** dissolves in toluene at concentrations below the μM level. However, increasing the concentration up to the mM range is not feasible, probably because strong intermolecular interactions arising from its highly planar π-conjugated framework led to aggregation and limited solubility. UV-vis absorption

and fluorescence spectra were measured for the homodimer **8** in a dilute toluene solution (Figure 1). To reveal the effect of macrocyclization on photophysics, the spectra of homodimer **8** were compared with those of a representative DBPHZ monomer **19** measured in a dilute dichloromethane.[1a] In toluene, the homodimer **8** exhibits a broad absorption band with a maximum at 456 nm that extends to around 500 nm. The maximum absorption wavelength of **8** is observed in a markedly lower energy region relative to that of the DBPHZ monomer **19** (λ_{max} = 416 nm), indicating that the π-conjugated system in **8** is effectively extended over the entire dimeric framework. In contrast, the molar absorption coefficient of the homodimer **8** is smaller than that of monomer **19**, which could be attributed to the higher structural symmetry of homodimer **8** compared to monomer **19**. Upon excitation at 405 nm, the homodimer shows bright yellow–green fluorescence in toluene with an emission maximum at 495 nm. The maximum emission wavelength of **8** again appears in a redder region compared to that of the DBPHZ monomer **19** (λ_{max} = 425 nm), consistent with the extended π-conjugation inferred from the absorption spectra. In the solid state, the homodimer displays yellow emission with a maximum at 565 nm. In both solution and the solid state, the emission lifetimes of **8** are in the range of nanoseconds, indicating prompt fluorescence from the singlet excited state. However, the photoluminescence quantum yield of **8** decreases markedly upon going from solution to the solid state. This behavior suggests that the solid-state emission of the homodimer is strongly influenced by aggregation and is likely associated with excimer-like emissive states formed in the aggregated phase.

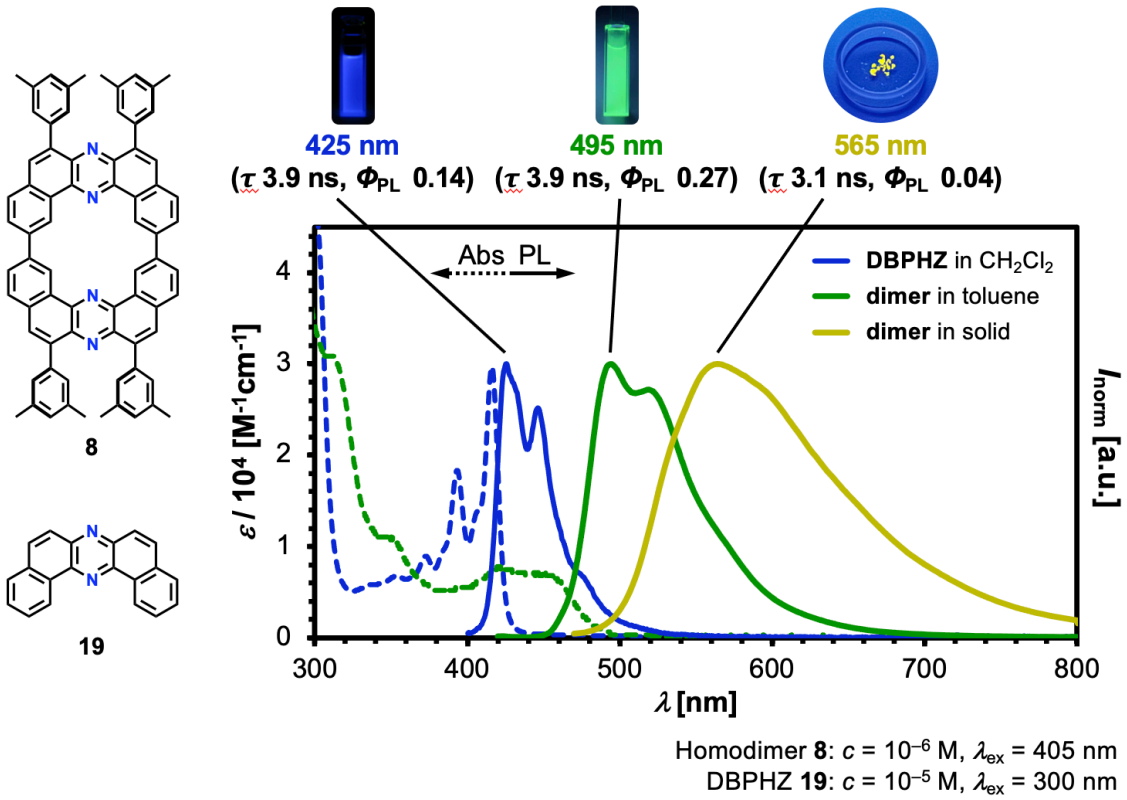


Figure 1. UV-vis absorption (Abs; dotted line) and photoluminescence (PL; solid line) of homodimer **8** and DBPHZ monomer **19**.

3-3. Frontier Molecular Orbitals of the Cyclic Homodimer of DBPHZ

To gain insight into the electronic structure of the homodimer **8**, the frontier molecular orbitals (FMOs) calculated using a quantum chemical method (PBE0/6-31G(d,p) level in $CHCl_3$) were analyzed. In the optimized geometry, both the HOMO and LUMO of **8** are delocalized over the entire dimeric DBPHZ framework (Figure 2). The calculated HOMO–LUMO energy gap (ΔE) for the homodimer is smaller (3.22 eV) than that of the DBPHZ monomer (3.75 eV), which is consistent with the experimental observation of red-shifts in absorption and emission spectra and thus supports the interpretation that macrocyclization leads to an effectively extended π-conjugated system. The calculated HOMO–LUMO gap (3.22 eV) of **8** is larger than the optical gap estimated from the crossing point of the absorption and emission spectra of the homodimer (E_{gap} = 2.66 eV, λ_{isec} = 466 nm). The optical bandgap is

much smaller than the HOMO–LUMO gap because photoexcitation generates bound excitons and therefore the required energy to absorb a photon to form an exciton pair is generally lower than that needed to produce free charge carriers. Both experimental and theoretical results consistently indicate that the macrocyclic structure reduces the energy gap relative to the monomer. Moreover, the distributions of FMOs suggest that the emissive excited state of the homodimer is dominated by locally excited (LE) character.

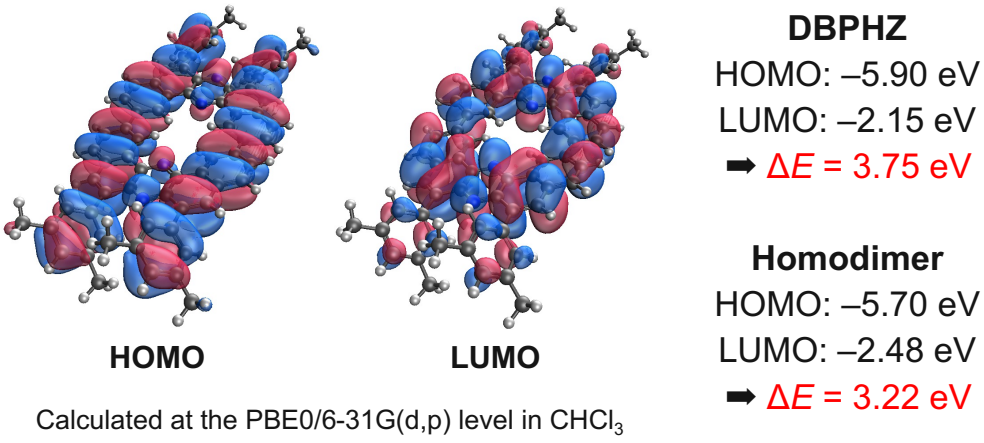


Figure 2. Frontier molecular orbitals (FMOs) of homodimer **8**.

3-4. Acid-Responsive Properties of the DBPHZ Cyclic Homodimer

Since the DBPHZ dimeric framework contains nitrogen atoms that have a lone pair, acid-responsive behavior is anticipated for the cyclic homodimer. Therefore, the photophysical properties of the homodimer **8** in an acidic solution were investigated. When an excess amount of trifluoroacetic acid (TFA) was added to a toluene solution of the homodimer **8**, the absorption band in the 400–500 nm region decreased, and a new broad band extending from 500 to 700 nm appeared (Figure 3). Concomitantly, the solution color changed distinctly from yellow to pink, indicating substantial modification of the electronic structure upon protonation.

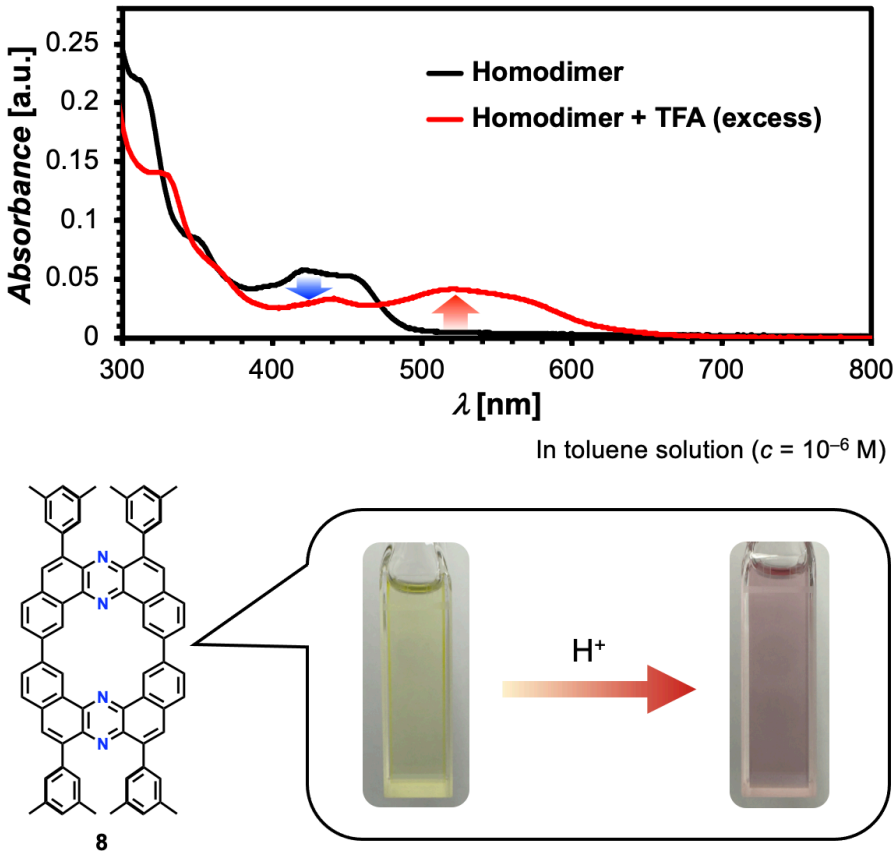
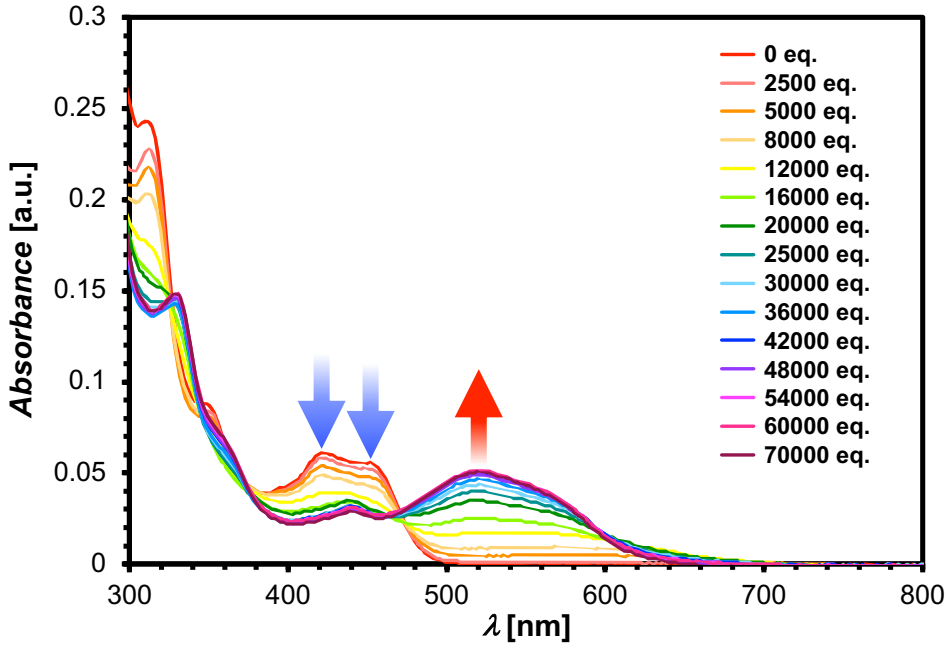


Figure 3. UV-vis absorption spectra of homodimer **8** with TFA and NEt_3.

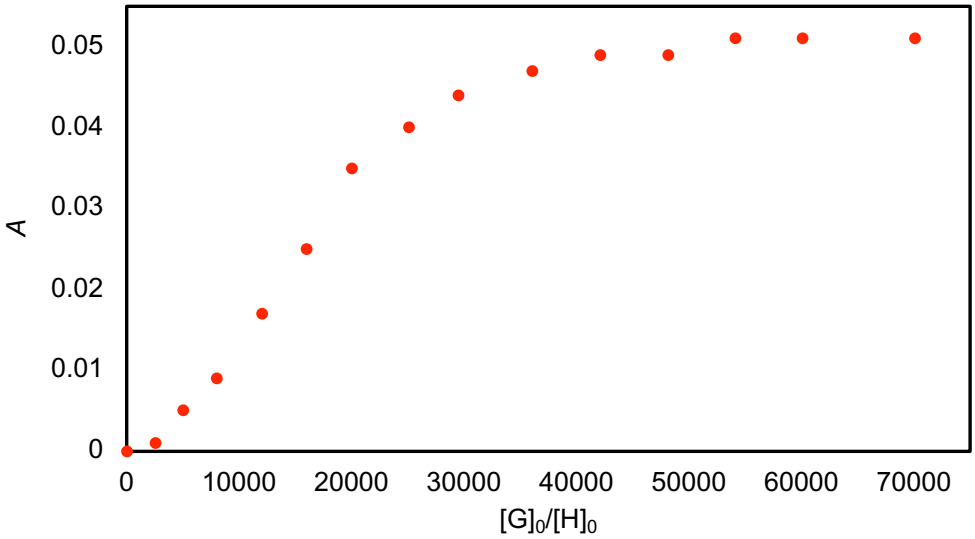
To analyze these photophysical changes more quantitatively, UV-vis absorption titration with TFA was performed (Figure 4). TFA was gradually added to a toluene solution of the homodimer while monitoring the absorption spectra. As the amount of TFA increased, the absorption band at 456 nm ascribed to the neutral homodimer gradually decreased, while the intensity of a new band at around 520 nm increased. The change in absorption spectra continued until the volume of added TFA reached approximately 70,000 equivalents. Fitting the isotherm of titration curve plotted from the absorbance at 520 nm with a 1:2 binding model afforded an association constant on the order of 10^1 M^{-1} (Figure 5).[2,3] Given the low basicity of the pyrazine nitrogen atoms (pK_{aH} = 0.37 in H_2O),[4] it is assumed that two equivalents of protons bind non-cooperatively to the pyrazine nitrogen of one macrocyclic host. It should be noted that the spectral changes were relatively small for the amount of acid added, because the

titration experiments were performed at very low concentrations (in the μM range). More accurate determination of the binding constants would ideally require measurements at higher concentrations (e.g., in the mM range) using ^{1}H NMR spectroscopy, but such experiments are hampered by the poor solubility of the homodimer. Thus, this experimental limitation inevitably leaves a certain degree of uncertainty in the association constant.



In toluene solution (c = 4.73 × 10^{-6} M) with TFA (c = 1.06 M) (λ_{ex} = 405 nm)

Figure 4. Absorption titration spectra of homodimer **8** with TFA.



In toluene solution (c = 4.73 × 10–6 M) with TFA (c = 1.06 M) (λ_{abs} = 520 nm)
K_a is determined by bindfit: http://supramolecular.org/bindfit.

Binding Constant of Homodimer for proton (H^+)

K_a = ~10^1 M^{-1} (Homodimer : H^+ = 1:2 model)

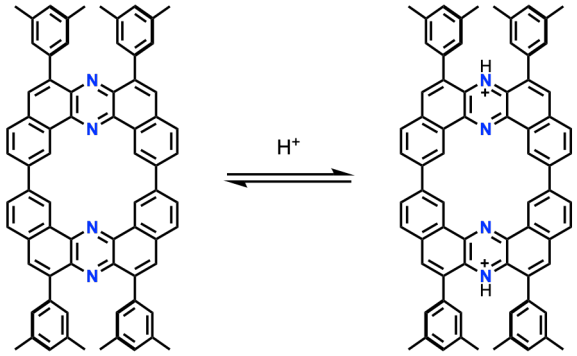
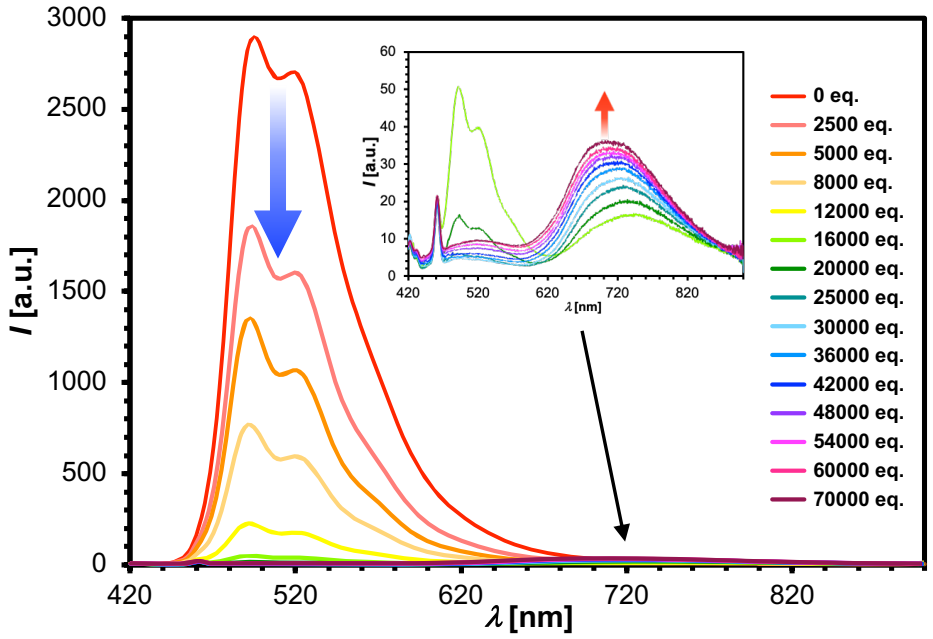


Figure 5. Titration curve and fitting model of homodimer **8** with TFA.

The titration emission spectra of the homodimer **8** were also investigated (Figure 6). Upon gradual addition of TFA, the emission band at around 500 nm ascribed to the neutral **8** decreases in intensity, and a weak new emission band appears at approximately 720 nm.



In toluene solution (c = 4.73 × 10^{-6} M) with TFA (c = 1.06 M) (λ_{ex} = 405 nm)

Figure 6. PL titration spectra of homodimer **8** with TFA.

When an excess amount of triethylamine (NEt_3) is added as a base to the TFA-treated solution, the original absorption and emission spectra of the neutral homodimer are recovered (Figure 7a). These observations demonstrate that the acid response of **8** is reversible and that the homodimer functions as a turn-off-type fluorescence switch (Figure 7b).

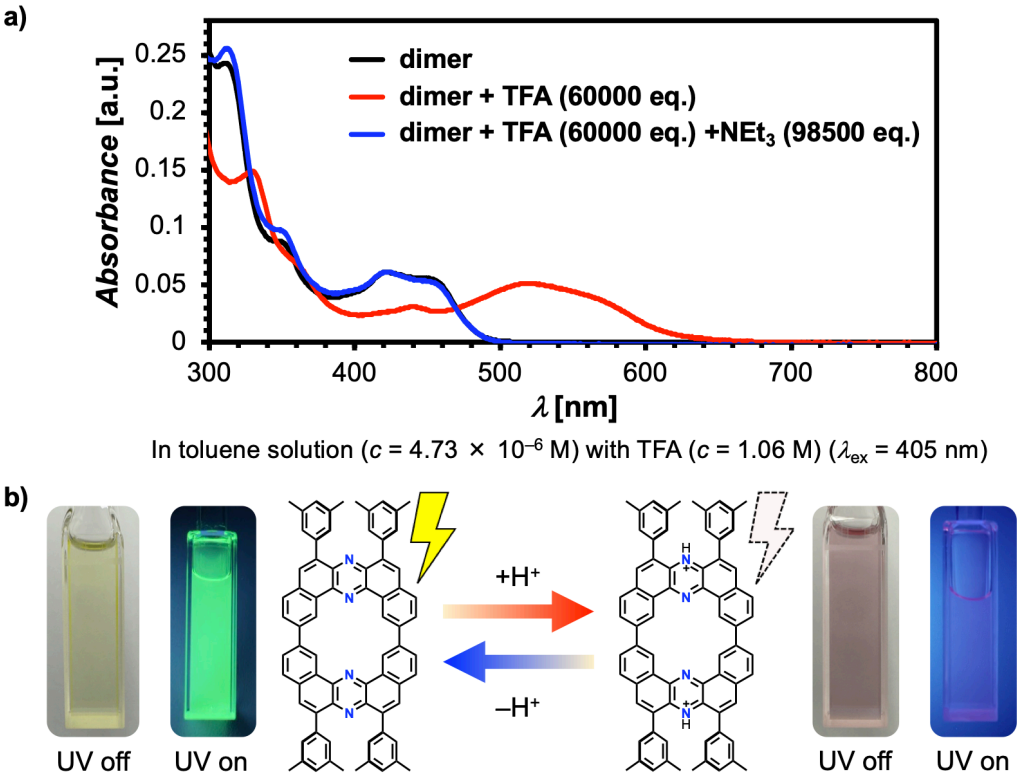


Figure 7. a) UV-vis absorption spectra of homodimer **8** with TFA and NEt_3 and b) The appearance of toluene solution of **8** (left) and **8** + TFA (right).

3-5. Prediction of Protonation Sites in the Cyclic Homodimer of DBPHZ

To identify the protonation sites in the homodimer, ^{1}H NMR spectra of DBPHZ monomer **20** and the cyclic homodimer **8** were measured in TFA-d_1 (Figure 8). For both monomer and cyclic homodimer, the signals corresponding to aromatic hydrogens of the DBPHZ framework were consistently shifted downfield upon protonation. On the other hand, ^{1}H NMR spectrum of a DBPHZ monomer derivative **21** in the form of its hydrochloride salt was also measured (Figure 9). In this case, the signals corresponding to the hydrogens at the 5,6- (or 7,8-) positions were clearly shifted downfield relative to those in the neutral state. This behavior suggests that protonation occurs at the outer pyrazine nitrogen atoms of the DBPHZ skeleton, leading to deshielding of the adjacent aromatic protons. Based on these results, it is reasonable to infer that, in the cyclic homodimer, both DBPHZ units would be preferentially

protonated at the outer pyrazine nitrogen atoms. The relatively small cavity of the optimized macrocyclic structure likely disfavors protonation at the inner nitrogen atoms for steric reasons (Figure 10). Thus, steric constraints play an important role in determining the protonation sites in the homodimer.

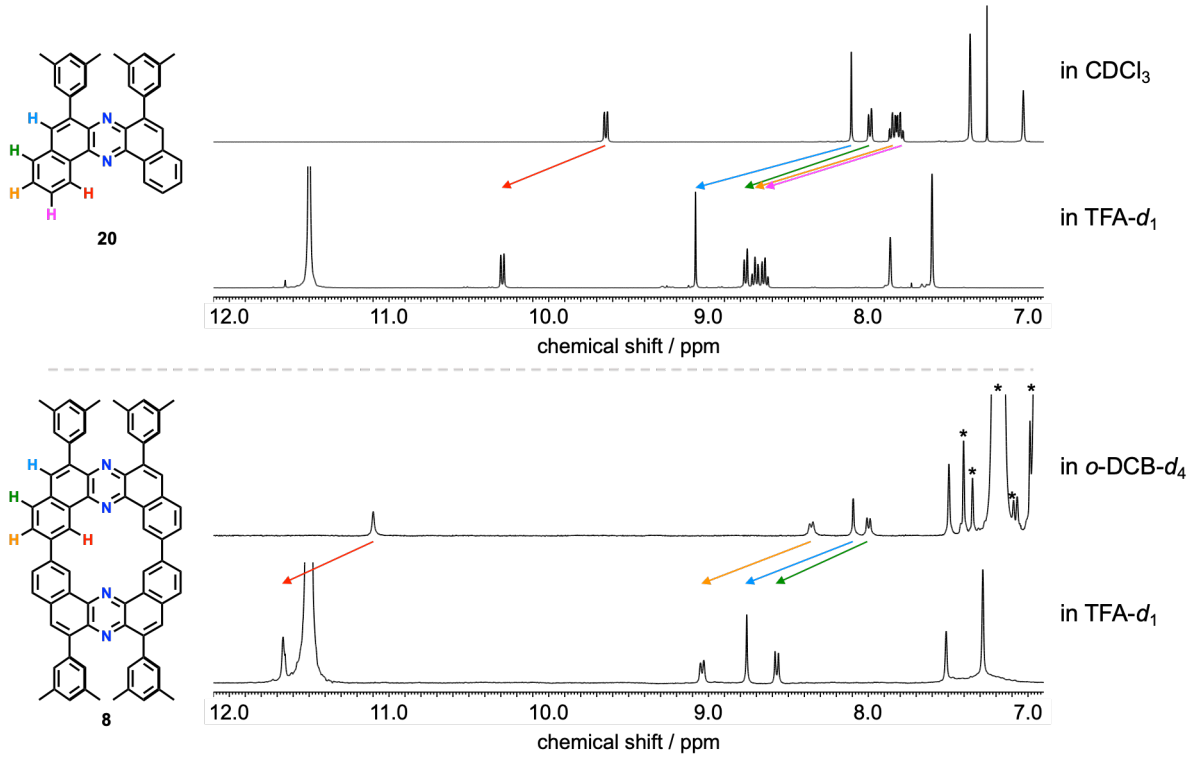


Figure 8. ^{1}H NMR spectra of DBPHZ monomer **20** and cyclic homodimer **8** in TFA-d_1.

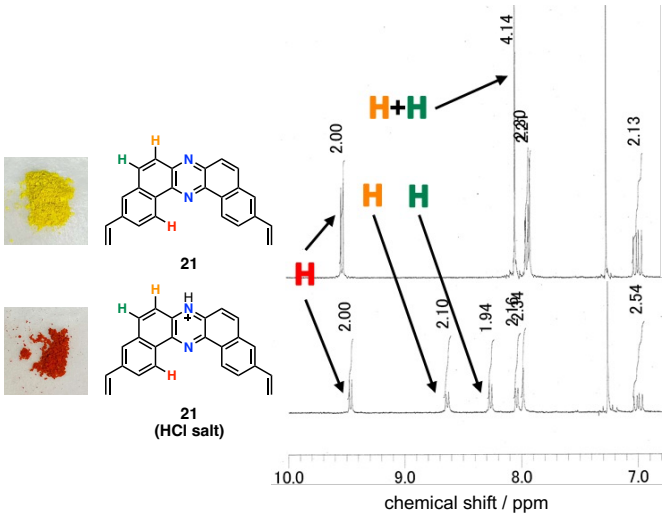


Figure 9. ^{1}H NMR spectra of DBPHZ derivative **21** and its HCl salt **21•HCl** in $CDCl_3$.

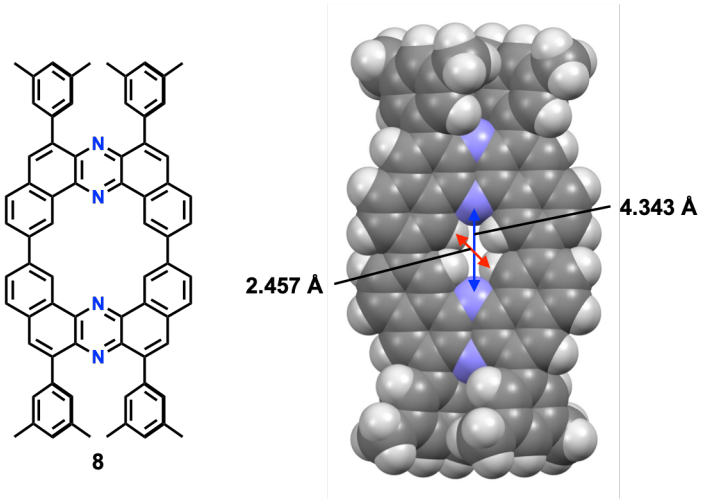


Figure 10. CPK model in the optimized structure of homodimer **8**.

3-6. Photophysical Properties of the Cyclic Heterodimer of DBPHZ in Solution

The author next investigated the photophysical properties of the cyclic heterodimer of DBPHZ synthesized in Chapter 2. Owing to the significantly improved solubility of the heterodimer **18** in organic solvents, systematic measurements could be carried out in a series of solvents with different polarities. The UV-vis absorption spectra of the heterodimer **18** in various dilute solutions show an absorption maximum at 437 nm that is essentially independent of solvent polarity (Figure 11). The maximum absorption wavelength of **18** appears in the bluer region relative to that of the homodimer (λ_{max} = 456 nm), indicating that the effective π-conjugation length of **18** is shorter than that of the homodimer **8**. This shortening in effective π-conjugation is ascribed to the increased twisting of the macrocyclic framework caused by steric repulsion between bulky siloxy groups and the bay-positioned C–H bonds, and the reduced number of aryl substituents at the periphery of the DBPHZ core in the heterodimer. In contrast to the absorption spectra, the emission spectra of the heterodimer **18** display slight positive solvatochromism: as the solvent polarity increases, the emission maximum shifts gradually to longer wavelength. This behavior suggests that the lowest excited state of the heterodimer has a weak charge-transfer (CT) character along with LE character.

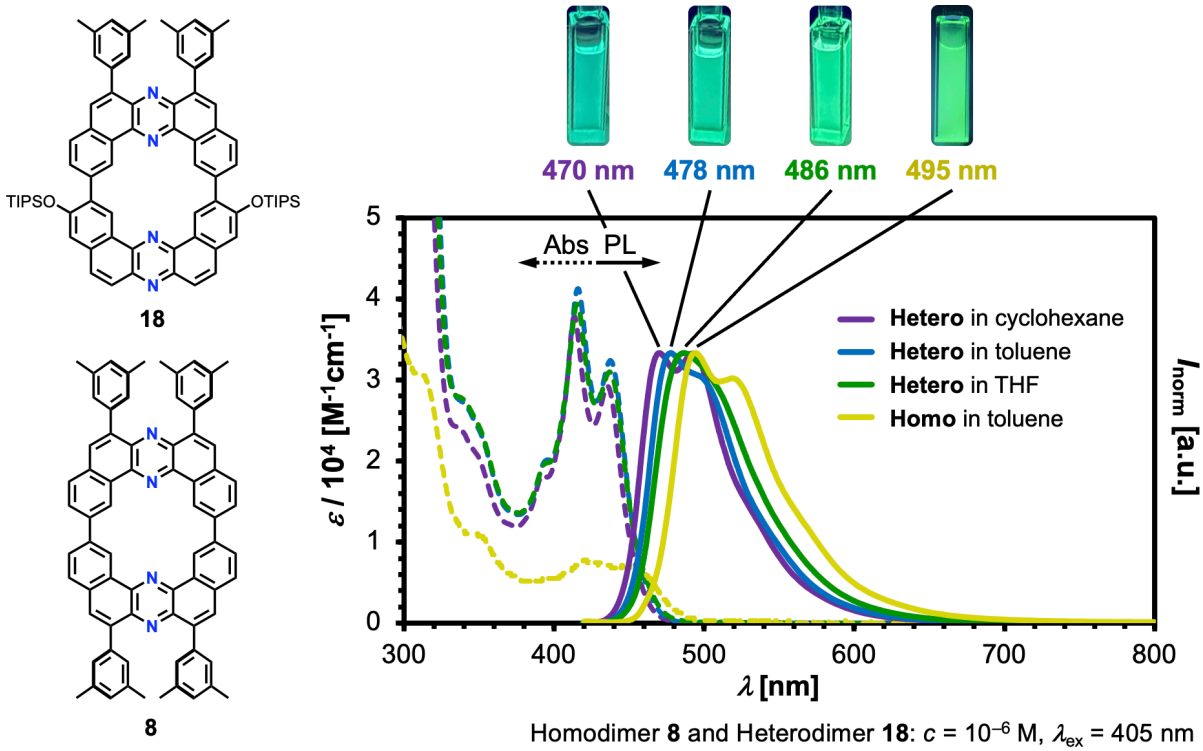


Figure 11. UV-vis absorption (Abs; dotted line) and photoluminescence (PL; solid line) of DBPHZ homodimer **8** and heterodimer **18**.

3-7. FMOs of the Cyclic Heterodimer of DBPHZ

To elucidate the electronic structure responsible for the photophysical behavior of the heterodimer, the FMOs were obtained by quantum-chemical calculations (Figure 12). As in the case of the homodimer, both the HOMO and LUMO of the heterodimer **18** are delocalized over the entire dimeric DBPHZ framework. Moreover, the HOMO of the heterodimer extends not only over the DBPHZ cores but also onto the oxygen atoms of the siloxy substituents. This distribution indicates that the siloxy groups act as weak electron donors, contributing to the HOMO and thereby inducing a charge-transfer (CT) character in the lowest excited state. This theoretical result is consistent with the experimentally observed weak solvatochromism in the emission spectra.

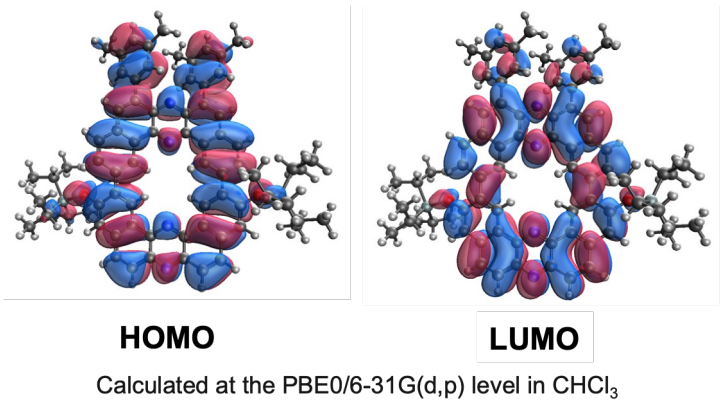


Figure 12. Frontier molecular orbitals (FMOs) of heterodimer **18**.

3-8. Photophysical Properties of the Cyclic Heterodimer of DBPHZ in Thin Films

The excellent solubility of the heterodimer **18** allowed the author to investigate its emission properties in the thin films. Thin films were prepared by dispersing the heterodimer at various concentrations in a nonpolar polymer matrix (Zeonex) and by forming neat films consisting of the heterodimer only. The photoluminescence spectra of these films were then measured (Figure 13). In the film with a dopant concentration of 0.1 wt%, the emission spectrum of **18** closely matches that observed in toluene solution, indicating that the heterodimer is homogeneously dispersed in the polymer matrix at this concentration. However, as the dopant concentration is increased from 0.1 to 10 wt%, the emission maximum gradually shifts to longer wavelength and the spectrum becomes broader. These trends suggest that aggregation of the heterodimer occurs progressively as the concentration increases. In the neat film composed of the heterodimer only, the emission is further red-shifted, and intense orange fluorescence with a maximum at 587 nm is observed. This pronounced bathochromic shift relative to the dilute film demonstrates that strong intermolecular interactions are operative in the neat film.

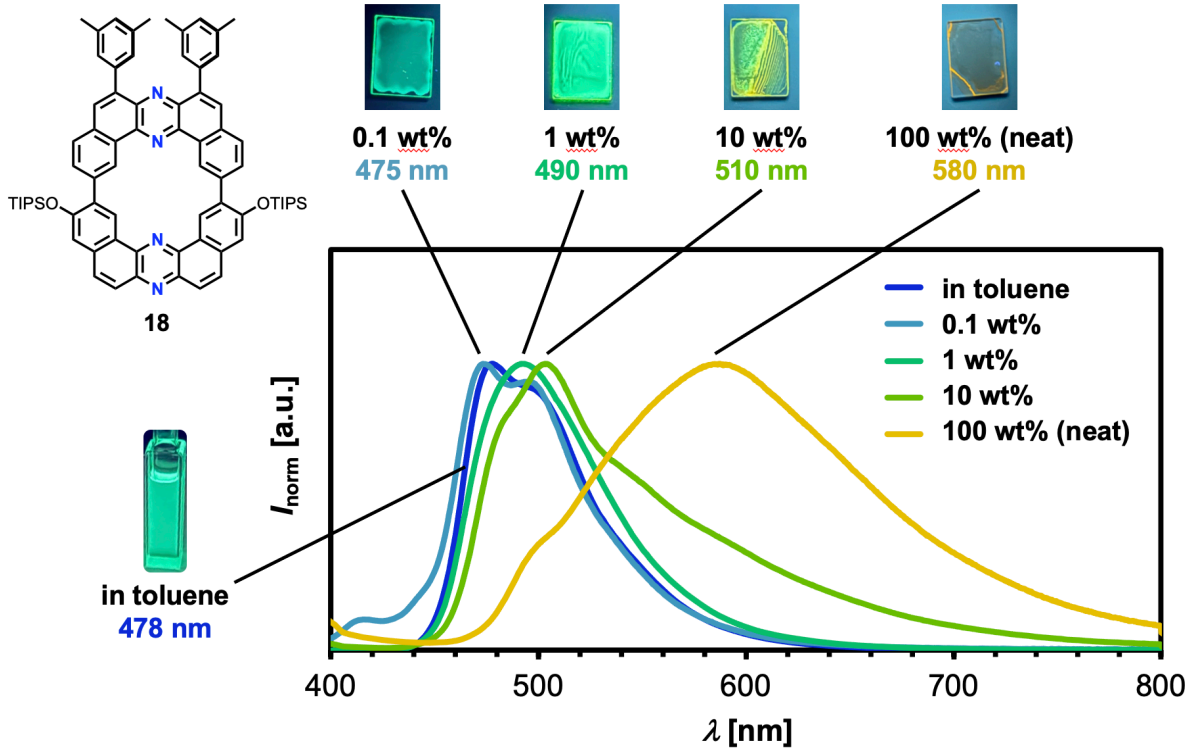


Figure 13. PL spectra of heterodimer **18** in thin films.

3-9. Elucidation of the Emission Process in Thin Films of the Cyclic Heterodimer

To clarify the emission mechanism of the heterodimer in thin films, photoluminescence quantum yields and emission lifetimes were measured for films with different dopant concentrations as well as for the neat film. As the concentration of the heterodimer in the Zeonex matrix increases, the photoluminescence quantum yield decreases, whereas the emission lifetime becomes progressively longer (Table 1). This combination of decreasing quantum yield and increasing lifetime indicates that the long-wavelength emission observed at higher concentrations originates from excimer-like states formed through intermolecular interactions. The concentration-dependent red-shift of the emission maximum is therefore attributed to the formation of such excimer-like emissive species. The author considers that this behavior is facilitated by the structural flexibility of the carbon–oxygen–silicon linkages in the siloxy substituents (Figure 14). Although these bulky groups enhance solubility in solution, the

flexible C–O–Si bonds allow rearrangement of the molecular packing in the condensed state, enabling close approach of neighboring macrocycles. As a result, strong intermolecular interactions such as π–π stacking can still operate in the films, giving rise to excimer-like emission that is sensitive to the degree of molecular aggregation.

Table 1. Summary of photophysics of heterodimer **18** in Zeonex films.

concentration (wt %)	0.1	1	10	100 (neat)
λ_{em} [nm]	475	490	510	580
Φ_{PL}	0.12	0.11	0.07	0.04
τ [ns]	2.27	3.04	3.14	4.67

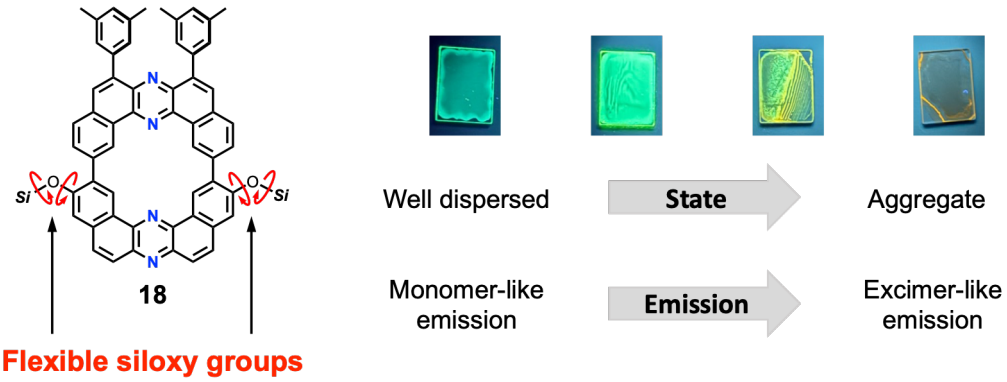


Figure 14. Summary of photophysical trend of heterodimer **18** in Zeonex films.

3-10. Summary

In Chapter 3, the photophysical properties of DBPHZ cyclic dimers were investigated and compared with those of monomeric DBPHZ derivatives. The results demonstrate that the cyclic dimer structures lead to effective extension of the π-conjugated system and to characteristic changes in the optical properties. For the cyclic homodimer, macrocyclization induces pronounced red-shifts in absorption and emission relative to the monomer, consistent

with delocalization of the frontier molecular orbitals over the entire macrocyclic framework. Taking advantage of the nitrogen atoms embedded in the cyclic π-conjugated skeleton, the homodimer exhibits reversible acid-responsive behavior, functioning as a turn-off-type fluorescence switch upon protonation. For the cyclic heterodimer, improved solubility enabled systematic studies in solution and in the thin films. The heterodimer shows a weakly charge-transfer excited state and displays concentration-dependent emission color changes in the solid state. In particular, the combination of flexible siloxy substituents and the macrocyclic framework leads to aggregation-induced formation of excimer-like emissive states, resulting in gradual red-shifts and lifetime elongation with increasing dopant concentration. Overall, these findings establish that DBPHZ-based cyclic dimers provide a versatile platform for tuning photophysical properties through macrocycle design, protonation, and control of aggregation, thereby opening new possibilities for functional organic materials based on nitrogen-embedded π-conjugated macrocycles.

3-11. Experimental Section

General Remarks.

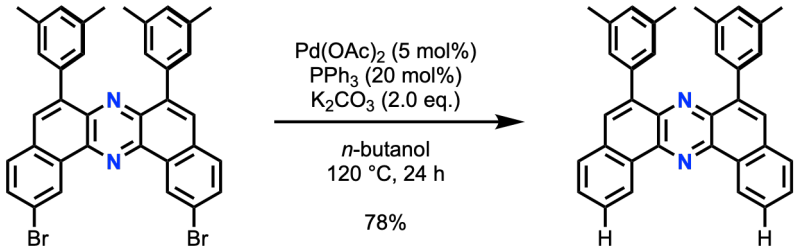
All reactions were carried out under an atmosphere of nitrogen unless otherwise noted. Products were purified by chromatography on silica gel Chromatorex BW-300 (Fuji Silysia Chemical Ltd.). Analytical thin-layer chromatography (TLC) was performed on pre-coated silica gel glass plates (Merck silica gel 60 F_{254} TLC plate, 0.25 mm thickness). Compounds were visualized with UV lamp. Melting points were determined using a Stanford Research Systems MPA100 OptiMelt Automated Melting Point System. All ^{1}H and ^{13}C NMR were recorded on a JEOL JNM-ECZL400S Spectrometer (^{1}H NMR: 400 MHz; ^{13}C NMR: 100 MHz). ^{1}H NMR chemical shifts were determined relative to tetramethylsilane (0.0 ppm) as an internal standard in $CDCl_3$ or the signals of residual non-deuterated trifluoroacetic acid (11.50 ppm) in trifluoroacetic acid-d_1. ^{13}C NMR chemical shifts were determined relative to $CDCl_3$ (77.00 ppm). Infrared spectra were acquired on a SHIMADZU IRAffinity-1 FT-IR Spectrometer. Mass spectra and high-resolution mass spectra were obtained on JEOL JMS-700 Mass Spectrometer or JEOL JMS-S3000 Mass Spectrometer. UV-Vis spectra were recorded on a Shimadzu UV-2550 spectrophotometer. Steady-state emission spectra were recorded on a HAMAMATSU Quantaurus-QY C11347-01 spectrometer with an integrating sphere. Lifetime measurement was conducted with a time-correlated single-photon counting (TCSPC) system HAMAMATSU Quantaurus-Tau C11367.

Materials.

Dibenzo[*a,j*]phenazine (**19**)[1a] and 3,11-dibromodibenzo[*a,j*]phenazine (**22**)[1a] were synthesized according to the reported procedures. Other commercial reagents were purchased from TCI or Wako Pure Chemical Industries, Ltd., and were used as received. Solvents of fluorescence spectroscopic grade for measurement of UV-Vis and emission spectra were purchased from Nacalai Tesque Inc.

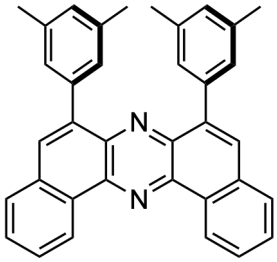
Synthetic Procedures and Spectroscopic Data of New Compounds.

6,8-bis(3,5-dimethylphenyl)dibenzo[*a,j*]phenazine (20)



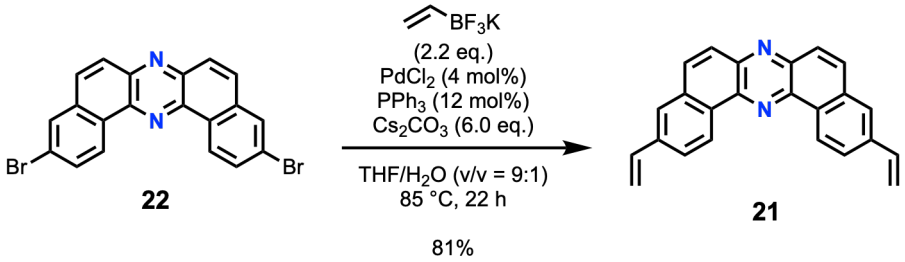
5c **20**

The title compound **20** was prepared according to a similar method reported in the literature[5] with a slight modification. A two-necked reaction tube (20 mL) equipped with a magnetic stirring bar and two rubber septa were dried in a vacuum oven at 80 °C for 2 hours before use. To the tube, were added 6,8-bis(3,5-dimethylphenyl)-2,12-dibromodibenzo[*a,j*]phenazine (**5c**) (129.3 mg, 0.200 mmol), $Pd(OAc)_2$ (2.2 mg, 10.0 μmol, 5 mol%), PPh_3 (10.5 mg, 40.0 μmol, 20 mol%), and K_2CO_3 (110.6 mg, 0.800 mmol, 4.0 eq.). The reaction tube was sealed with two rubber septa, evacuated, and refilled with nitrogen gas through a syringe needle connected to a double vacuum manifold for three times. *n*-Butanol (4.0 mL) were added to the tube, and the resulting mixture was stirred at room temperature for 10 min. The reaction mixture was stirred in a Personal Organic Synthesizer (EYELA, *Chemi-Station*) equipped with a cooling system (aluminum block temperature: 120 °C) for 24 hours. The reaction mixture was allowed to cool down to room temperature, and toluene and EtOH were removed under reduced pressure. Water (10 mL) was added to the mixture, and the organic layer was extracted with $CHCl_3$ (30 mL×3). The combined organic extracts were dried over Na_2SO_4 and filtered, and the solvents in the filtrate were removed under reduced pressure to give yellowish crude solid. The solid residue was purified by flash short column chromatography on silica gel (eluent: *n*-hexane/$CHCl_3$ = 9:1–7:3) to give yellow solid containing DBPHZ **20** and small quantities of impurities, which was then reprecipitated from $CHCl_3$/*n*-hexane (> 1:20) to provide the title compound **20** in 78% yield (76.2 mg, 0.156 mmol) as a yellow solid.



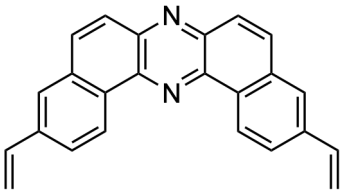
^{1}H NMR (400 MHz, $CDCl_3$) δ 9.64 (d, J = 7.6 Hz, 2H), 8.10 (s, 2H), 7.99 (d, J = 7.2 Hz, 2H), 7.86–7.78 (m, 4H), 7.36 (s, 4H), 7.02 (s, 2H), 2.22 (s, 12H).

3,11-divinyldibenzo[*a,j*]phenazine (21)



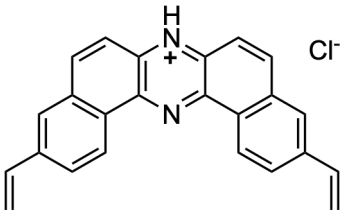
The title compound **21** was prepared according to a similar method reported in the literature[6] with a slight modification. A two-necked reaction tube (20 mL) equipped with a magnetic stirring bar and two rubber septa were dried in a vacuum oven at 80 °C for 2 hours before use. Dehydrated THF and deionized water were degassed through freeze-pump-thaw cycling three times before use. To the tube, were added 3,11-dibromodibenzo[*a,j*]phenazine (**22**) (87.6 mg, 0.200 mmol), Potassium Vinyltrifluoroborate (58.9 mg, 0.440 mmol, 2.2 eq.), $PdCl_2$ (1.4 mg, 7.9 μmol, 4 mol%), PPh_3 (6.3 mg, 24 μmol, 12 mol%), and Cs_2CO_3 (391.0 mg, 1.20 mmol, 6.0 eq.). The reaction tube was sealed with two rubber septa, evacuated, and refilled with nitrogen gas through a syringe needle connected to a double vacuum manifold for three times. Dehydrated THF (3.6 mL) and deionized water (0.4 mL) were added to the tube, and the resulting mixture was stirred at room temperature for 10 min. The reaction mixture was stirred in a Personal Organic Synthesizer (EYELA, *Chemi-Station*) equipped with a cooling system (aluminum block temperature: 85 °C) for 22 hours. The reaction mixture was allowed to cool down to room temperature, and toluene and EtOH were removed under reduced pressure. Water (10 mL) was added to the mixture, and the organic layer was extracted with $CHCl_3$ (20 mL×3). The combined organic extracts were dried over Na_2SO_4 and filtered, and the solvents in the filtrate were removed under reduced pressure to give yellowish crude solid (80.3 mg). The solid residue was purified by flash short column chromatography on NH silica gel (eluent:

n-hexane/EtOAc = 9:1) to give yellow solid containing DBPHZ **21** and small quantities of impurities, which was then reprecipitated from $CHCl_3$/*n*-hexane (> 1:20) to provide the title compound **21** in 81% yield (53.9 mg, 0.162 mmol) as a yellow solid.



mp 329 °C (dec.); R_f 0.37 (*n*-hexane/EtOAc 8:2, NH silica); ^{1}H NMR (400 MHz, $CDCl_3$) δ 9.52 (d, J = 8.4 Hz, 2H), 8.04 (brs, 4H), 7.94 (dd, J = 8.4, 1.8 Hz, 2H), 7.91 (d, J = 1.8 Hz, 2H), 6.99 (dd, J = 17.6, 10.8 Hz, 2H), 6.03 (d, J = 17.6 Hz, 2H), 5.47 (d, J = 10.8 Hz, 2H); ^{13}C NMR (100 MHz, $CDCl_3$) δ 142.7, 140.5, 138.5, 136.5, 133.5, 132.4, 130.8, 127.3, 126.2, 125.5, 125.2, 115.7; IR (ATR, cm^{-1}): 3065, 3034, 3007, 2914, 2874, 1686, 1616, 1603, 1474, 1447, 1418, 1344, 1204, 1103, 991, 883, 851, 793, 723; MS (EI^+): *m*/*z* (relative intensity, %): 333 ($[M+1]^+$, 28), 332 (M^+, 100), 166 ($[M/2]^+$, 13), 152 ($[M/2–N]^+$, 7); HRMS (EI^+): *m/z* calcd for $C_{24}H_{16}N_2$ (M) 332.1313, found 332.1308.

3,11-divinyldibenzo[*a,j*]phenazine hydrochloride (21•HCl)



^{1}H NMR (400 MHz, $CDCl_3$) δ 9.46 (d, J = 8.8 Hz, 2H), 8.63 (d, J = 9.2 Hz, 2H), 8.26 (d, J = 9.2 Hz, 2H), 8.04 (d, J = 8.8 Hz, 2H), 7.98 (s, 2H), 7.00 (dd, J = 17.6, 11.2 Hz, 2H), 6.08 (d, J = 17.6 Hz, 2H), 5.56 (d, J = 11.2 Hz, 2H).

Photophysical Measurements.

*Measurement of cyclic homodimer **8***

All the steady-state UV-Vis absorption and PL spectra were measured at room temperature with diluted solutions (10^{-6} M), which were prepared from degassed spectroscopic grade solvents (N_2 for 30 min).

TCSPC measurements

For the TCSPC measurements, the solutions were degassed by performing freeze-thaw cycles (3 times). PL decay curves were deconvoluted with instrumental responsive function (IRF), and decay function $G(t)$ was fitted with the following equation to extract lifetimes:

$$G(t) = \sum_{i=1}^{n} A_i \exp\left(-\frac{t}{\tau_i}\right)$$

where τ_i are lifetimes of each emission component and A_i are the corresponding fractional amplitudes.

Also, intensity average lifetime $<\tau>$ was calculated by the following equation:

$$<\tau> = \frac{\sum_{i=1}^{n} \tau_i^2 A_i}{\sum_{i=1}^{n} \tau_i A_i}$$

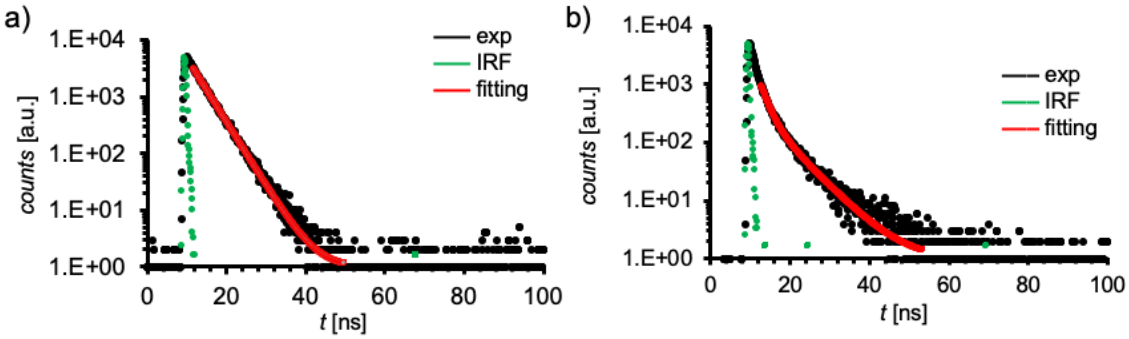


Figure 15. Emission decay profiles of a) toluene solution of **8** (c = 10^{-6} M) and b) solid **8**. Black and green plots indicate experimental photocounting and instrumental responsive function (IRF), respectively. Red lines indicate fitting deconvolution curves.

Table 2. Summary of parameters of cyclic homodimer **8** obtained by TCSPC measurement.

	τ_1 (ns)	A_1	τ_2 (ns)	A_2	$<\tau>$ (ns)	χ^2
solution	3.86	767.3	—	—	3.86	1.03
solid	1.86	534.3	6.29	61.3	3.10	1.06

*UV-Vis Absorption Titration of **8** with TFA and reversibility test*

Dehydrated toluene (spectroscopic analysis grade) was deaerated through babbling N_2 gas for 30 min. To a volumetric flask (100 mL), were added **8** (460 μg, 0.473 μmol) and toluene to make 100 mL of solution (c = 4.73 μM) (*Solution A*). In another volumetric flask (20 mL), were added TFA (2.42 g, 21.2 mmol) and the *Solution A* to make 20 mL of solution (the concentration of TFA = 1.06 M, the concentration of **8** = 4.34 μM,) (*Solution B*). In a quartz cell (optical path length: 1 cm), were added *Solution A* (2.2 mL) and a stirring bar. The UV-Vis absorption spectrum was acquired. *Solution B* (25 μL, TFA 2500 equiv.) was added, and the resulting solution was stirred for 10 min, and the UV-Vis absorption spectrum was acquired. In a similar manner, a portion of *Solution B* was added (25, 31, 43, 44, 46, 60, 55, 86, 84, 89, 94, 100, and 182 μL), and the UV-Vis absoption spectrum was acquired. After adding TFA, NEt_3 (200 μL, 1.44 mmol, 98500 eq.) was added to the cell, and the resulting solution was stirred for 10 min, and the UV-Vis absorption spectrum was acquired.

*PL Titration of **8** with TFA*

Dehydrated toluene (spectroscopic analysis grade) was deaerated through babbling N_2 gas for 30 min. To a volumetric flask (100 mL), were added **8** (460 μg, 0.473 μmol) and toluene to make 100 mL of solution (c = 4.73 μM) (*Solution A*). In another volumetric flask (20 mL), were added TFA (2.42 g, 21.2 mmol) and the *Solution A* to make 20 mL of solution (the concentration of TFA = 1.06 M, the concentration of **8** = 4.34 μM,) (*Solution B*). In a quartz cell (optical path length: 1 cm) filled with N_2 gas, were added *Solution A* (2.2 mL) deaerated with freeze-threw cycles (3 times) and a stirring bar. The PL spectrum was acquired (λ_{ex} = 405 nm). *Solution B* (25 μL, TFA 2500 equiv) was added, and the resulting solution was stirred for 10 min, and the PL spectrum was acquired. In a similar manner, a portion of *Solution B* was added (25, 31, 43, 45, 45, 60, 55, 86, 84, 89, 94, 100, and 182 μL), and the PL spectrum was acquired. After adding TFA, NEt_3 (200 μL, 1.44 mmol, 98500 eq.) was added to the cell, and the resulting solution was stirred for 10 min, and the PL spectrum was acquired.

*Measurement of cyclic heterodimer **18***

All the steady-state UV-Vis absorption and PL spectra were measured at room temperature with diluted solutions (2.0×10^{-5} M), which were prepared from degassed spectroscopic grade solvents (N_2 for 30 min).

Procedure for preparation of Zeonex® film

Zeonex® (1.0 mg) was dissolved in toluene (10 mL) to afford a Zeonex® stock solution (100 g L^{-1}). Compound **18** (1.98 mg) was dissolved in toluene (2.0 mL). The Zeonex® solution and the solution of compound **18** were mixed in desired ratios to prepare blended solutions with different doping concentrations (0.1 wt% = 9:1, 1 wt% = 1:1, and 10 wt% = 1:9 by volume). A quartz substrate (20 mm×20 mm) was washed with acetone. The mixed solutions were dropped onto the substrates and dried under ambient conditions.

TCSPC measurements

For the TCSPC measurements, the solutions were degassed by performing freeze-thaw cycles (3 times). PL decay curves were deconvoluted with instrumental responsive function (IRF), and decay function $G(t)$ was fitted with the following equation to extract lifetimes:

$$G(t) = \sum_{i=1}^{n} A_i \exp\left(-\frac{t}{\tau_i}\right)$$

where τ_i are lifetimes of each emission component and A_i are the corresponding fractional amplitudes.

Also, intensity average lifetime $<\tau>$ was calculated by the following equation:

$$<\tau> = \frac{\sum_{i=1}^{n} \tau_i^2 A_i}{\sum_{i=1}^{n} \tau_i A_i}$$

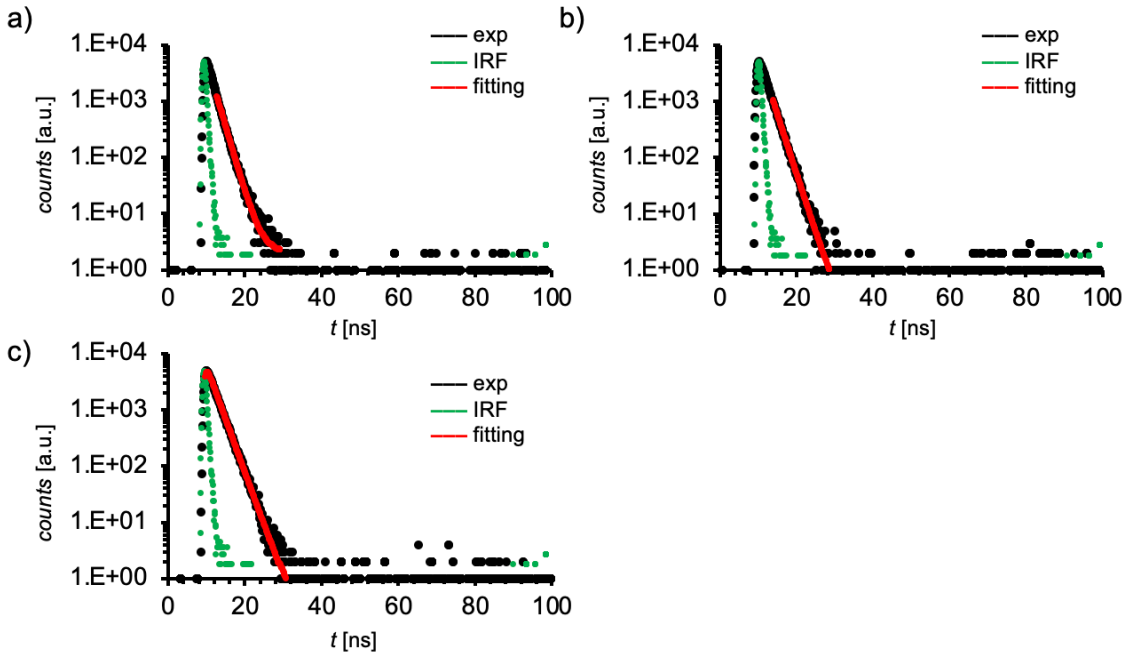


Figure 16. Emission decay profiles of **18** (c = 2.0 × 10^{-5} M) in a) cyclohexane, b) toluene, and c) THF. Black and green plots indicate experimental photocounting and instrumental responsive function (IRF), respectively. Red lines indicate fitting deconvolution curves.

Table 3. Summary of photophysics of **18** in solutions (c = 2.0 × 10^{-5} M).

solvent	λ_{abs} (nm)	ε ($M^{-1}cm^{-1}$)	λ_{em} (nm)	Φ_{PL}	τ (ns)	χ^2	k_r (s^{-1})
CyH	413	37,900	470, 493	0.10	1.84	0.955	5.43×10^7
	436	29,100					
toluene	417	41,000	478	0.14	2.04	1.004	6.86×10^7
	437	32,400					
THF	417	38,500	486	0.13	2.29	0.932	5.68×10^7
	438	30,900					

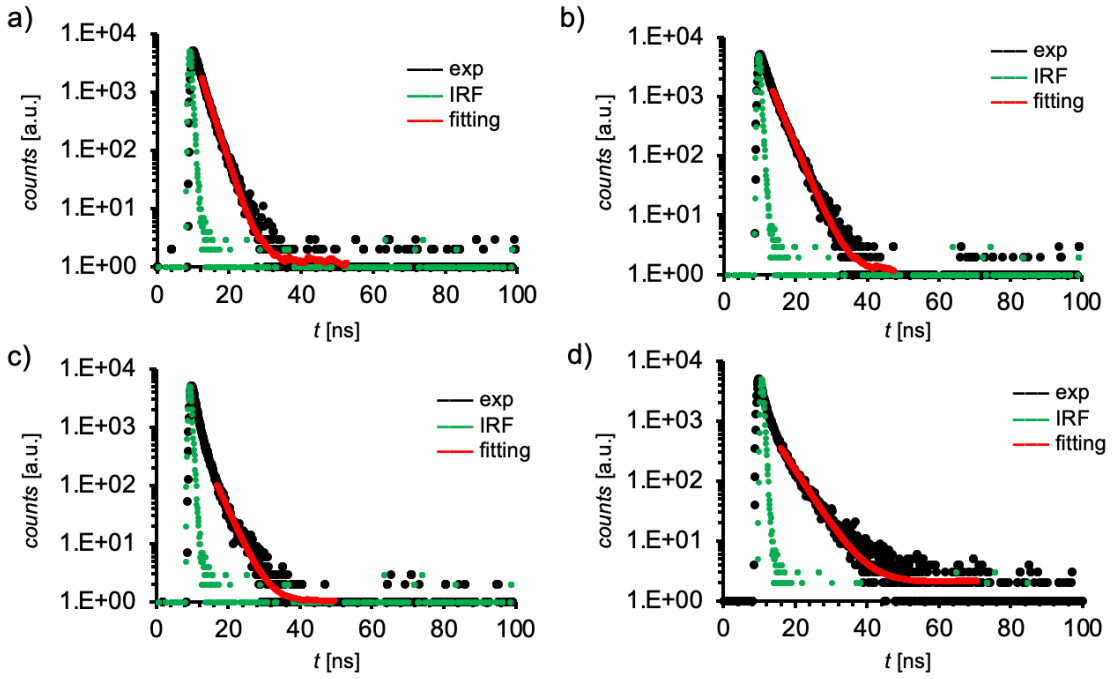


Figure 17. Emission decay profiles of **18** (c = 10^{-5} M) in zeonex® films. a) 0.1 wt%, b) 1.0 wt%, c) 10 wt%, and d) 100 wt% (neat). Black and green plots indicate experimental photocounting and instrumental responsive function (IRF), respectively. Red lines indicate fitting deconvolution curves.

Table 4. Summary of photophysics of **2** in Zeonex® films.

Concentration (wt%)	λ_{em} (nm)	Φ_{PL}	τ (ns)	χ^2	k_r (s^{-1})
0.1	475	0.12	2.27	1.021	5.29×10^7
1.0	490	0.11	3.04	0.950	3.62×10^7
10	510	0.07	3.14	0.915	2.23×10^7
100 (neat)	580	0.04	4.67	1.098	8.57×10^6

Quantum Chemical Calculations

All quantum chemical calculations were performed using Gaussian 16. Geometry optimizations were carried out at the PBE0/6-31G(d,p) level with the IEFPCM solvation model ($CHCl_3$). Geometry coordinates are available as xyz files online.

3-12. References

1. (a) Takeda, Y.; Okazaki, M.; Minakata, S. *Chem. Commun.* **2014**, *50*, 10291–10294. (b) Takeda, Y.; Data, P.; Minakata, S. *Chem. Commun.* **2020**, *56*, 8884–8894. (c) Takeda, Y. *Acc. Chem. Res.* **2024**, *57*, 2219–2232.
2. Thordarson, P. *Chem. Soc. Rev.* **2011**, *40*, 1305–1323.
3. http://app.supramolecular.org/bindfit/.
4. (a) Albert, A.; Phillips, J. N. *J. Chem. Soc.* **1956**, 1294–1304. (b) Lõkov, M.; Tshepelevitsh, S.; Heering, A.; Plieger, P. G.; Vianello, R.; Leito, I. *Eur. J. Org. Chem.* **2017**, *30*, 4475–4489.
5. Chen, J.; Zhang, Y.; Yang, L.; Zhang, X.; Liu, J.; Li, L.; Zhang, H. *Tetrahedron* **2007**, *63*, 4266–4270.
6. Molander, G. A.; Brown, A. R. *J. Org. Chem.* **2006**, *71*, 9681–9686.

Conclusion

The present Thesis has focused on the design, synthesis, and functional exploration of novel nitrogen-embedded π-extended arylene macrocycles based on dibenzo[*a,j*]phenazine (DBPHZ). The results obtained through the studies are summarized as follows:

Chapter 1 described the development of 6,8-diarylated DBPHZ derivatives as solubility-enhanced building blocks and their application to the synthesis of DBPHZ cyclic homodimer **8**. Introduction of bulky alkylated aryl substituents at the 6,8-positions effectively suppressed intermolecular aggregation and improved the solubility of DBPHZ building blocks. ^{1}H NMR spectroscopy and DFT calculations showed that the resulting cyclic homodimer adopts a rigid helical framework. Moreover, analysis of HOMA values and NICS indices revealed that the aromaticity of **8** is localized on the benzene rings rather than being delocalized over the entire macrocycle, consistent with a Clar's π-sextet electronic structure.

Chapter 2 described the development of a tetra-functionalized DBPHZ building block **10** designed to further enhance the solubility of DBPHZ cyclic dimers. Compound **10**, bearing two bromo functionalities at the 2,12-positions and two triisopropylsiloxy groups at the 3,11-positions, was synthesized via a practical synthetic route from a naphthol precursor while retaining all key functionalities. The DBPHZ cyclic heterodimer **18**, obtained from DBPHZ **10** and **7**, readily dissolved in common organic solvents, in contrast to the poorly soluble homodimer **8**. ^{1}H NMR analysis and DFT calculations indicated that heterodimer **18** is C_2-symmetry with a more twisted and helical structure than homodimer **8** due to the increased steric congestion around the biphenylene bridge. These findings clearly demonstrate that the introduction of siloxy groups significantly contributes to improved solubility.

Chapter 3 described the photophysical properties of the DBPHZ cyclic dimers synthesized in Chapter 1 and Chapter 2, compared them with those of monomeric DBPHZ, and explored functions arising from the characteristic structures and properties of the cyclic dimers.

Both cyclic dimers exhibit red-shifted absorption and emission relative to the DBPHZ monomer, reflecting an effectively extended π-conjugation pathway. Furthermore, for the cyclic homodimer **8**, acid titration experiments revealed protonation-induced spectral changes, and binding analysis supported a non-cooperative 1:2 binding model between the macrocycle and protons. NMR studies suggested that protonation occurs preferentially at the outer pyrazine nitrogen atoms, and the homodimer demonstrates reversible turn-off type luminescence switching behavior upon protonation. For the cyclic heterodimer **18**, its good solubility enabled detailed photophysical studies in various solvents and in thin films. In solution, the heterodimer shows weak solvatochromic emission, indicating a lowest excited state with charge-transfer character. DFT calculations show HOMO contribution from the siloxy groups. In thin films, the heterodimer exhibits concentration-dependent emission color changes, indicating the formation of excimer-like emissive states governed by intermolecular interactions between macrocycles, mediated by the flexible C–O–Si linkages.

Through this Thesis, it has been clarified that macrocyclization of appropriately functionalized DBPHZ units is an effective strategy for constructing novel nitrogen-embedded arylene macrocycles. The molecular design principles established here—combining a preorganized U-shaped N-arylene core, strategically positioned halogen functionalities for intramolecular coupling, and aryl or siloxy substituents for enhancing solubility—are expected to contribute to the further development of functional N-arylene macrocycles and related organic photofunctional materials.

The findings obtained in this study provide design guidelines for nitrogen-doped cycloarylene molecules and offer useful insights into the development of new organic luminescent materials and supramolecular functional materials.

List of Publications

The content of this thesis has been published in the following papers.

1) Synthesis of Solubility-Enhanced 6,8-Diarylated Dibromodibenzo[*a,j*]Phenazines via Pd-Catalyzed C–H Arylation and Skeletal Rearrangement

   Naohiro Namba, Norimitsu Tohnai, Satoshi Minakata, Youhei Takeda

   Asian J. Org. Chem. **2025**, *14*, e70211.

2) Synthesis and Photophysical Properties of Cyclic Homodimer of U-Shaped Dibenzophenazinylene

   Naohiro Namba, Satoshi Minakata, Youhei Takeda

   Org. Lett. **2025**, *27*, 11480–11484.

3) Highly Soluble Cyclic Dibenzophenazine Heterodimer Enabled by a Tetra-Functionalized Building Block

   Naohiro Namba, Fumiya Ogura, Marc K. Etherington, Satoshi Minakata, Youhei Takeda

   Chem. Lett. **2025**, *54*, upaf216.

Copyrights

The author has obtained the permissions to reuse contents. The author wishes to express his thanks to Creative Commons, Copyright Clearance Center, Wiley-VCH GmbH, American Chemical Society, and Oxford University Press.

Credits

Reprinted with permission from Namba, N.; Tohnai, N.; Minakata, S.; Takeda, Y. *Asian J. Org. Chem.* **2025**, *14*, e70211. Copyright 2025 Wiley-VCH GmbH.

Reprinted with permission from Namba, N.; Minakata, S.; Takeda, Y. *Org. Lett.* **2025**, *27*, 11480–11484. Copyright 2025 American Chemical Society.

Reprinted with permission from Namba, N.; Ogura, F.; Etherington, M. K.; Minakata, S.; Takeda, Y. *Chem. Lett.* **2025**, *54*, upaf216. Copyright 2025 Oxford University Press.

Acknowledgement

The author would like to express his sincere gratitude to Professor Dr. Satoshi Minakata, for his continuous guidance, many invaluable suggestions, and encouragement with warm enthusiasm throughout this work. The author is also deeply grateful to Professor Dr. Norimitsu Tohnai for kindly reviewing this Thesis with thoughtful comments and suggestions, and for performing the single crystal X-ray structure analysis. The author wishes to express his deepest thanks to Professor Dr. Ken-ichi Nakayama for reviewing this Thesis and providing helpful comments and suggestions.

The author owes a great debt of gratitude to Associate Professor Dr. Youhei Takeda for his continuous guidance and invaluable advice during the course of this study. The author is sincerely grateful to Assistant Professor Dr. Kensuke Kiyokawa for his helpful discussions and encouragement.

The author is indebted to Assistant Professor Dr. Marc K. Etherington, Northumbria University for his assistance in UV-vis and PL measurements and his valuable discussions.

Thanks are also due to the Instrumental Analysis Center, Graduate School of Engineering, the University of Osaka, for measurements of spectral and analytical data. The author would especially like to thank Mr. Hiroaki Tanaka for his kind support and insightful comments on the MALDI-TOF mass measurements.

The author deeply thanks Ms. Junko Ohmagari for her kind help and heartwarning encouragement.

The author is deeply indebted to Mr. Fumiya Ogura for his valuable discussions and active collaboration. The author would like to offer his special thanks to all members of the Minakata group for their hearty encouragement, constant support and kind friendship.

The author is grateful for the financial support by the Japan Science and Technology Agency (JST) as a part of Support for Pioneering Research Initiated by the Next Generation (SPRING) program.

Furthermore, the author is deeply grateful to his family–Ms. Maho Namba, Mr. Hitoki Namba, Ms. Ryoko Kobayashi, and Mr. Senshi Kobayashi–for their full understanding and unfailing support, which enabled him to complete his doctorate.

Finally, his appreciation cannot be expressed in words for all the people who helped him during his doctoral studies.

Naohiro Namba